

Extreme precipitation and temperature events in the Colombian Andes during ENSO and Neutral years

Isabel Cristina Acero Ramírez

Tesis de maestría presentada para optar al título de Magíster enIngeniería Ambiental

Directora
Sara Cristina Vieira Agudelo, PhD

Universidad de Antioquia
Facultad de Ingeniería, Escuela Ambiental
Maestría en Ingeniería Ambiental
Medellín
2024

Cita	(Acero Ramírez, 2024)
Referencia **Estilo APA 7 (2020)**	Acero Ramírez, I.C. (2024). *Extreme precipitation and temperature events in the Colombian Andes during ENSO and Neutral years* [Tesis de maestría]. Universidad de Antioquia, Medellín, Colombia).

creative commons

BY NC SA

Maestría en Ingeniería Ambiental.
Grupo de Investigación Ingeniería y Gestión Ambiental (GIGA).
Centro de Investigaciones Ambientales y de Ingeniería (CIA).

UNIVERSIDAD DE ANTIOQUIA
Vicerrectoría de Docencia

Sistema de Bibliotecas

Biblioteca Carlos Gaviria Díaz

Repositorio Institucional: http://bibliotecadigital.udea.edu.co

Universidad de Antioquia - www.udea.edu.co

Rector: John Jairo Arboleda.
Decano/Director Julio César Saldarriaga.
Jefe departamento: Lina María Berrouet Cadavid.

El contenido de esta obra corresponde al derecho de expresión de los autores y no compromete el pensamiento institucional de la Universidad de Antioquia ni desata su responsabilidad frente a terceros. Los autores asumen la responsabilidad por los derechos de autor y conexos.



Extreme precipitation and temperature events in the Colombian Andes during ENSO and Neutral years

Isabel Cristina Acero Ramírez

Thesis submitted as partial fulfilment of the requirements towards the degree of:
Master of Environmental Engineering

Director:
Sara Cristina Vieira Agudelo PhD

Universidad de Antioquia
Facultad de Ingeniería - Escuela Ambiental
Medellín, Colombia
2023

Acknowledgments

Antes de mostrar este trabajo me gustaría agradecer a las personas que estuvieron apoyando, impulsando y motivando mi camnino para la realización de esta investigación. Personas que me valoran y quieren verme seguir hacia adelante y merecen este espacio como mi agradecimiento por este acompañamiento.

En primer lugar quiero agaradecer a la profesora Sara Vieira mi asesora quién no solo es una excelente profesora sino también una gran persona con su empatía y comprensión, y la cual tuvo mucha paciencia cuando tuve momentos dificiles en este proceso.

A mi familia, mi hermana Carolina Acero, mi padre Jorge Mario Acero, mi tía Martha Ramírez quienes son las primeras personas presentes para ayudarme en todo lo que he necesitado tanto material como emocionalmente. A mi madre por ser la mujer que me han inspirado, siempre, por enseñarme a ser humano compasivo y seguir hacia adelante. Ella es mi inspiración y aprecio muchos sus sacrificios y esfuerzos por sacarnos hacia adelante y tengamos bienestar mi hermana y yo.

Me siento infinitamente agradecida con Julián Sepúlveda quién su amabilidad contribuyó en asesoría en este trabajo de investigación, aportando ideas, conocimiento y críticas. Es una persona que se ha destacado en la investigación y quién admiro por su labor.

También a Omar Pimienta quién fue la persona que caminó casi todo este proceso conmigo. La persona que me enseñó valores para la vida y fue el apoyo en los momentos donde pensé que no había salida.

A Juan Diego Mantilla, mi pareja que a pesar del recorrido corto que hemos tenido juntos él ha sido fundamental en la finalización de este proceso, no solo por darme su apoyo y ánimo constantemente sino por su contribución en ideas, ayuda en algunos casos el procesamiento y revisión.

Puedo decir que soy afortunada por tener muchos amigos valiosos. Quiero darle las gracias a mis amigas Estefanía González, María del mar Vásquez, Camila Díaz, Yeresmin Arias y Melisa Zea. Amigas desde hace muchos años, mis confidentes, que me han aconsejado, escuchado, levantado y han creído en mi.

A Braian Silva y los gimnásticos Cristina Vásquez, Roobert Gallego, James Morales, Norfy Sierra, Juan Vanegas, Sebastián Arias, Jonathan Grajales, Julián Zapata, Melisa Patiño y Daniela Marin. Los amigos que encontré practicando un deporte y se han mantenido en el camino, desde sus saberes y experiencias, estuvieron dándome consejos, sacándome de rutinas y disfrutando de la vida.

También a mis amigos de maestría Juliana Mejía, Diver Marín y Natalia Bernal, quie-

nes juntos trasnochamos en muchas ocasiones, nos retroalimentamos y aprendimos entre nosotros.

A SIATA y a mis compañeros y amigos de allí en particular Duvan Nieves, Isabel Correa y Laura Ortíz que me han dado la oportunidad de conocerlos como profesionales y de los cuales he aprendido mucho, además por abrirme un espacio en sus vidas donde hemos podido construir una amistad.

Por último, también quiero reconocerme a mi misma el esfuerzo y sacrificios que realicé, por las trasnochadas y la incertidumbre. Escoger hacer una maestría indica tal vez el deseo de continuar aprendiendo o tal vez no. Sabemos que implicará un reto, frustración, odio, amor y muchas reflexiones. Para mí la enseñanza no solo fue académica sino también para la vida, por las experiencias, decisiones a tomar y sobre todo por el aprendizaje que obtenemos de las persona que conocemos en el camino. También a no dejar de último mi bienestar y prestar más atención a mi salud física y mental.

Abstract

The Andes of Colombia is a region highly influenced by changes in the mean and extreme precipitation and temperature fields during El Niño–Southern Oscillation (ENSO). Here we study the influence of the ENSO phenomenon on extreme precipitation events (EPE) and extreme temperature events (ETE) and explore the atmospheric circulation patterns that contribute to the EPEs. EPEs were characterized from the 95th and 99th percentiles and ETEs through the 99th percentile for daytime and nighttime maxima (TXx) and minima (TNn). Our results suggest that EPEs do not show differences in intensity between La Niña (LN), EN (EN), and neutral years; however, the frequency is higher during LN and the September-October-November season. Additionally, a cluster analysis was performed where five regions with similar characteristics were found for their intensity in the EPEs. This finding is consistent with the spatial patterns observed at the in situ stations. On the other hand, diurnal and nocturnal TXx and TNn were more intense during EN. While TXx are more frequent during EN, and TNn are more frequent during LN, in both nocturnal and diurnal. Transitioning our analysis to the atmospheric context, the circulation patterns exhibited favorable conditions for the onset of EPEs during LN in northern South America; in addition, the horizontal fields showed agreement between the 2010-2012 LN event and the composite, except for the vertical profile where the atmospheric conditions may be different from other LN events in some months. The moisture flux in the vertical showed that moisture sources are available during the year but may change during EN, LN, and neutral years.

Keywords: Extreme Precipitation Events (EPEs); Extreme Temperature events (ETEs); El Niño-Southern Oscillation (ENSO); Neutral years; cluster analysis; Andes; Circulation Pattern.

Abbreviations

EPTEs	Extreme precipitation and temperature events
EPEs	Extreme precipitation events
ETEs	Extreme temperature events
ENSO	El Niño-Southern Oscillation
DJF	December, January, February
MAM	March, Apil, May
JJA	June, July, August
SON	Septiembre, Octubre, Noviembre
ETCCDI	Expert Team on Climate Detection and Change Indices
SST	Sea Surface Temperature
TEOF	Trend Empirical Orthogonal Function
GPD	Generalized Pareto Distribution
TXx	Maximum Value of Daily Maximum Temperature
TNn	Monthly Minimum Value of Daily Minimum Temperature

List of Figures

2-1. Annual rainfall cycle for the Andes of Colombia comparing average spatial data from TRMM and CHIRPS satellite sources with mean measurements from IDEAM stations. Gray shaded band corresponds to the range of variation across IDEAM stations. 13

2-2. The threshold value for characterized extreme and heavy precipitation, a) 95th TRMM, b) 95th CHIRPS, c) 95th rain gauge IDEAM, d) 99th TRMM, e) 99th CHIRPS, and f) 99th rain gauge IDEAM. 14

2-3. Heatmaps of extreme precipitation events for percentiles 99th , based on TRMM (1998-2019) and CHIRPS (1981-2019) data sets. a) Intensity events percentile 99th TRMM, b) Intensity events percentile 99th CHIRPS, c) frequency events percentile 99th TRMM and d) frequency events percentile 99th CHIRPS. 15

2-4. Heatmaps of extreme precipitation events for percentiles 95th and 99th across IDEAM station(1991–2019). a) Intensity events percentile 95th, b) Intensity events percentile 99th h, c) frequency events percentile 95th and d) frequency events percentile 99th. 16

2-5. Heatmaps of extreme precipitation events for percentiles 95th and 99th in stations IDEAM, between 1991–2019, a) Intensity events percentile 95th, b) Intensity events percentile 99th, c) frequency events percentile 95th and d) frequency events percentile 99th. 17

2-6. Characterization of extreme precipitation events, categorized by the intensity at the 95th (top three rows) and 99th percentiles (bottom three rows), during DJF. Data is sourced from TRMM at the 95th (a, d, g) and 99th percentiles (j, m, p), CHIRPS at the 95th (b, e, h) and 99th percentiles (k, n, q), and IDEAM stations at the 95th (c, f, i) and 99th percentiles (l, o, r). The labels in each row signify the phases of the ENSO, encapsulating LN years, EN years, and neutral years. Regions shaded in white denote the absence of extreme events during the respective season. 20

2-7. Characterization of extreme precipitation events, categorized by the frequency at the 95th (top three rows) and 99th percentiles (bottom three rows), during DJF. Data is sourced from TRMM at the 95th (a, d, g) and 99th percentiles (j, m, p), CHIRPS at the 95th (b, e, h) and 99th percentiles (k, n, q), and IDEAM stations at the 95th (c, f, i) and 99th percentiles (l, o, r). The labels in each row signify the phases of the ENSO, encapsulating LN years, EN years, and neutral years. Regions shaded in white denote the absence of extreme events during the respective season. 21

2-8. Characterization of extreme precipitation events, categorized by the intensity at the 95th (top three rows) and 99th percentiles (bottom three rows), during MAM. Data is sourced from TRMM at the 95th (a, d, g) and 99th percentiles (j, m, p), CHIRPS at the 95th (b, e, h) and 99th percentiles (k, n, q), and IDEAM stations at the 95th (c, f, i) and 99th percentiles (l, o, r). The labels in each row signify the phases of the ENSO, encapsulating LN years, EN years, and neutral years. Regions shaded in white denote the absence of extreme events during the respective season. 23

2-9. Characterization of extreme precipitation events, categorized by the frequency at the 95th (top three rows) and 99th percentiles (bottom three rows), during MAM. Data is sourced from TRMM at the 95th (a, d, g) and 99th percentiles (j, m, p), CHIRPS at the 95th (b, e, h) and 99th percentiles (k, n, q), and IDEAM stations at the 95th (c, f, i) and 99th percentiles (l, o, r). The labels in each row signify the phases of the ENSO, encapsulating LN years, EN years, and neutral years. Regions shaded in white denote the absence of extreme events during the respective season. 24

2-10. Characterization of extreme precipitation events, categorized by the intensity at the 95th (top three rows) and 99th percentiles (bottom three rows), during JJA. Data is sourced from TRMM at the 95th (a, d, g) and 99th percentiles (j, m, p), CHIRPS at the 95th (b, e, h) and 99th percentiles (k, n, q), and IDEAM stations at the 95th (c, f, i) and 99th percentiles (l, o, r). The labels in each row signify the phases of the ENSO, encapsulating LN years, EN years, and neutral years. Regions shaded in white denote the absence of extreme events during the respective season. 26

2-11. Characterization of extreme precipitation events, categorized by the frequency at the 95th (top three rows) and 99th percentiles (bottom three rows), during JJA. Data is sourced from TRMM at the 95th (a, d, g) and 99th percentiles (j, m, p), CHIRPS at the 95th (b, e, h) and 99th percentiles (k, n, q), and IDEAM stations at the 95th (c, f, i) and 99th percentiles (l, o, r). The labels in each row signify the phases of the ENSO, encapsulating LN years, EN years, and neutral years. Regions shaded in white denote the absence of extreme events during the respective season. 27

2-12.Characterization of extreme precipitation events, categorized by the intensity at the 95th (top three rows) and 99th percentiles (bottom three rows), during SON. Data is sourced from TRMM at the 95th (a, d, g) and 99th percentiles (j, m, p), CHIRPS at the 95th (b, e, h) and 99th percentiles (k, n, q), and IDEAM stations at the 95th (c, f, i) and 99th percentiles (l, o, r). The labels in each row signify the phases of the ENSO, encapsulating LN years, EN years, and neutral years. Regions shaded in white denote the absence of extreme events during the respective season. 29

2-13.Characterization of extreme precipitation events, categorized by the frequency at the 95th (top three rows) and 99th percentiles (bottom three rows), during SON. Data is sourced from TRMM at the 95th (a, d, g) and 99th percentiles (j, m, p), CHIRPS at the 95th (b, e, h) and 99th percentiles (k, n, q), and IDEAM stations at the 95th (c, f, i) and 99th percentiles (l, o, r). The labels in each row signify the phases of the ENSO, encapsulating LN years, EN years, and neutral years. Regions shaded in white denote the absence of extreme events during the respective season. 30

2-14.Difference between ENSO and neutral years by the intensity at the 95th (top three rows) and 99th percentiles (bottom three rows), during DJF. Data is sourced from TRMM at the 95th (a, d, g) and 99th percentiles (j, m, p), CHIRPS at the 95th (b, e, h) and 99th percentiles (k, n, q), and IDEAM stations at the 95th (c, f, i) and 99th percentiles (l, o, r). The labels in each row signify the phases of the ENSO, encapsulating LN-Neutral years, EN-Neutral years, and LN-EN. Grid points signify significant differences at a 95% confidence level. 33

2-15.Difference between ENSO and neutral years by the frequency at the 95th (top three rows) and 99th percentiles (bottom three rows), during DJF. Data is sourced from TRMM at the 95th (a, d, g) and 99th percentiles (j, m, p), CHIRPS at the 95th (b, e, h) and 99th percentiles (k, n, q), and IDEAM stations at the 95th (c, f, i) and 99th percentiles (l, o, r). The labels in each row signify the phases of the ENSO, encapsulating LN-Neutral years, EN-Neutral years, and LN-EN. Grid points signify significant differences at a 95% confidence level. 34

2-16.Difference between ENSO and neutral years by the intensity at the 95th (top three rows) and 99th percentiles (bottom three rows), during MAM. Data is sourced from TRMM at the 95th (a, d, g) and 99th percentiles (j, m, p), CHIRPS at the 95th (b, e, h) and 99th percentiles (k, n, q), and IDEAM stations at the 95th (c, f, i) and 99th percentiles (l, o, r). The labels in each row signify the phases of the ENSO, encapsulating LN-Neutral years, EN-Neutral years, and LN-EN. Grid points signify significant differences at a 95% confidence level. 36

2-17.Difference between ENSO and neutral years by the frequency at the 95th (top three rows) and 99th percentiles (bottom three rows), during MAM. Data is sourced from TRMM at the 95th (a, d, g) and 99th percentiles (j, m, p), CHIRPS at the 95th (b, e, h) and 99th percentiles (k, n, q), and IDEAM stations at the 95th (c, f, i) and 99th percentiles (l, o, r). The labels in each row signify the phases of the ENSO, encapsulating LN-Neutral years, EN-Neutral years, and LN-EN. Grid points signify significant differences at a 95% confidence level. 37

2-18.Difference between ENSO and neutral years by the intensity at the 95th (top three rows) and 99th percentiles (bottom three rows), during JJA. Data is sourced from TRMM at the 95th (a, d, g) and 99th percentiles (j, m, p), CHIRPS at the 95th (b, e, h) and 99th percentiles (k, n, q), and IDEAM stations at the 95th (c, f, i) and 99th percentiles (l, o, r). The labels in each row signify the phases of the ENSO, encapsulating LN-Neutral years, EN-Neutral years, and LN-EN. Grid points signify significant differences at a 95% confidence level. 40

2-19.Difference between ENSO and neutral years by the frequency at the 95th (top three rows) and 99th percentiles (bottom three rows), during JJA. Data is sourced from TRMM at the 95th (a, d, g) and 99th percentiles (j, m, p), CHIRPS at the 95th (b, e, h) and 99th percentiles (k, n, q), and IDEAM stations at the 95th (c, f, i) and 99th percentiles (l, o, r). The labels in each row signify the phases of the ENSO, encapsulating LN-Neutral years, EN-Neutral years, and LN-EN. Grid points signify significant differences at a 95% confidence level. 41

2-20.Difference between ENSO and neutral years by the intensity at the 95th (top three rows) and 99th percentiles (bottom three rows), during SON. Data is sourced from TRMM at the 95th (a, d, g) and 99th percentiles (j, m, p), CHIRPS at the 95th (b, e, h) and 99th percentiles (k, n, q), and IDEAM stations at the 95th (c, f, i) and 99th percentiles (l, o, r). The labels in each row signify the phases of the ENSO, encapsulating LN-Neutral years, EN-Neutral years, and LN-EN. Grid points signify significant differences at a 95% confidence level. 42

2-21.Difference between ENSO and neutral years by the frequency at the 95th (top three rows) and 99th percentiles (bottom three rows), during SON. Data is sourced from TRMM at the 95th (a, d, g) and 99th percentiles (j, m, p), CHIRPS at the 95th (b, e, h) and 99th percentiles (k, n, q), and IDEAM stations at the 95th (c, f, i) and 99th percentiles (l, o, r). The labels in each row signify the phases of the ENSO, encapsulating LN-Neutral years, EN-Neutral years, and LN-EN. Grid points signify significant differences at a 95% confidence level. 43

2-22.Cluster classification in the Colombian Andes in the 95th percentile. a) TRMM and b) CHIRPS. 47

2-23.Cluster classification in the Colombian Andes in the 99th percentile. a) TRMM and b) CHIRPS. 48

2-24.Annual rainfall cycle for the Andes of Colombia comparing average spatial data from TRMM and CHIRPS satellite sources with mean measurements from IDEAM stations. a) Cluster 1, b) Cluster 2, c) Cluster 3, c) Cluster 4, d) Cluster 4. 49

2-25.Histograms of monthly EPEs intensities distribution were found at the 95th percentile for each cluster and discretized by LN, EN, and neutral years. The first column corresponds to the groups found in TRMM and the second in CHIRPS. 50

2-26.Histograms of monthly EPEs intensities distribution were found at the 99th percentile for each cluster and discretized by LN, EN, and neutral years. The first column corresponds to the groups found in TRMM and the second in CHIRPS. 51

2-27.The p-values of the stations were obtained from the U-test conducted by the EPEs intensity series at the 95th percentile, LN-neutral years (blue), En-neutral years (red), and LN-EN (gray). The number of stations corresponds to those found in each cluster in TRMM or CHIRPS. The red line has the value of -0.05 and 0.05, and the black line of -0.08 and 0.08. Stations with p-value < 0.05 fall in the range of the red line values. CHIRPS regions 4 and 5 are not plotted because there are no stations within these zones. 53

2-28.The p-values of the stations were obtained from the U-test conducted by the EPEs intensity series at the 99th percentile, LN-neutral years (blue), En-neutral years (red), and LN-EN (gray). The number of stations corresponds to those found in each cluster in TRMM or CHIRPS. The red line has the value of -0.05 and 0.05, and the black line of -0.08 and 0.08. Stations with p-value < 0.05 fall in the range of the red line values. CHIRPS regions 4 and 5 are not plotted because there are no stations within these zones. 54

2-29.The p-values of the stations were obtained from the U-test conducted by the EPE frequency series at the 95th percentile, LN-neutral years (blue), En-neutral years (red), and LN-EN (gray). The number of stations corresponds to those found in each cluster in TRMM or CHIRPS. The red line has the value of -0.05 and 0.05, and the black line of -0.08 and 0.08. Stations with p-value < 0.05 fall in the range of the red line values. CHIRPS regions 4 and 5 are not plotted because there are no stations within these zones. 55

2-30.The p-values of the stations were obtained from the U-test conducted by the EPE frequency series at the 99th percentile, LN-neutral years (blue), En-neutral years (red), and LN-EN (gray). The number of stations corresponds to those found in each cluster in TRMM or CHIRPS. The red line has the value of -0.05 and 0.05, and the black line of -0.08 and 0.08. Stations with p-value < 0.05 fall in the range of the red line values. CHIRPS regions 4 and 5 are not plotted because there are no stations within these zones. 56

3-1. Linear trends for daily temperature in two periods: a) 1979-1999, b) 2000-2019, and c) difference between both periods. In a) hatched areas show significant trends with a confidence level of 95%, while in b) the whole shaded area corresponds to statistically significant temperature trends. 61

3-2. Time series of extreme values indices: daily TXx 90th percentile and daily TNn 10th percentile in daytime and nighttime. a) Intensity and b) Frequency. The blue shading refers to LN events, and the red shading to EN events. . . 62

3-3. Correlation between sea surface temperature (SST) anomalies of the Niño 3.4 region and the frequency of the ETEs indices. a) Daytime TXx extremes, b) Nighttime TXx extremes, c) Daytime TNn extremes, and d) Nighttime TNn extremes. Panels a) to d) depict the correlation, with hatched regions indicating significant associations at a 0.05 p-value. The second row represents the scatter plot only for the Andes between the same variables; the points are discriminated in the values corresponding to LN (blue), EN (red), and neutral (gray). e) Daytime TXx extremes, f) Nighttime TXx extremes, g) Daytime TNn extremes, and h) Nighttime TNn extremes. 64

3-4. Correlation between sea surface temperature (SST) anomalies of the Niño 3.4 region and the frequency of the ETEs indices. a) Daytime TXx extremes, b) Nighttime TXx extremes, c) Daytime TNn extremes, and d) Nighttime TNn extremes. The second row represents the scatter plot only for the Andes between the same variables; the points are discriminated in the values corresponding to LN (blue), EN (red), and neutral (gray). e) Daytime TXx extremes, f) Nighttime TXx extremes, g) Daytime TNn extremes, and h) Nighttime TNn extremes. 66

3-5. The index indicates the intensity of extreme events that occur during the daytime. These events include a) TXx in DJF, b) TXx in JJA, c) TNn in DJF, and d) TNn in JJA. Furthermore, the extreme events are categorized in the first row as occurring during LN years, in the second row as occurring during EN years, and in the third row as occurring during neutral years. . . 68

3-6. The index indicates the intensity of extreme events that occur during the nighttime. These events include a) TXx in DJF, b) TXx in JJA, c) TNn in DJF, and d) TNn in JJA. Furthermore, the extreme events are categorized in the first row as occurring during LN years, in the second row as occurring during EN years, and in the third row as occurring during neutral years. . . 69

3-7. The index indicates the frequency of extreme events that occur during the daytime. These events include a) TXx in DJF, b) TXx in JJA, c) TNn in DJF, and d) TNn in JJA. Furthermore, the extreme events are categorized in the first row as occurring during LN years, in the second row as occurring during EN years, and in the third row as occurring during neutral years. . . 70

3-8. The index indicates the frequency of extreme events that occur during the nighttime. These events include a) TXx in DJF, b) TXx in JJA, c) TNn in DJF, and d) TNn in JJA. Furthermore, the extreme events are categorized in the first row as occurring during LN years, in the second row as occurring during EN years, and in the third row as occurring during neutral years. . . 71

3-9. Comparative analysis of daytime ETEs Index intensity during different ENSO Phases and Neutral years. The first row shows the difference between LN and EN, the second row shows the difference between EN and Neutral years, and the third row shows the difference between LN and EN. The events analyze a) TXx in DJF, b) TXx in JJA, c) TNn in DJF, and d) TNn in JJA. Grid points signify significant differences at a 95% confidence level. 74

3-10.Comparative analysis of nighttime ETEs Index intensity during different ENSO Phases and Neutral years. The first row shows the difference between LN and EN, the second row shows the difference between EN and Neutral years, and the third row shows the difference between LN and EN. The events analyze a) TXx in DJF, b) TXx in JJA, c) TNn in DJF, and d) TNn in JJA. Grid points signify significant differences at a 95% confidence level. 75

3-11.Comparative analysis of daytime ETE Index frequency during different ENSO Phases and Neutral years. The first row shows the difference between La Niña and El Niño, the second row shows the difference between El Niño and Neutral years, and the third row shows the difference between La Niña and El Niño. The events analyze a) TXx in DJF, b) TXx in JJA, c) TNn in DJF, and d) TNn in JJA. Grid points signify significant differences at a 95% confidence level. 77

3-12.Comparative analysis of nighttime ETEs Index frequency during different ENSO Phases and Neutral years. The first row shows the difference between La Niña and El Niño, the second row shows the difference between El Niño and Neutral years, and the third row shows the difference between La Niña and El Niño. The events analyze a) TXx in DJF, b) TXx in JJA, c) TNn in DJF, and d) TNn in JJA. Grid points signify significant differences at a 95% confidence level. 78

3-13.Comparative distribution of monthly intensity of ETEs indices during EN (Red), LN (Blue), and Neutral Years (Light Gray) in the Andes: a) TXx daytime, b) TXx nighttime, c) TNn daytime, and d) TNn nighttime. 80

4-1. 200 hPa geopotential height anomalies from August to December, in the 2010 LN event (first row), EN composite (second row), LN composite (third row), and neutral years composite (fourth row). 85

4-2. 500 hPa omega anomalies from August to December, in the 2010 LN event (first row), EN composite (second row), LN composite (third row), neutral years composite (fourth row), and climatology (fifth row). 86

4-3. 200 hPa velocity potential (shades) and divergence (vectors) anomalies from August to December, in the 2010 LN event (first row), EN composite (second row), LN composite (third row), neutral years composite (fourth row), and climatology (fifth row). 87

4-4. 200 hPa divergence magnitude anomalies from August to December, in the 2010 LN event (first row), EN composite (second row), LN composite (third row), and neutral years composite (fourth row). 90

4-5. 850 hPa specific humidity anomalies from August to December, in the 2010 LN event (first row), EN composite (second row), LN composite (third row), and neutral years composite (fourth row). 92

4-6. Vertically integrated moisture flux (vectors) and moisture convergence (shades) anomalies from August to December in the 2010 LN event (first row), EN composite (second row), LN composite (third row), and neutral years composite (fourth row). Vertically integrated moisture flux magnitude is indicated by the arrow at the right-bottom corner for the composite, but the event magnitude corresponds to 200 kgm-1s-1. 94

4-7. Meridional specific humidity anomalies cross-section from August to December in the 2010 LN event (first row), EN composite (second row), LN composite (third row), and neutral years composite (fourth row). 97

4-8. Meridional omega (shades) and geopotential height (contours) anomalies cross-section from August to December in the 2010 LN event (first row), EN composite (second row), LN composite (third row), and neutral years composite (fourth row). Solid (dotted) contours indicate positive (negative) geopotential height anomalies. 98

A-1. Regional cluster classification in the Colombian Andes. The shading is the TRMM classification, the overlay (black) contour is the CHIRPS classification and the triangle symbol corresponds to the IDEAM stations. For a) 95th percentile and b) 99th percentile. 106

List of Tables

2-1. The p-values were obtained from the U-test in each cluster classification in TRMM and CHIRPS. Values with an asterisk (*) are statistically significant. 52

3-1. Differences between the distributions at a 5% significance level (sig. < 0.05) by U-test. Values associated with an asterisk indicate that they are not statistically significant. 80

B-1. Information from IDEAM stations located in the Andes region. 110

Contents

Acknowledgments iv

Abbreviations vii

Figures List viii

Tables List xvii

1. Introduction 2

2. Characterization and comparison of extreme precipitation events 8
2.1. Methodology . . . 8
2.1.1. Extreme precipitation and temperature definition . . . 8
2.1.2. Data . . . 10
2.1.3. Characterization and comparison . . . 11
2.1.4. Cluster analysis . . . 12
2.2. Results and discussion . . . 12
2.2.1. Rainfall Annual cycle . . . 12
2.2.2. Characterization of EPE . . . 14
2.2.3. Comparison between ENSO and neutral years . . . 31
2.2.4. Cluster analysis . . . 46
2.3. Conclusions . . . 56

3. Characterization and comparison of extreme temperature events 59
3.1. Data and methods . . . 59
3.2. Results and discussion . . . 61
3.2.1. The impact of ENSO on extreme temperature events . . . 61
3.2.2. Characterization and comparison of ETEs . . . 67
3.3. Conclusions . . . 81

4. Atmospheric circulation patterns related to EPEs 82
4.1. Methodology . . . 82
4.2. Results and discussion . . . 83
4.3. Conclusions . . . 99

5. General conclusions **102**

A. Appendix: Complementary Figures **106**

B. Appendix: Complementary Tables **107**

Bibliography **110**

1. Introduction

Colombia, specifically the Andean Cordillera, is highly vulnerable to hazards triggered by extreme events due to its complex topography (Poveda et al., 2020). The Colombian Andes are characterized by interactions between vegetation, topography, and atmosphere, resulting in different atmospheric circulations at various spatial scales. This region experiences a distinct biannual precipitation cycle in March- April- May and September- October- November, attributed to the double passage of the Intertropical Convergence Zone (ITCZ).

Studies in the region have shown that the Colombian Andes are sensitive to the El Niño–Southern Oscillation (ENSO) response (Grimm and Natori, 2006; Poveda et al., 2011). Strong correlations have been found between Niño 3 and Niño 4 regions with rainfall in the tropical Andes. Moreover, research conducted in Colombia has demonstrated that the impacts of the ENSO appear earlier and with greater intensity in the western Andes. At the same time, they exhibit a delayed onset in the eastern region (Poveda et al., 2011). Negative precipitation anomalies are observed almost everywhere across the Andes during El Niño (EN) events, resulting in reduced soil moisture, which, in turn, is associated with decreased evaporation, reduced streamflow levels, and increased mean air temperature (Poveda et al., 1996, 2005). During El Niño years, the surface temperature tends to increase, leading to prolonged periods of drought due to negative precipitation anomalies. Changes in pressure in tropical South America lead to changes in the convection centers of the ITCZ, which can cause disturbances in land-atmosphere interactions (Cai et al., 2020; Trenberth, 2019). The effects of EN have been associated with adverse impacts on agriculture, energy production, water supply, and other economic activities (Bastianin et al., 2018; Erfanian et al., 2017; Martínez et al., 2017). For example, the EN events of 1991 - 1992 were associated with a drought that caused a crisis in hydropower in energy generation (Poveda et al., 2002), and 2015-2016 was categorized as an extreme ENSO generating damage in different regions (Santoso et al., 2017; Aceituno et al., 2009; Dracup and Gutie, 2001; Poveda, 2004; Waylen and Poveda, 2002).

In their study, Grimm and Tedeschi (2009) demonstrated that South America exhibits heightened sensitivity to the ENSO, particularly in relation to the frequency of extreme precipitation events. Their findings emphasize that this sensitivity is more pronounced when assessing extreme events rather than focusing on the monthly accumulated rainfall in the region. The authors employed the gamma distribution to characterize the events during each phase of the ENSO. In later research, Tedeschi et al. (2015) and 2016 investigated the

relationship between the tropical regions of the central and eastern Pacific during ENSO with Extreme Precipitation Events (EPEs). Their research revealed that for two seasons of the year, the precipitation pattern is different in some regions of South America when analyzed with the central and eastern tropical Pacific region. Moreover, in Brazil, trends analysis has revealed that during La Niña (LN), the wet conditions decrease (Borges et al., 2018).

ENSO affects mean temperature fields and extreme temperature events (ETEs). The warmest days in extreme maximum temperature events are found to be significantly influenced by ENSO (Arblaster and Alexander, 2012; Sun et al., 2017; Tan et al., 2021). During the peak of EN events, regions such as Australia, Canada, southernmost Asia, southern Africa, and northern South America experience higher and more frequent maximum temperature extremes compared to LN events. Conversely, extreme events are more pronounced in areas like the United States and Siberia during LN years. Some authors (Arblaster and Alexander, 2012; Gershunov, 1998) found that ENSO teleconnections exhibit similarities with mean temperature values and temperature extremes.

Given the increase in the planet's average temperature, studies worldwide have focused on global warming and its effect on precipitation and extreme temperature events (Alexander, 2016; de Barros Soares et al., 2017; Ghasemi, 2015; Grimm, 2011; Barkhordarian et al., 2018; Almazroui et al., 2021; IPCC, 2021). While it is true that rising temperatures and changes in precipitation patterns in both intensity and frequency have been linked to more frequent and severe heat waves, droughts, floods, and storms. This line of research is pivotal in enhancing our understanding of developing effective early warning systems and formulating adaptive strategies to address the challenges posed by climate change. However, it is also essential to acknowledge the role of the ENSO phenomenon, acting as a modulator of interannual variability and influencing short-term temperature changes. This phenomenon has been observed in South America. Rusticucci et al. (2017) analyzed the influence of ENSO on minimum and maximum temperatures; they observed positive trends in the surface temperature series and found that the change in the South Atlantic anticyclone affected temperature changes. In particular, they found that over Argentina, minimum temperatures are uniformly affected throughout the year under EN conditions, favoring warm nights. Additionally, they observed seasonal variations in maximum temperature extremes. Complementing this, Arblaster and Alexander (2012) provided evidence that, during warm ENSO events, the composite of monthly maximum daily temperatures for the December-January-February period exhibited elevated values over central Argentina.

ETEs in South America have undergone significant changes in recent decades, with a warming trend, a decrease in the frequency of cold nights, and an increase in the occurrence of warm nights (Meseguer-Ruiz et al., 2018; Rusticucci, 2012; Salvador and de Brito, 2018). Similar patterns have been observed in the Andean and Caribbean regions, with a higher frequency of extreme dry spells and fewer wet days per year (Arias et al., 2015; Pabón-

Caicedo, 2012; Rodríguez et al., 2019). In Uruguay, for example, extreme temperature events are strongly correlated with changes in the evolution of ENSO and vortex circulation at higher levels and have been modified by changes in these phenomena (Renom et al., 2011). In addition, more warm nights across South America and a decrease in cold nights are projected to occur in the future, as well as significant changes in precipitation extremes and droughts (Marengo et al., 2009). Nevertheless, denser and more extensive databases and additional regional studies are needed to improve confidence in continental-scale results.

Studies on extreme events in the Andes region have analyzed trends or atmospheric patterns when a particular ENSO event occurs. Cerón et al. (2022) used four precipitation indices associated with extreme rainfall patterns, recommended by the Expert Team on Climate Detection and Change Indices (ETCCDI). They found an increase in the indexes examined during December-February and March-May in almost the entire territory of Colombia. Conversely, they noted a decrease in total precipitation in June-August in the Andes. Moreover, Ávila et al. (2019) reported negative trends in total annual rainfall in the Cauca basin in March-April-May, June-July-August, and September-October-November, while an increase in the extreme indices is observed during December-January and February. They also indicated a significant correlation with a one-month lag between the Niño 3.4 region and the extreme precipitation indices. These results are in agreement with Rodríguez et al. (2019), who found increases in wet spells (consecutive wet days) during LN and dry spells (consecutive dry days) during EN. Understanding the distribution and changes of precipitation and temperature extremes is crucial for effective risk management, especially in the Andean region, where these events are frequent. There is still a significant knowledge gap in the spatial and temporal patterns of these extremes and how they are affected by ENSO events. It is imperative to address this gap to mitigate the potential impacts of extreme weather events.

Understanding the teleconnections and mechanisms of ENSO in South America is crucial due to the region's sensitivity and its adverse effects on the population (Aceituno et al., 2009; Cai et al., 2020; Hoyos et al., 2013a). The impact of EN and LN phases are believed to be symmetrical and opposite, causing deviations in average precipitation and surface air temperature conditions. These atmospheric conditions change due to the warming or cooling of sea surface temperature associated with ENSO, which affects Walker's circulation (Julian and Chervin, 1978). As a result, subsidence over the equatorial east of South America and the equatorial west of the Atlantic inhibits the equatorward movement of the South Atlantic convergence zone (SACZ) and contributes to negative precipitation anomalies (Krishnamurthy and Misra, 2010; Reboita et al., 2021). The impacts of ENSO events may vary during different seasons due to teleconnection efficiencies across tropical and extratropical pathways and, in turn, moisture transport in a given place (Reboita et al., 2021).

Numerous inquiries persist regarding the hydroclimatic anomalies in Colombia during both El Niño and La Niña (ENSO) phases, as explored by various studies (Aceituno, 1989; Poveda

et al., 2011; Poveda and Mesa, 1997; Tootle et al., 2008). In Colombia, some mechanisms have been identified that contribute to hydrological changes during LN or EN events. When the sea surface temperature (SST) is warmer (colder) than normal conditions in EN (LN), the SST gradient east of the Colombian Pacific can weaken (strengthen), changing the transport of moisture and weakening (strengthening) the low-level Chocó jet producing increased (decreased) precipitation over Colombia. This alteration affects the moisture transport and modifies the intensity of the low-level Chocó jet, ultimately leading to increased (decreased) precipitation across Colombia. Furthermore, other mechanisms come into play, such as variations in the equatorial jet at 700 hPa, the influence of tropical waves from the east over the North Atlantic, the displacement of the ZCIT due to anomalies in the Hadley cell over the American tropics, and positive feedback between land-atmosphere processes and the alteration of the atmospheric moisture balance at lower levels (Bedoya-Soto et al., 2019; Poveda, 2004; Poveda et al., 2011, 2020). As highlighted by the works of Ruiz-vásquez et al. (2021) and Arias et al. (2015), the mechanisms are further modified by moisture sources during EN and LN (Hoyos et al., 2018). In addition, Builes-Jaramillo et al. (2023) found changes in moisture transport over the low-level Caribbean, Orinoco, and Chocó jets and changes in precipitation patterns during the transition from LN to EN and vice versa. These findings demonstrate the complex interplay of various factors shaping the hydrological dynamics of Colombia during EN and LN events

The impact of ENSO on the occurrence of EPEs has been a subject of great interest. Unraveling the intricate mechanisms behind the development of these events poses a compelling question that warrants exploration. The first chapter of this research will explain, that the expansive scope of extreme event definition introduces an element of variability, which consequently impacts the conclusions drawn from different choices. Likewise, studying atmospheric circulation patterns also has a wide variety of methodologies. In the literature, the methods used to understand the antecedent and precedent conditions of the atmosphere of an EPEs relies heavily on the study's specific objectives. Time scale is a key factor in analyzing the evolution of the EPEs, i.e., diurnal, daily, monthly, seasonal, and intraseasonal variations. For example, research focused on EPEs associated with atmospheric rivers (Jennrich et al., 2020; Ridder et al., 2018; Tan et al., 2022; Warner et al., 2012), often operates on a daily scale, making it more beneficial to scrutinize atmospheric variables. Others have also looked for ways to discern the most relevant spatial patterns of variability using techniques such as Principal Component Analysis (PCA) and Empirical Orthogonal Functions (EOF). Additionally, methodologies incorporating three-dimensional analyses have also been employed to identify the spatial patterns, as demonstrated in studies by Hu et al. (2020) and Wang et al. (2022a).

EPEs generally occur at an hourly scale; however, since finding information at that resolution is difficult (Barlow et al., 2019; Beck et al., 2015). Consequently, researchers often resort to utilizing data from in situ stations, satellite observations, and reanalysis at the

daily scale. However, it is worth noting that extreme events unfold on a sub-daily scale, leading to a discernible discrepancy in the analysis (Meseguer-Ruiz et al., 2018; Schumacher et al., 2020; Valencia et al., 2023). Satellite observation databases have been instrumental in deciphering diverse meteorological and climatic phenomena in regions with low station densities. Although these observations still carry a degree of uncertainty, their accuracy has steadily improved over time from one version to the next. Given that ENSO impacts the diurnal precipitation cycle in the Andes and, consequently, affects extreme events, it is important to consider the simultaneous influence of multiple phenomena. Hirata and Grimm (2016) identified that both ENSO at the synoptic scale and the Madden-Julian Oscillation at the intraseasonal scale are related to the life cycle of EPEs during the summer in South America. In this sense, atmospheric conditions are studied days before and after the event to analyze daily events' evolution (Huang et al., 2019). But, these methods may have limitations as they only enable the investigation of extremes occurring on specific days, months, or seasons. EPEs are not isolated in the year, and at any time, they can occur.

Extreme precipitation and temperature events exhibit significant regional variations, primarily influenced by the specific geographic location of each site. In the mountainous areas of the tropics, such as the Colombian Andes, complex topography can generate ETEs due to factors such as altitude, solar exposure, humidity, and local atmospheric circulation. Topography influences temperature and precipitation distribution, and in the Colombian Andes, for example, the three mountain ranges with their steep orography and numerous valleys can generate microclimates and the presence of different ecosystems. In addition, solar exposure and humidity can vary according to the relief orientation (Espinoza et al., 2020; Poveda et al., 2011, 2020). However, mountains with snow-capped peaks have been affected by the gradual increase in temperature over the years, which has caused a decrease in snow cover on snow-capped cliffs, the migration of species to different altitudes, and the loss of ecosystems.

In this study, we investigate extreme precipitation and temperature events in the Colombian Andes during events of ENSO and neutral years. In Chapter 2 and Chapter 3, the aim is to characterize and compare daily extreme precipitation and temperature events during ENSO and neutral years. While it has been established that ENSO modifies average precipitation and mean temperature (resulting in increased (decreased) rainfall during La Niña (El Niño) (Poveda et al., 2011), we seek to analyze whether there are discernible differences in the intensity and occurrence of extreme precipitation and temperature events within each ENSO phase. Finally, in Chapter 4, we conduct an exploratory analysis comparing the effects of selected atmospheric variables during a month identified as highly active in extreme precipitation events within an extreme La Niña event. We compare the fields of that specific period with a composite of the same month from La Niña, El Niño, and neutral years. The primary objective of this chapter is to identify whether the pattern of hydroclimatic variables changes between a singular event and the composite and whether the underlying mechanisms are consistent over time or unique to an event occurring during the active phase

of ENSO.

2. Characterization and comparison of extreme precipitation events

Abstract

The research on extreme precipitation events (EPEs) in the Colombian Andes is relevant due to the uncertainty associated with their social, economic, and environmental impact. Although the intensity and frequency of EPEs have changed due to environmental changes, it is necessary to deepen the understanding of EPEs when El Niño Southern Oscillation (ENSO) is active. In this sense, this study aimed to characterize extreme precipitation events in intensity and frequency. The 95th and 99th percentile definition was used to find a threshold using TRMM and CHIRPS station databases. Our results reveal that the events do not present differences in the magnitude of intensity between La Niña, El Niño, and neutral years. However, during La Niña, the occurrence of events is higher. Additionally, regions with homogeneous daily intensity events were found by clustering analysis, which may be associated with phenomena on other spatial and temporal scales that act throughout the region, moisture input, similar characteristics in the atmosphere, or a combination of these. On the other hand, the results between the databases were congruent for analyzing the events by intensity. However, there were discrepancies in the frequency, mainly with CHIRPS, which identified an important number of EPEs in June-July-August.

Keywords

Extreme Precipitation Events (EPEs), El Niño-Southern Oscillation (ENSO); Andes; intensity; frequency; Cluster analysis.

2.1. Methodology

2.1.1 Extreme precipitation and temperature definition

The diversity of climatic conditions and spatial-temporal phenomena globally poses a challenge in defining extreme precipitation globally. There are no apparent differences between methods for studying EPEs according to large-scale meteorological patterns and extreme events related to teleconnections such as ENSO. Methodologies are generally designed ac-

cording to the research question; some may be based on the spatial variations of the EPEs or the response of a circulation pattern (Grotjahn et al., 2016; Barlow et al., 2019). .

Three distinct approaches for defining extreme events have been used in the context of EPEs. These approaches include compositing based on the events, pattern-based analysis of circulation or thermodynamic fields during these events, and case studies (Grotjahn et al., 2016).

In this sense, the appropriate definition of extremes and the associated questions heavily depend on the chosen metrics, as well as the spatial and temporal scales. The use of metric measures involves determining a threshold magnitude, for example, top 1%, values greater than 5 cm, and period return. The choice of spatial scale typically depends on the region under study and considerations such as station-based, grid box, area average, and the extent of contiguous rain area. In contrast, the temporal scale choice examines events' intensity, duration, and frequency concerning accumulation over hours, days, or the whole event (Barlow et al., 2019). Disagreement on the definitions used can complicate the conclusions drawn from the study. Moreover, it is essential to consider different hazard triggers, e.g., flash flooding, agricultural damage, water management, etc.

In recent years, the extreme precipitation indices proposed by ETCCDI under the auspices of the World Meteorological Organization's CLIVAR program (Tank et al., 2009) have been widely used in the study of extreme events in climate change and natural variability worldwide, including South America (Ávila et al., 2019; Cerón et al., 2022; Rodríguez et al., 2019). These indices aim to provide homogeneous measurements that can be used in any climate and regional setting.

Conservely, researchers in the northern region of South America have consistently used the extreme value theory, while others consider a Generalized Pareto Distribution (GPD) (Hoyos et al., 2013b). The advantage of the GPD method is that it allows for multiple thresholds to be obtained rather than a single value, which helps to infer the statistical properties of the tail distribution. Another less common method is the use of gamma distribution to calculate percentile from daily values.

Investigations into extreme events span a wide range of factors, encompassing metrics, as well as spatial and temporal scales. These elements significantly shape the characterization and definition of what qualifies as an extreme event. However, the choice of these aspects depends on the specific research interest, and in the case of South American regional researchers, the preferred definition may vary. A critical consideration when selecting a measure of extreme values is how to appropriately compare extreme events, accounting for the influence of patterns at various spatial scales and whether the focus is on short-lived or climatological-scale events (Hellström, 2005). For instance, selecting an appropriate threshold value should adequately represent the tail distribution of the data, considering the sample size and the limitations of the threshold. Furthermore, whether the threshold includes all

days or just wet days can significantly impact the conclusions drawn from the results. In this sense, each extreme definition responds to specific questions involving spatial, temporal, or both analyses, such as comparing different periods (trend analysis) or several regions.

In this study, we characterized spatial and temporal EPE. In the following, we defined extreme events as those falling within the 95th and 99th percentiles without considering zero daily rainfall values. Using the 95th and 99th percentile thresholds provides a means to examine the extremities of the precipitation series within a particular location. Moreover, this approach will ensure its practicality across varying climatic regions. It recognizes the impracticality of imposing a uniform threshold in areas characterized by distinct precipitation variabilities. By tailoring thresholds to the 95th and 99th percentiles, we enhance our analysis's precision, accounting for each location's unique characteristics and fostering a more comprehensive understanding of extreme weather patterns. Deciding on the temporal resolution of the data is critical in studying extreme events. Some authors consider that using sub-daily information can better describe the intensity and frequency of events, while daily data can hide it. However, limited sub-daily databases are available in the Colombian Andes region, making daily data the most accessible source. Additionally, observations from satellite data may be necessary to supplement the available information (Barlow et al., 2019; Grotjahn et al., 2016; Beck et al., 2015).

2.1.2 Data

To understand the relationship between synoptic phenomena, precipitation, and extreme temperatures, it is essential to have access to in-situ data for the region of interest. To this end, the station information was supplied by Instituto de Hidrología, Meteorología y Estudios Ambientales (IDEAM) of Colombia. Specifically, data with a daily temporal resolution from 100 stations located in the Andes region of Colombia was acquired. The period of record for each station is provided in Table **B-1**.

We employed the Tropical Rainfall Measuring Mission (TRMM-3B42-V7) Multi-satellite Precipitation Analysis (TMPA) product to identify extreme daily precipitation. This mission, which monitors rainfall in tropical regions, is a joint endeavor of the National Aeronautics and Space Administration (NASA) and the Japan Aerospace Exploration Agency (JAXA) (Huffman et al., 2010). The TRMM data has a spatial resolution of 0.25° and is available at `https://gpm.nasa.gov/data/directory`. Although the original temporal resolution is 3 hours, the data can be aggregated to provide daily information.

TRMM data have been extensively used in the region of interest (Palomino-Ángel et al., 2018; Condom et al., 2020), and its performance has also been evaluated in conjunction with the new Global Precipitation Measurement – GPM mission for daily precipitation in high altitudes regions in northeast South America. They found that TRMM can capture the spa-

tial and temporal distribution of mean daily rainfall. Nonetheless, it tends to underestimate the precipitation over high altitudes of the Andes Mountains range, and overestimates its values in medium to low altitudes. Other studies used TRMM for precipitation anomalies analysis (Arias et al., 2015; Salas et al., 2020) and model validation (Posada-Marín et al., 2019).

The extreme precipitation events were also characterized using the Climate Hazard Group Infrared Precipitation with Station Data – CHIRPS (Funk et al., 2015). Specifically, our study used daily precipitation data from CHIRPS, which has a spatial resolution of 0.05°. This dataset was developed by the Earth Resources Observation and Science Center of the U.S. Geological Survey and the Climate Risk Group of the University of California, Santa Barbara. CHRIPS historical record spans from 1981 to the present, providing daily, monthly, annual, and pentad temporal resolutions. Rainfall is estimated from satellite images and station data *in situ*, and the daily resolution is available at 0.05° (5km) and 0.25° (28km), the database has been validated in Colombia by Funk et al. (2015) and Urrea et al. (2019). Previous studies in the Argentinean Andes found that CHIRPS can capture some precipitation characteristics. However, it overestimates the values in cold periods, which may be associated with poor representation in reproducing precipitation characteristics above 1000 m above sea level (Rivera et al., 2018).

2.1.3 Characterization and comparison

This study aims to characterize EPTE in the active phases of ENSO. The intensities found are those that exceed the threshold given by the percentile, and the frequencies are zero and one values that indicate whether or not the condition is met. This methodology is commonly used and employed in the percentile-based ETCCDI indices (Borges et al., 2018; Kim et al., 2020; Peng et al., 2018; Tencer et al., 2016; Meseguer-Ruiz et al., 2018; Ávila et al., 2019; Rodríguez et al., 2019; Banauthor et al., 2015). To classify ENSO events we used the Oceanic Niño Index (ONI) (`https://origin.cpc.ncep.noaa.gov/products/analysis_monitoring/ensostuff/ONI_v5.php`) to classify LN, EN, and neutral year events. Based on the ONI index, we estimated two types of composites using the intensity and frequency of EPTE during LN, EN, and neutral years. The first composite consisted of seasonal data, while the second composite included all events. To track the evolution of EPE month by month and for each year, we created heatmaps for the entire Andes. On the other hand, the differences between ENSO and neutral years, as well as LN and EN years were calculated to determine during which events the extremes increase or decrease. Finally, the parametric t-test was used to assess the significance of the differences.

Our goal was to investigate whether extreme daily precipitation events are more frequent and intense during an ENSO phase than under normal conditions. Based on the daily distributions of the extreme values of precipitation and temperature (i.e., histograms), a

comparison was made between EN and LN concerning the neutral years. The Mann – Whitney U-test was applied to measure if the medians were statistically significant. This non – non-parametric test is more suitable for this type of data because it does not require a normality assumption. Comparison between the ENSO phases and neutral years are performed with a 5% significance level.

2.1.4 Cluster analysis

The Andes region is characterized by a high spatial precipitation variability due to the presence of the mountain range division. To better understand the spatial behavior of EPEs, we performed a clustering analysis that groups pixels based on their similarity in intensity. Specifically, we used the agglomerative K-means method (Steinley, 2006) along with Ward's method for optimal process classification (Ward, 1963). This procedure aims to minimize within-cluster variance, without defining a specific distance between clusters. Ward's method, which is based on the error sum of a square, has the advantage of maximizing the homogeneity within each group. Therefore, it has been used in literature to identify homogeneous regions based on their climatic conditions (Carvalho et al., 2016; Wang et al., 2022b; Firat et al., 2012). To apply the clustering procedure, we used daily precipitation extreme series. In addition to the clustering analysis, we also created histograms for both ENSO periods and neutral years for each region identified by the cluster. This allowed us to compare the distribution of precipitation extremes across different regions.

2.2. Results and discussion

2.2.1 Rainfall Annual cycle

Figure **2-1** illustrates the annual precipitation cycle in the Colombian Andes according to data provided by TRMM, CHIRPS, and IDEAM. The figure highlights two essential points regarding the behavior of the entire Andes region: capturing patterns and performance. TRMM and CHIRPS effectively capture the bimodal precipitation pattern observed in the IDEAM stations. Moreover, the performance of the three datasets differs in terms of amplitude. The mean values of all stations indicate that the satellite database overestimates rainfall in the entire Andes region. Moreover, TRMM shows better consistency than CHIRPS.

The Andean Region experiences its highest precipitation levels during two distinct periods: December - January - February and September - October - November. Due to that patterns are largely influenced by the Intertropical Convergence Zone (ITCZ), which plays a crucial role in modulating rainfall in the Andes. The ITZC moves latitudinally, following

the apparent displacement of the sun with respect to the Earth. The double passage of the ITCZ generates a bimodal cycle in the region (as seen in Figure **2-1**). The ITCZ is displaced southward in October and November, reaching its maximum southern displacement during January. This shift results in the second wet season and the beginning of the first dry season over the Andes. Then, during April and May, the ZCIT is displaced northward, with its maximum northern displacement occurring in July. This results in wet first and dry second seasons (Leon et al., 2000; Poveda, 2004).

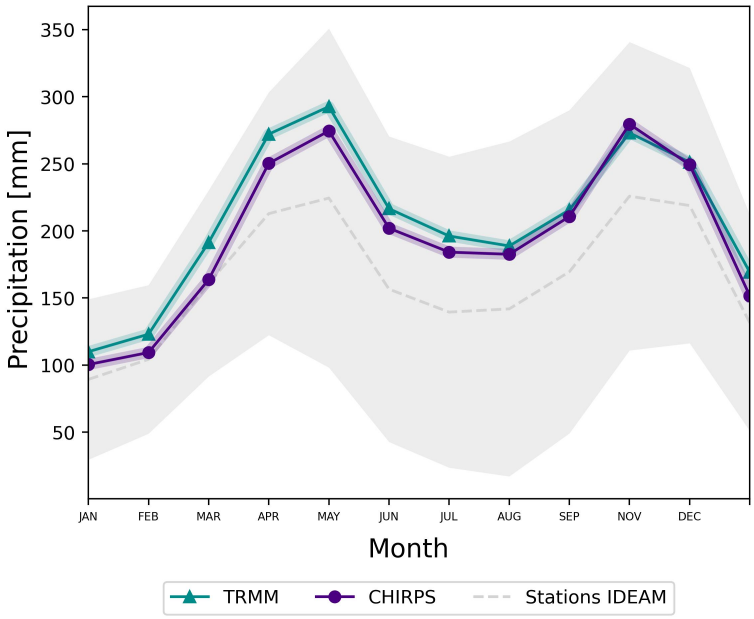

Figure **2-1**.: Annual rainfall cycle for the Andes of Colombia comparing average spatial data from TRMM and CHIRPS satellite sources with mean measurements from IDEAM stations. Gray shaded band corresponds to the range of variation across IDEAM stations.

In contrast to in-situ databases, TRMM tends to overestimate precipitation values between January and September, whereas CHIRPS shows better agreement during this period. However, TRMM and CHIRPS tend to overestimate precipitation magnitudes in the Andes region compared to rain gauges. TRMM and CHIRPS exhibit similar performance in estimating precipitation values from September to December.

The amount of rainfall can vary widely within the Andes due to differences in altitude and the presence of mountain systems. For example, in the high-altitude of the Andes, precipitation is lower; meanwhile, in lower elevations, it is mainly influenced by warm and humid winds coming from the Pacific Ocean (Poveda et al., 2005, 2011). However, other phenomena at different spatial and temporal scales, and the interaction between topography and vegetation, can also modify the rainfall pattern (Espinoza et al., 2020; Poveda, 2004; Poveda et al., 2005; Urrea et al., 2019).

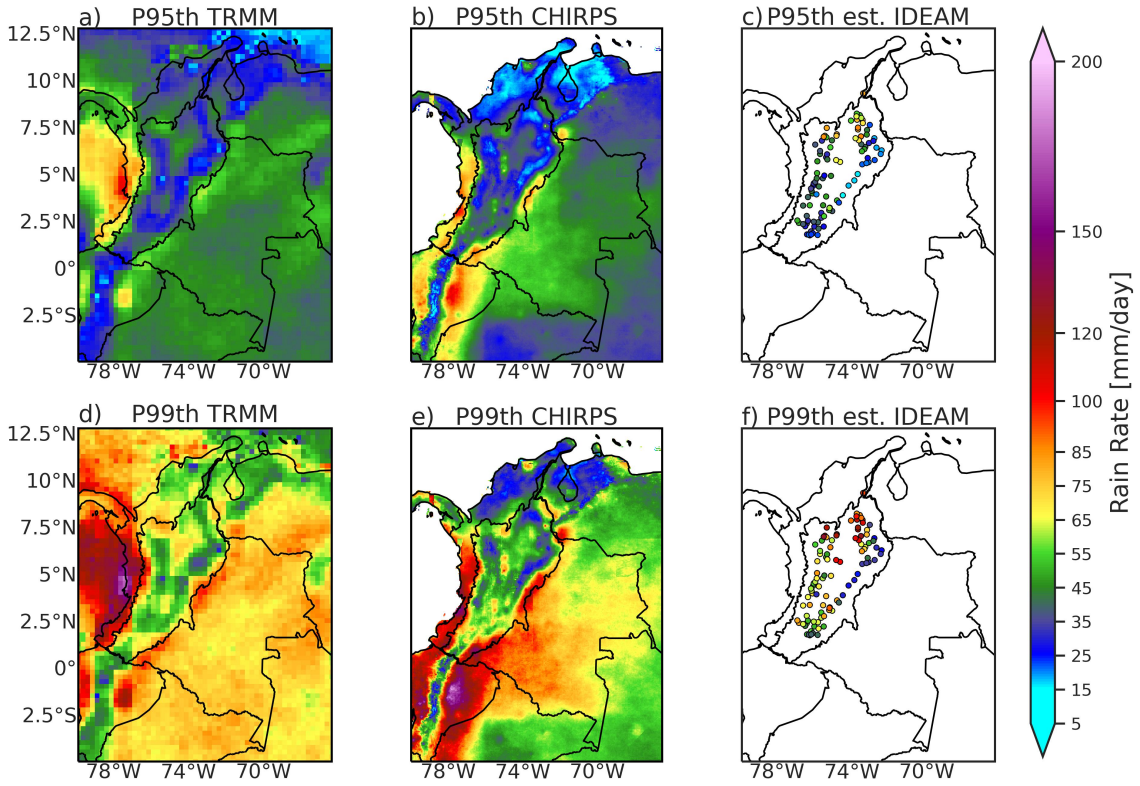

Figure **2-2**.: The threshold value for characterized extreme and heavy precipitation, a) 95th TRMM, b) 95th CHIRPS, c) 95th rain gauge IDEAM, d) 99th TRMM, e) 99th CHIRPS, and f) 99th rain gauge IDEAM.

2.2.2 Characterization of EPE

Climate variability in different regions makes establishing standard definitions of extreme events difficult. This study used a threshold based on a percentile to determine extreme and heavy precipitation events. To prevent skewing of extreme values due to regional climatic variations, a unique value was determined for each pixel in the case of satellite observations, and a threshold was established for each station. The threshold based on percentiles 95th and 99th for classifying extreme and very extreme events presents high spatial variability in the territory. Values between 45 and 100 mm/day are observed in the Inter-Andean valleys and their surroundings in the Pacific coast region and the Colombian eastern plains, regions of low altitudes. The Pacific region of Colombia is known for having high precipitation magnitudes during the wettest periods of the year and is considered the rainiest region of the world; therefore, it is expected to show high values in the thresholds (Poveda and Mesa,

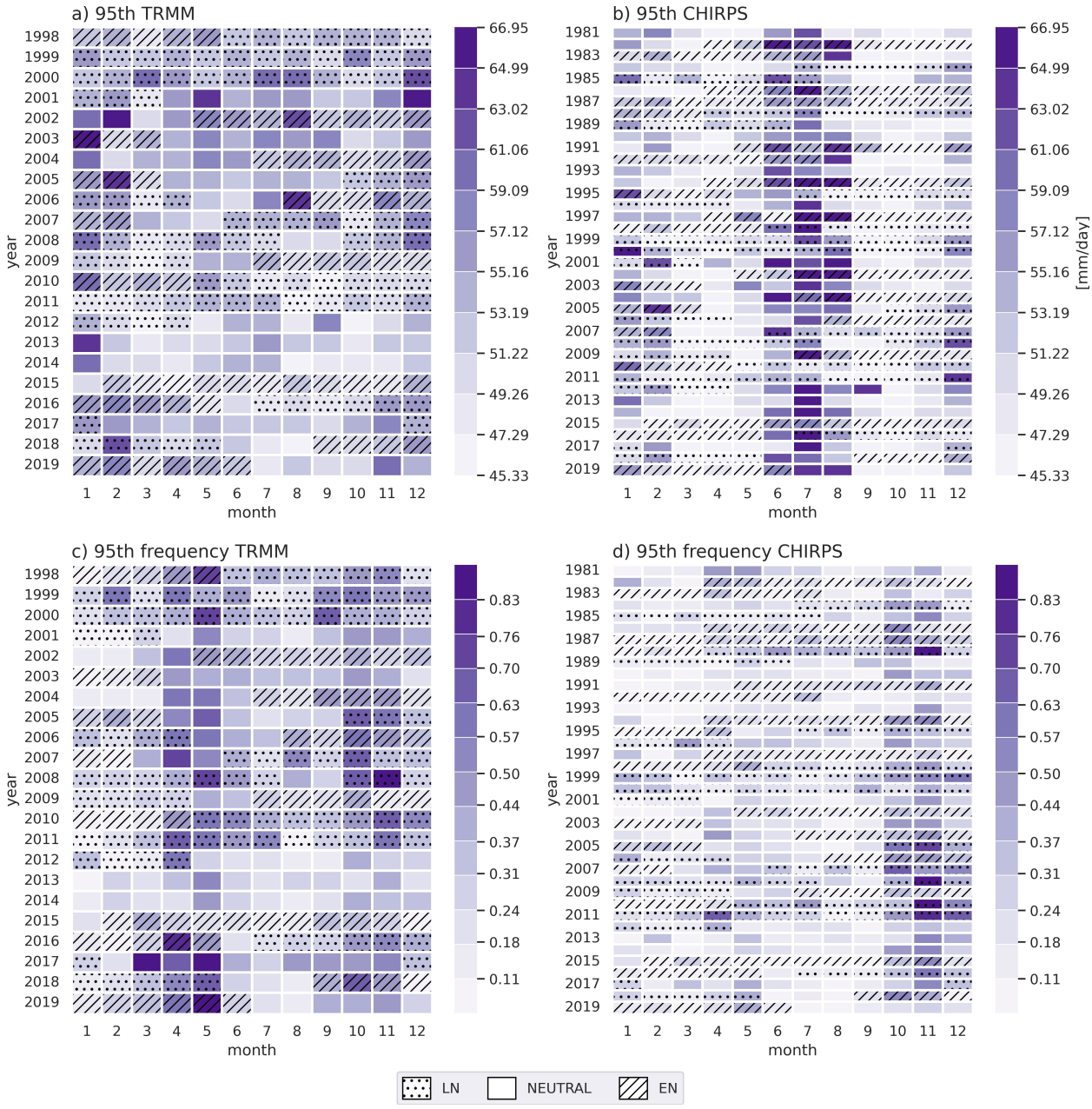

Figure **2-3**.: Heatmaps of extreme precipitation events for percentiles 99th , based on TRMM (1998-2019) and CHIRPS (1981-2019) data sets. a) Intensity events percentile 99th TRMM, b) Intensity events percentile 99th CHIRPS, c) frequency events percentile 99th TRMM and d) frequency events percentile 99th CHIRPS.

2000).

The spatial patterns are similar in the three databases, but their magnitudes differ, higher magnitude is observed at the 95th and 99th percentile in the northern region in the rain

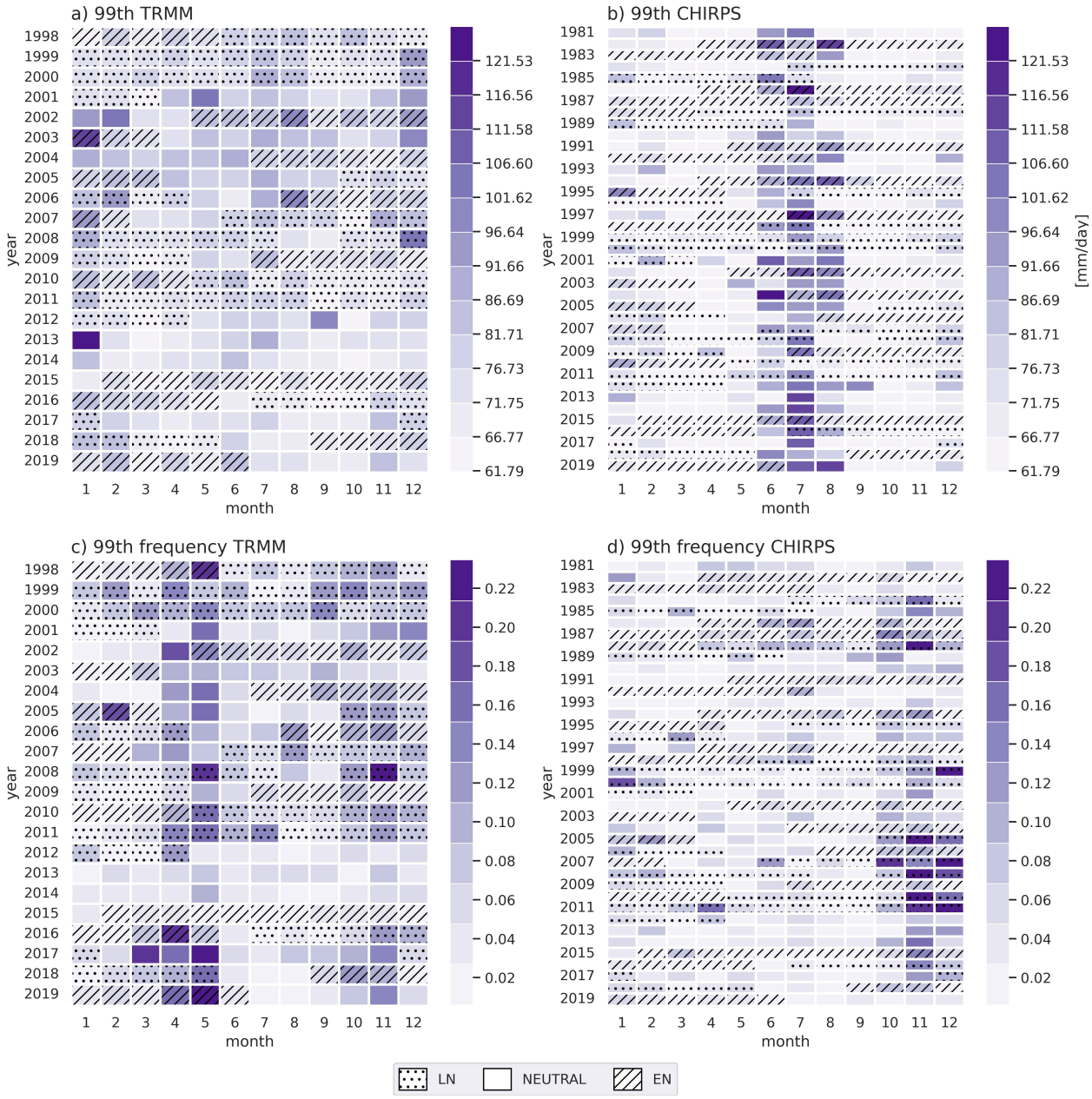

Figure **2-4**.: Heatmaps of extreme precipitation events for percentiles 95th and 99th across IDEAM station(1991–2019). a) Intensity events percentile 95th, b) Intensity events percentile 99th h, c) frequency events percentile 95th and d) frequency events percentile 99th.

gauges (Figures **2-2** c and f). However, in the satellite databases, the magnitudes may be lower, leading to an underestimation of extreme precipitation in the high mountains. As mentioned above, it has been found that the TRMM 3B43 V7 product does not adequately capture the amplitude of rain at high altitudes, which is usually underestimated. As a result,

it tends to show underestimates in the inter-Andean valleys (Vallejo-Bernal et al., 2021). On the other hand, CHIRPS shows spatial similarities with TRMM, but the magnitude values are generally larger in the center Andes. When comparing satellite databases, researchers tend to focus on evaluating mean values, where similar patterns have often been found

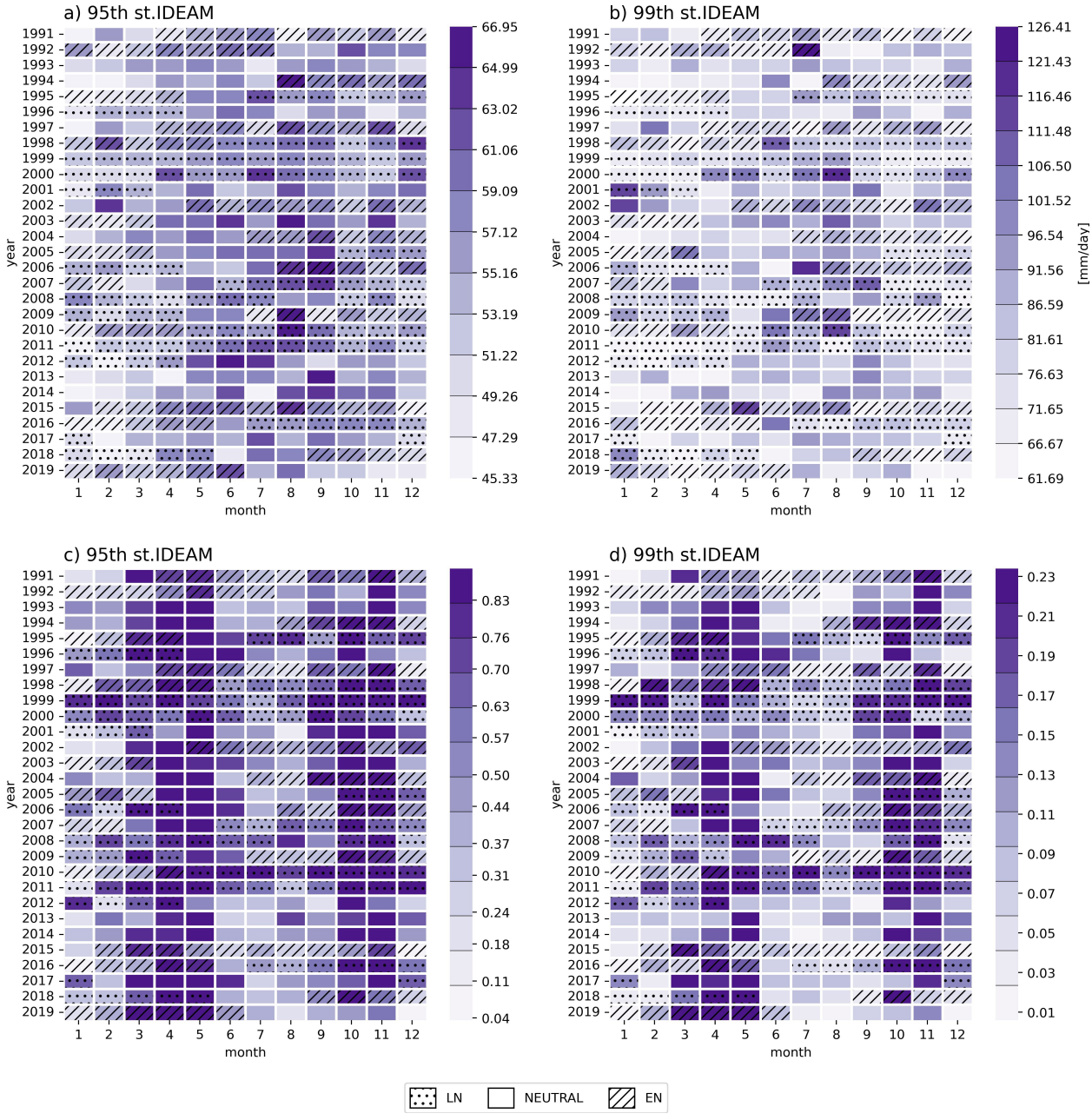

Figure **2-5**.: Heatmaps of extreme precipitation events for percentiles 95th and 99th in stations IDEAM, between 1991–2019, a) Intensity events percentile 95th, b) Intensity events percentile 99th, c) frequency events percentile 95th and d) frequency events percentile 99th.

with data from ground-based rain gauges. However, satellite database algorithms can have problems capturing extreme values because they cannot adequately represent the formation of the convective system (Salio et al., 2015). For example, Araujo et al. (2020) found that CHIRPS tends to underestimate precipitation extremes at the 99th percentile, while for TRMM the bias is more negligible than for CHIRPS.

Over the Andean Region, precipitation at the interannual time scale is mainly modulated by the ENSO phenomenon, in which rainfall amplitude changes have been observed. Understanding the frequency and intensity of extreme precipitation events during El Niño-Southern Oscillation (ENSO) events compared to neutral years is crucial, particularly in the Andes region where Colombia's population and economic activities are concentrated. Although observing the spatial pattern of precipitation extremes is essential, a temporal analysis allows us to understand the magnitude of intensities and frequency of rainfall extremes during active ENSO phases (Figures **2-3**, **2-4**, and **2-5**). The LN, EN, and neutral years do not differ in the magnitude of intensity and frequency, i.e., in all three situations, very intense and extreme high-frequency events can occur. However, it can be observed in extreme ENSO events; for example, the 2010-2011 and 2011-2012 LN events presented extreme values in both percentiles high in intensity and frequency (Arias et al., 2015). Conversely, during periods of generally high precipitation, the impact of EN led to a decrease in rainfall, as evidenced in the 2015-2016 EN event (Figures **2-3**, **2-4**, and **2-5**).

Significant differences in the intensities and frequencies of extreme events are observed among the TRMM, CHIRPS, and station data. The most notable differences are evident in the intensity magnitudes for 95th percentile during November – December - January - February for both TRMM and stations data, and June - July - August in CHIRPS data (Figures **2-3**a, **2-3**b, and **2-5**a). The highest frequencies across data sources are found during April - May and October – November in the 95th percentile (Figures **2-3**c, **2-3**d, and **2-5**c). For the 99th percentile, TRMM and station data show that November-February has the most intense events, while CHIRPS data reveals the same intense months as in the 95th percentile (Figures **2-4**a, **2-4**b, and **2-5**b). The occurrence of events was higher in the same months as in the 99th percentile for TRMM and CHIRPS (Figures **2-4**c, **2-4**d, and **2-5**d).

The Andes experience two distinct wet seasons: one in March-April-May and another in September-October-November. During the LN event, the wet season tends to last longer and increases rainfall, while the EN event leads to decreased rainfall. However, when examining the heatmaps of the 95th and 99th percentiles (Figures **2-3**, **2-4**, and **2-5**), there is no significant seasonality in intensity. On the other hand, in terms of frequency, an increase in precipitation does not necessarily imply an increase in EPE intensities. Instead, it may simply facilitate their occurrence. Even then, the results of the intensities of extreme precipitation events presented by CHIRPS differ from those of TRMM and the stations. Notably, both percentiles exhibit precipitation seasonality, particularly in June-July and August. To validate the data, we created histograms of extreme event series for June, July, and August,

up to the 95th and 99th percentiles (not shown). There we found that the distribution of the event data of CHIRPS is slightly skewed to the right compared to TRMM and the stations (not shown). This indicates that the magnitudes are higher and may be associated with problems of the database algorithm to represent the extremes adequately.

The intensity and average frequency of extreme daily precipitation events are characterized spatially for LN, EN, and neutral years in the seasons of December - January - February (DJF), March - April - May (MAM), June - July - August (JJA), and September - October - November (SON). Furthermore, after performing a month-by-month analysis (not shown), the convenience of analyzing the information by season will enable us to observe the transition of the intensity and frequency of events. The results are also presented in a way that highlights the difference in extremes during LN, EN, and neutral years.

DJF

During the DJF period, the highest magnitudes for extreme daily events in the 95th percentile are found along the ocean and Pacific coast. Higher magnitudes are seen at the lower altitudes in the Andes, while lower values occur at high elevations (Figure **2-6** a, b, c, d, e, f, g, h, i). This distribution resembles the pattern shown in Figures **2-2**a and **2-2**b. During episodes of LN, EN, and neutral years, the intensities of the events show no notable differences.

For this season, no extreme events have been recorded in the northeastern region of the study area and the Caribbean. CHIRPS agrees with the results presented by TRMM, in northeastern South America. The absence of events may be associated with the dry season from November to February in the Orinoco affecting the low-level jet and inhibiting the transport of moisture into the continent's interior. On the other hand, CHIRPS shows lower intensity values in the north of Colombia and the high mountains of the Andes.

The results from the rain gauges reveal a pattern of lower extreme values east of the Andes, intermediate values to the west, and higher values in the central northern region of the Magdalena-Cauca basin (Figure **2-6** c, f, i). These results are similar during both ENSO phases and neutral years. Additionally, both CHIRPS and TRMM datasets exhibited a similar pattern to the one shown by the rain gauges.

The 99th percentile represents heavy precipitation events, exhibiting greater magnitudes of intensity than those shown in the 95th percentile (Figure **2-6** j, k, l, m, n, o, p, q, r). The spatial pattern for this season closely resembles the one observed for the 95th percentile.

Notably, there is a region with more considerable spatial extension without extreme events during EN events compared to neutral years. However, in both TRMM and CHIRPS, the most extreme precipitation events stand out on the Pacific coast, especially in the study area's southwestern region near Ecuador during LN episodes. Additionally, in CHIRPS, it

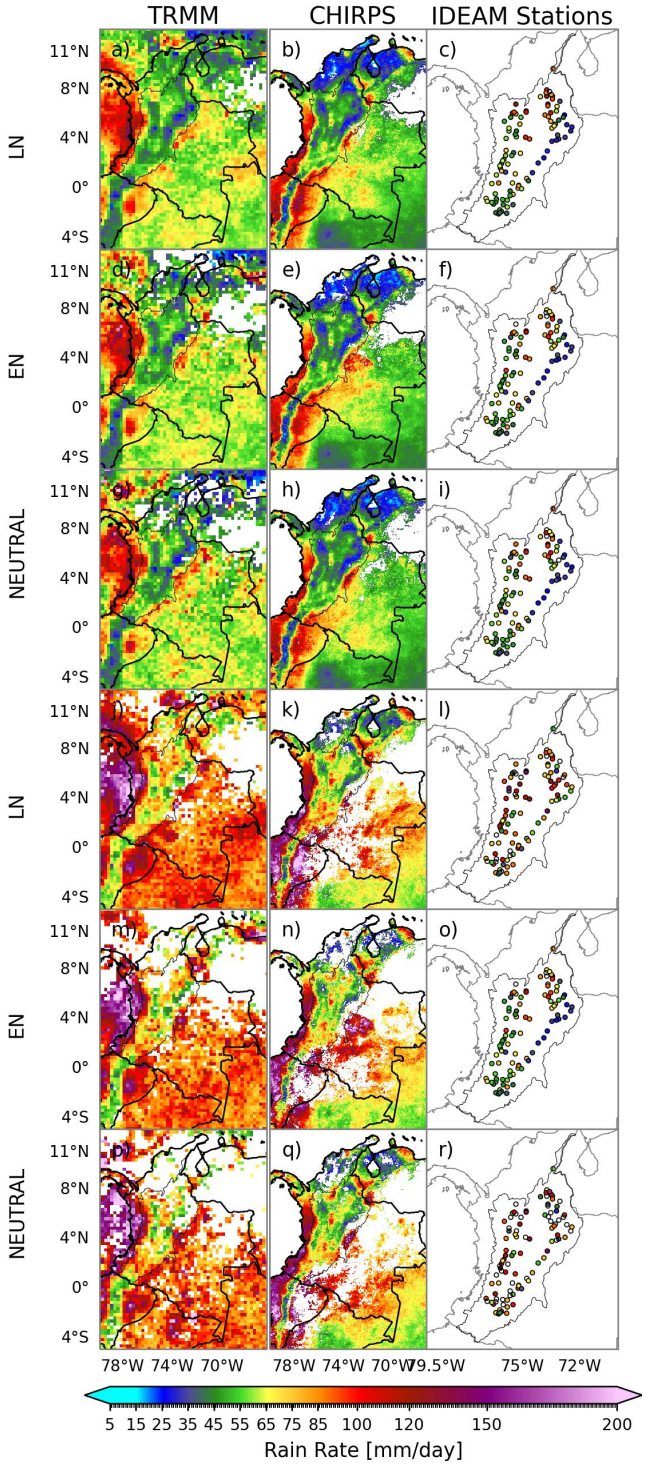

Figure **2-6**.: Characterization of extreme precipitation events, categorized by the intensity at the 95th (top three rows) and 99th percentiles (bottom three rows), during DJF. Data is sourced from TRMM at the 95th (a, d, g) and 99th percentiles (j, m, p), CHIRPS at the 95th (b, e, h) and 99th percentiles (k, n, q), and IDEAM stations at the 95th (c, f, i) and 99th percentiles (l, o, r). The labels in each row signify the phases of the ENSO, encapsulating LN years, EN years, and neutral years. Regions shaded in white denote the absence of extreme events during the respective season.

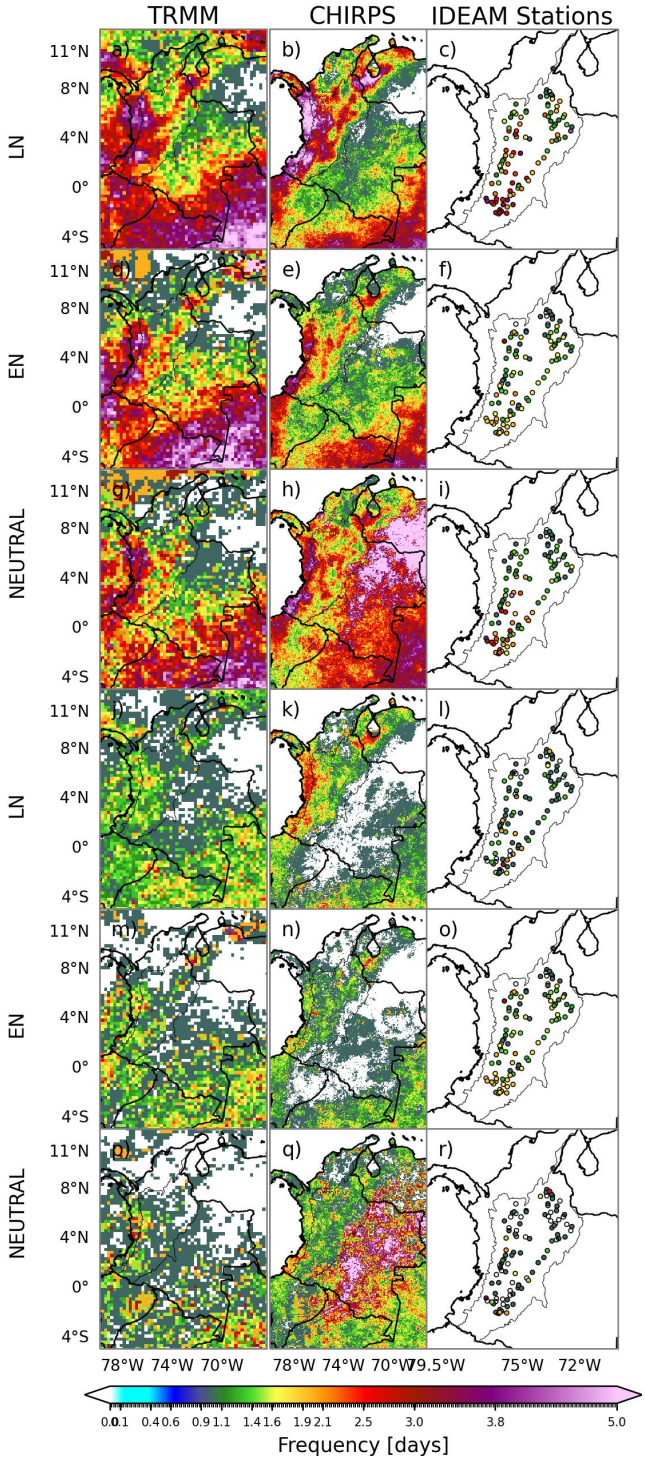

Figure **2-7**.: Characterization of extreme precipitation events, categorized by the frequency at the 95th (top three rows) and 99th percentiles (bottom three rows), during DJF. Data is sourced from TRMM at the 95th (a, d, g) and 99th percentiles (j, m, p), CHIRPS at the 95th (b, e, h) and 99th percentiles (k, n, q), and IDEAM stations at the 95th (c, f, i) and 99th percentiles (l, o, r). The labels in each row signify the phases of the ENSO, encapsulating LN years, EN years, and neutral years. Regions shaded in white denote the absence of extreme events during the respective season.

is observed that during LN, there are higher values of precipitation intensity in the Andes compared to EN and neutral years.

On the other hand, in TRMM, lower extreme precipitation values are observed in the high mountains, but they are still slightly higher compared to CHIRPS. Additionally, in the rain gauge stations, as in the 95th percentile, there are lower magnitude values in the east of the Andes, intermediate values in the west, and high values in the north. In summary, the results of the satellite databases consistently align with the rain gauge measurements.

The results of the 95th percentile frequency in TRMM and CHIRPS have a pattern within precipitation seasonality. During the austral summer in TRMM, a very marked pattern is observed in the frequency of events along the Pacific coast, south of the Andean region, and the southern part of the territory, averaging 3 to 5 events per quarter. Conversely, the lowest occurrence of events occurs north of the Andes, on the Caribbean coast, and eastern portion of the territory (Figure **2-7** a, b, c, d, e, f, g, h, i). CHIRPS also shows a similar pattern, with high values in the north and west of the Andes and along the Pacific coast, while the lowest frequency is found on the Caribbean coast and in the eastern region (Figure **2-7**). Events during LN are more prominent in the Andes than during EN and neutral years. In the 99th percentile, TRMM and CHIRPS exhibit fewer events and comparable spatial patterns (Figure **2-7** j, k, l, m, n, o, p, q, r).

The rain gauges in the south-central Andes exhibit the highest occurrence, as evidenced by the 95th percentile data shown in Figure **2-7** c, f, and i. At the same time, lower frequencies are observed in the eastern and northern regions of the Andes. Conversely, the 99th percentile indicates lower values across the rain gauges, with some stations in the east and north of the Andes not recording any events and a few others to the south registering marginally higher values (Figure **2-7** l, o, r).

MAM

The spatial pattern observed in the MAM season remains consistent with that found in the DJF season, with the most significant difference being the absence of extreme events in certain Caribbean regions during EN (Figure **2-8** a, b, c, d, e, f, g, h, i). However, even at the 99th percentile, the Caribbean experiences no extreme precipitation events, mainly during EN events and neutral years in TRMM (Figure **2-8** j, m, o). CHIRPS highlights high-intensity values in the Andes during LN, with magnitudes around 200 mm/day near Ecuador's territory (Figure **2-8** k, n, q). The stations display significant differences in intensity magnitude between ENSO and neutral years, but high values are observed to the north and south, moderate values to the west, and low values to the east of the Andes (Figure **2-8** l, o, r).

During this season, the occurrence of events in the 95th percentile is prominent in TRMM.

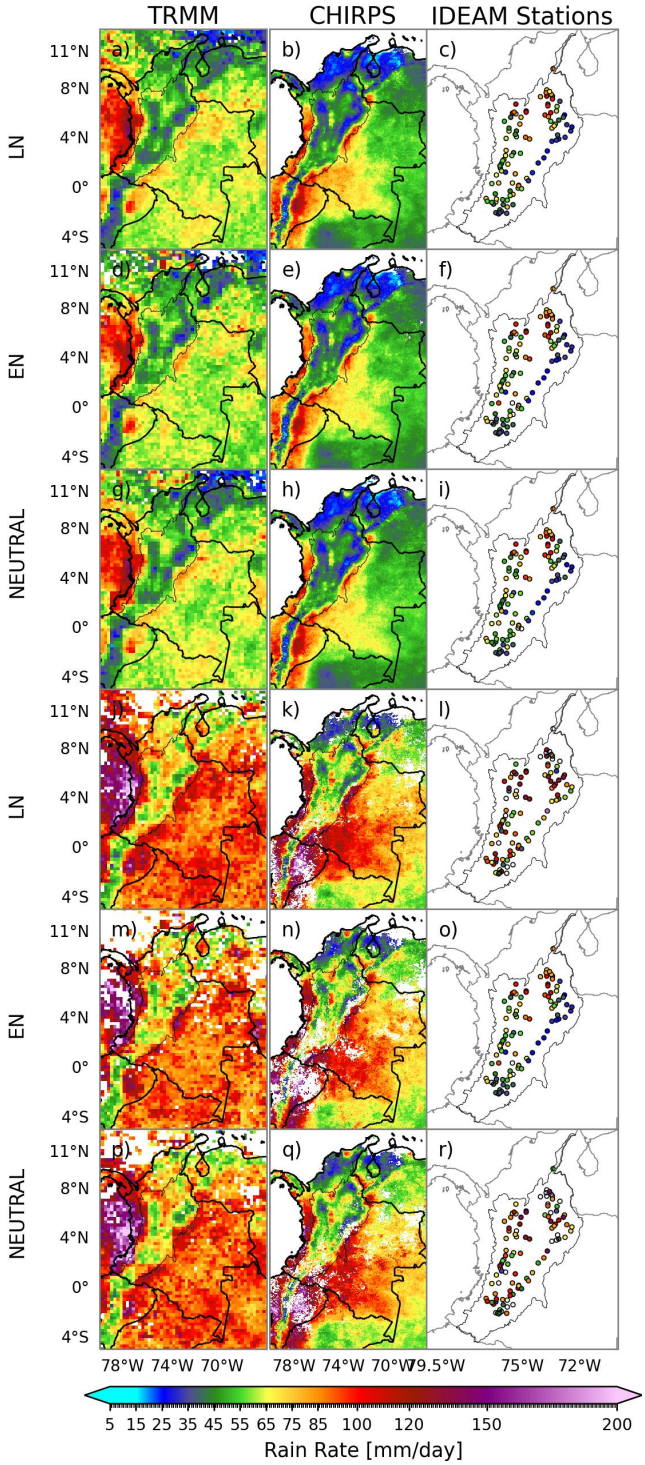

Figure **2-8**.: Characterization of extreme precipitation events, categorized by the intensity at the 95th (top three rows) and 99th percentiles (bottom three rows), during MAM. Data is sourced from TRMM at the 95th (a, d, g) and 99th percentiles (j, m, p), CHIRPS at the 95th (b, e, h) and 99th percentiles (k, n, q), and IDEAM stations at the 95th (c, f, i) and 99th percentiles (l, o, r). The labels in each row signify the phases of the ENSO, encapsulating LN years, EN years, and neutral years. Regions shaded in white denote the absence of extreme events during the respective season.

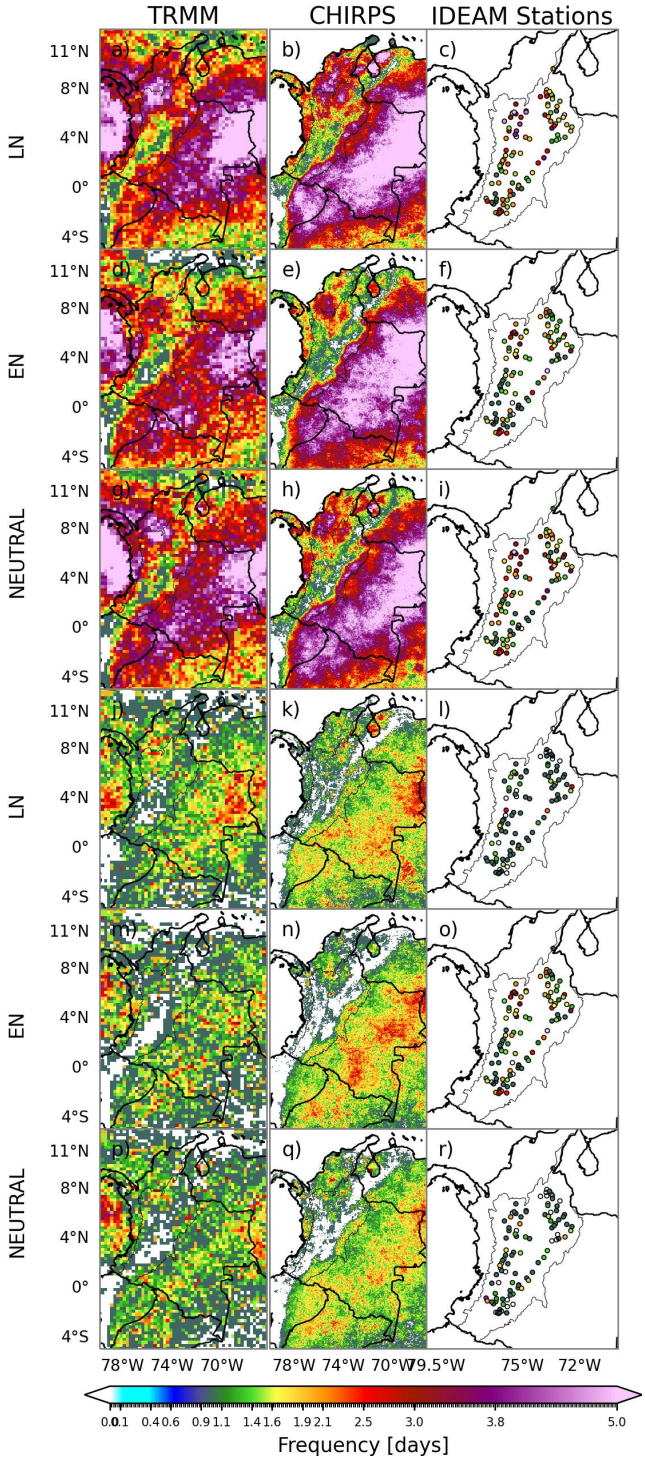

Figure **2-9**.: Characterization of extreme precipitation events, categorized by the frequency at the 95th (top three rows) and 99th percentiles (bottom three rows), during MAM. Data is sourced from TRMM at the 95th (a, d, g) and 99th percentiles (j, m, p), CHIRPS at the 95th (b, e, h) and 99th percentiles (k, n, q), and IDEAM stations at the 95th (c, f, i) and 99th percentiles (l, o, r). The labels in each row signify the phases of the ENSO, encapsulating LN years, EN years, and neutral years. Regions shaded in white denote the absence of extreme events during the respective season.

The highest values are along the Andes, with an average of 2.5 and 5 events, while the lowest frequencies are concentrated in the Caribbean and Pacific Oceans (Figure **2-9** a, d, g). CHIRPS exhibits a similar pattern to that described by TRMM but with slightly lower values, and the highest values in the Andes are concentrated in the center-north (Figure **2-9** b, e, h). The satellite databases agree with the stations' results, identifying the northern Andes as the area with the highest occurrence of events. No differences between ENSO and neutral years events are observed in the satellite databases. However, stations indicate marginally higher values during LN (Figure **2-9** c, f, i).

The frequency at the 99th percentile in TRMM shows that areas with outstanding values are located in the center-north of the Andean region and southern Colombia (Figure **2-9** j, m, p). This behavior is similar to the results given by CHIRPS, locating the values further south than TRMM, and in the stations to the east of the Andes, where most stations do not present events (Figure **2-9** k, n, q, i, o, r).

JJA

During the boreal summer, the intensities pattern at the 95th percentile does not show significant changes in the Colombian Andes compared to previous months. Some areas in the Caribbean Sea and Ecuador do not record events during EN and neutral years in TRMM (Figure **2-10** a, d, g). While the CHIRPS dataset shows no substantial differences in event magnitudes between ENSO events and neutral years, it does indicate that several Andean areas do not register events during EN and neutral years, as illustrated in Figure **2-10** b, e, and h. This pattern is inconsistent with the rain gauges, where all stations recorded events in this percentile and season (Figure **2-10** c, f, i). Figure **2-10** j, m, and p, highlights the absence of records of events in the 99th percentile in the south of the Andes during EN and neutral years in TRMM, while in CHIRPS is observed during LN events (Figure **2-10** k, n, q).

Another notable observation is the values approaching 200 mm/day between the Andes mountain range in Ecuador and southern Colombia at the 99th percentile in CHIRPS, shown in Figure **2-10** k, n, and q. Similar to the MAM season, the JJA season exhibits the highest records in rain gauges to the west and center of the Andes, while the eastern regions continue to display the lowest intensity levels, as demonstrated in Figure **2-10** l, o, and r.

TRMM and CHIRPS data show a distinctive pattern in the frequency values at the 95th percentile during JJA for LN, EN, and neutral year, with high extreme precipitation events occurring throughout almost the entire Andes region (Figure **2-11** a, d, g and Figure **2-11** b, e, h). However, notable differences exist between the TRMM and CHIRPS datasets. TRMM registers the highest precipitation records along the coast and the Pacific Ocean. while CHIRPS exhibits the highest frequencies in the eastern plains, north of the Andes, on the Caribbean coast, at the border of the eastern cordillera, and eastward across the

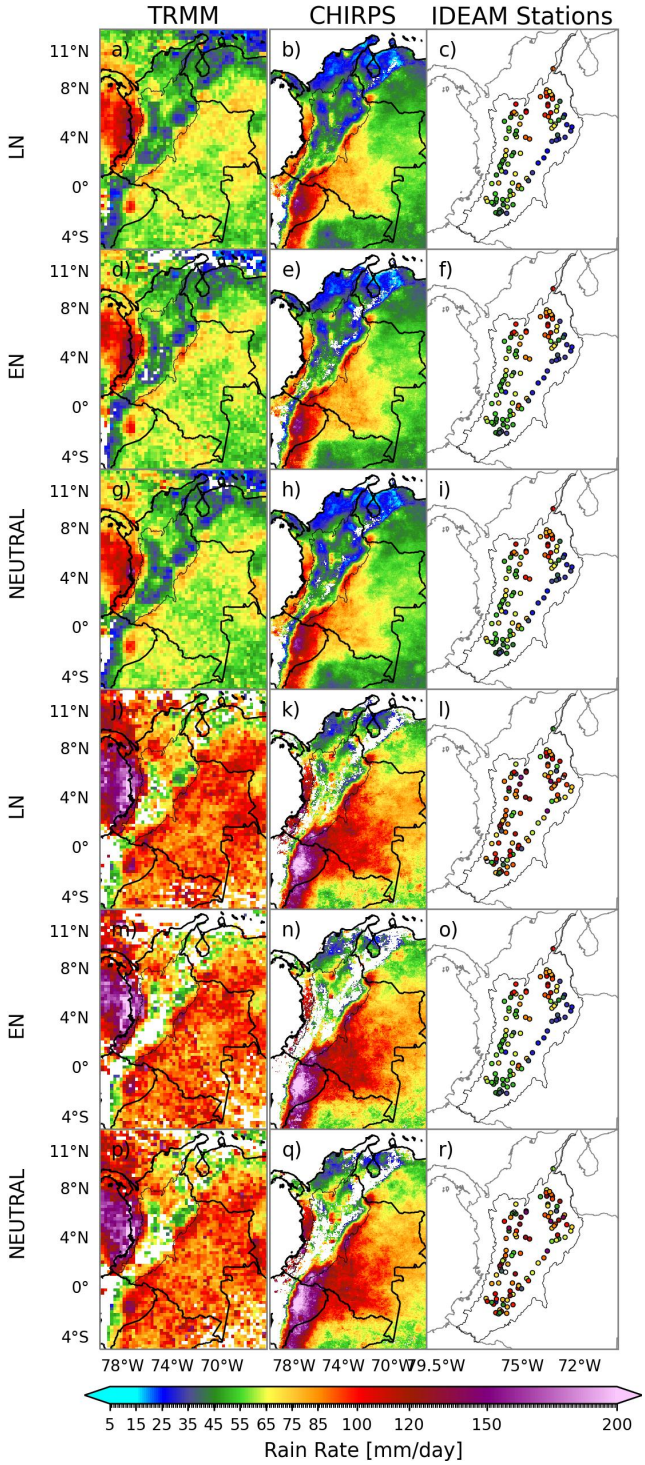

Figure **2-10**.: Characterization of extreme precipitation events, categorized by the intensity at the 95th (top three rows) and 99th percentiles (bottom three rows), during JJA. Data is sourced from TRMM at the 95th (a, d, g) and 99th percentiles (j, m, p), CHIRPS at the 95th (b, e, h) and 99th percentiles (k, n, q), and IDEAM stations at the 95th (c, f, i) and 99th percentiles (l, o, r). The labels in each row signify the phases of the ENSO, encapsulating LN years, EN years, and neutral years. Regions shaded in white denote the absence of extreme events during the respective season.

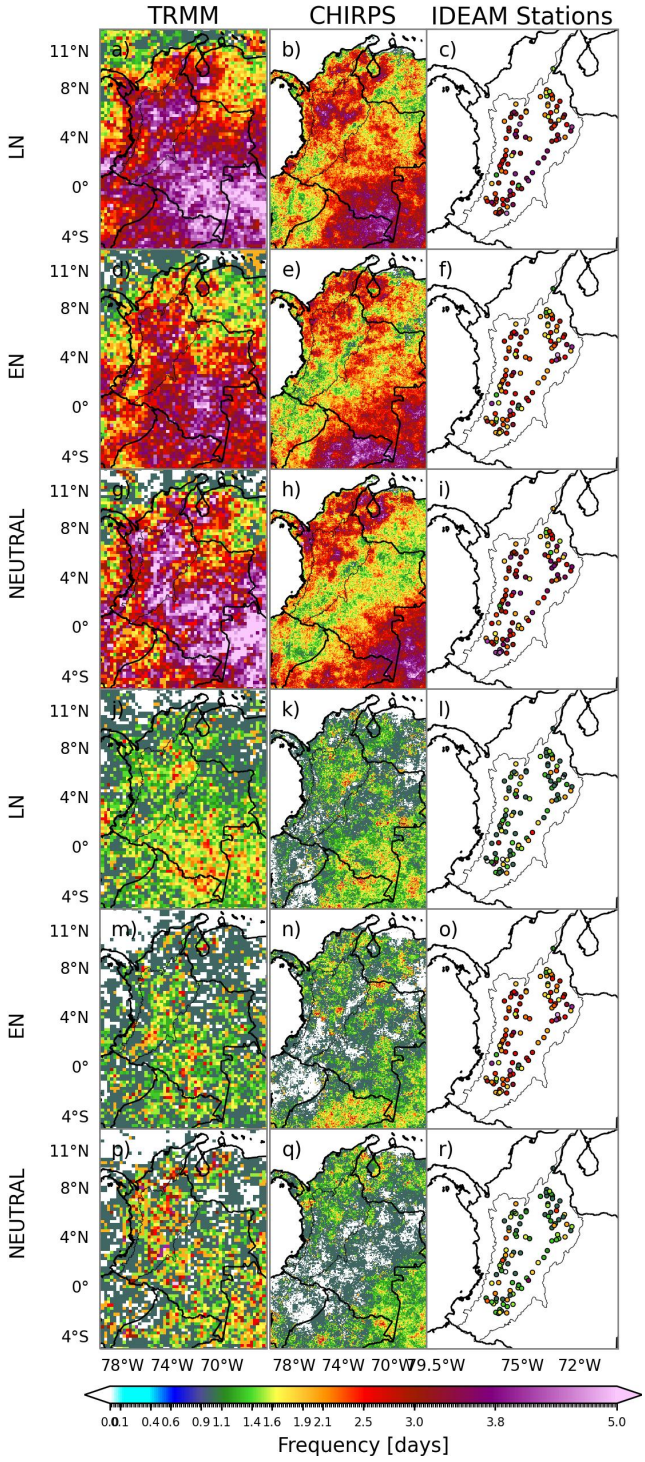

Figure **2-11**.: Characterization of extreme precipitation events, categorized by the frequency at the 95th (top three rows) and 99th percentiles (bottom three rows), during JJA. Data is sourced from TRMM at the 95th (a, d, g) and 99th percentiles (j, m, p), CHIRPS at the 95th (b, e, h) and 99th percentiles (k, n, q), and IDEAM stations at the 95th (c, f, i) and 99th percentiles (l, o, r). The labels in each row signify the phases of the ENSO, encapsulating LN years, EN years, and neutral years. Regions shaded in white denote the absence of extreme events during the respective season.

territory.

Some stations in the north and east of the Andes present the highest frequency values during LN, whereas stations in the south and northeast display lower values (Figure **2-11** c, f, i). All rain gauges exhibit common values in the 99th percentile frequency during ENSO events and neutral years (Figure **2-11** l, o, r).

SON

During this season, the 99th percentile of TRMM reveals that the most extreme precipitation events are found along the Pacific coast and northwestern region of the Caribbean Sea. The Andes also experience significant rainfall intensities, with magnitudes between 45 and 85 mm/day (Figure **2-12** j, m, p). It is noteworthy that during EN and neutral years, some areas do not experience any extreme events. On the other hand, the CHIRPS database presents a different pattern. During LN episodes, there are no events in most of eastern Colombia, and the events that do occur are less intense compared to those in EN and neutral years (Figure **2-12** k, n, q). The stations show a pattern similar to the one found on JJA (Figure **2-12** l, o, r).

The frequency at the 95th percentile in TRMM reveals significant findings; during LN, EN, and neutral years, the Andes experience the highest intensities of extreme events. These events span the entire Andean region up to the Caribbean, with LN showing the most extensive coverage of extremely severe occurrences. Notably, the boundary between the Andes and eastern Colombia experiences events with reduced intensity (Figure **2-13** a, d, g). CHIRPS datasets exhibit similar spatial pattern that TRMM (Figure **2-13** b, e, h), aligning with the station data, where the lowest values are located in the east of the mountain range (Figure **2-13** c, f, i). Consequently, the 99th percentile frequency results are congruent with the 95th percentile. During LN The TRMM data reveals high frequencies in the Andes, similar to what is seen in CHIRPS (Figure **2-13** j, m, p Figure **2-13** k, n, q). However, the station data does not display correspondingly high values in the Andes, despite events occurring at all stations (Figure **2-13** l, o, r).

The intensities and frequencies found in the 95th and 99th percentiles exhibit different outcomes across the four seasons. The 95th and 99th percentile intensities show similarities in their spatial and temporal pattern in three databases, and ENSO events and, neutral years; only some differences are observed at the 99th percentile during monthly analyses (not shown).

The study of the change of EPEs in climate change has become very relevant because, for the north of South America, we still have many unknowns of how it may affect the population and ecosystems. Therefore, the research developed in the region has focused on analyzing trends to observe changes in EPEs. However, researchers have taken into account the effects

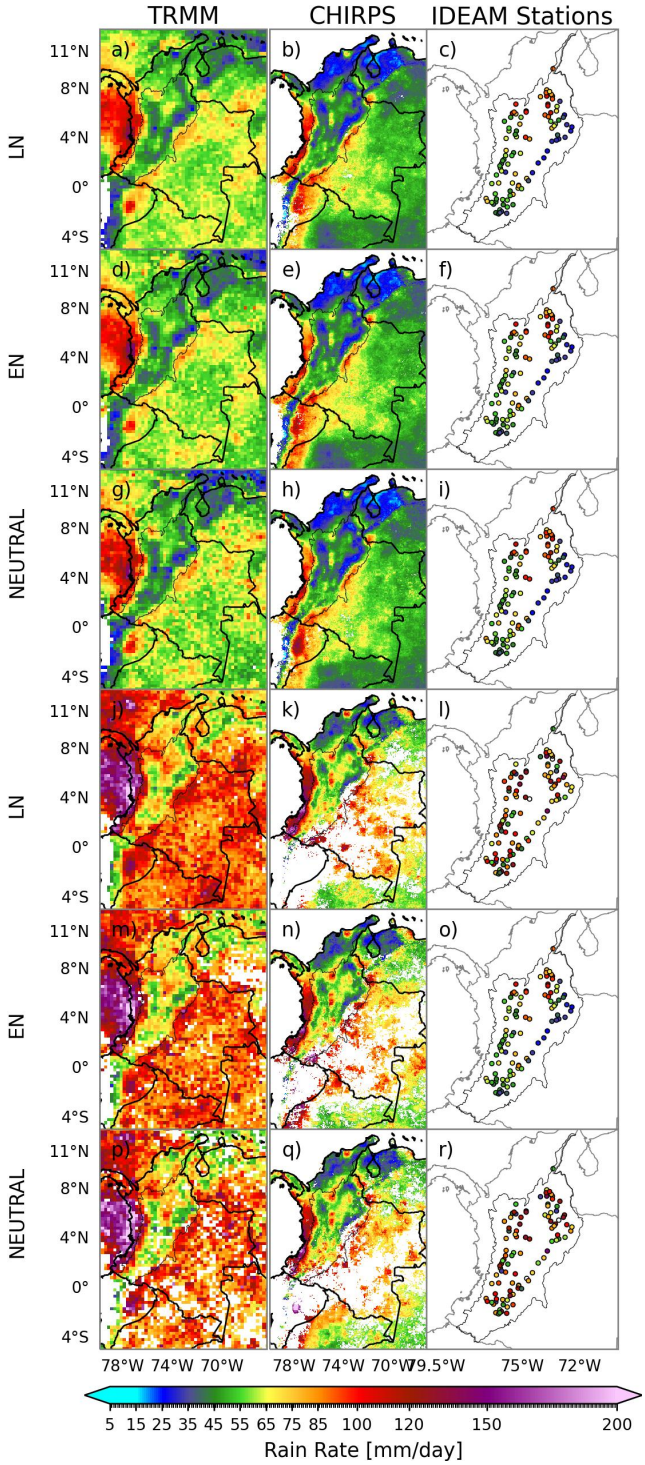

Figure **2-12**.: Characterization of extreme precipitation events, categorized by the intensity at the 95th (top three rows) and 99th percentiles (bottom three rows), during SON. Data is sourced from TRMM at the 95th (a, d, g) and 99th percentiles (j, m, p), CHIRPS at the 95th (b, e, h) and 99th percentiles (k, n, q), and IDEAM stations at the 95th (c, f, i) and 99th percentiles (l, o, r). The labels in each row signify the phases of the ENSO, encapsulating LN years, EN years, and neutral years. Regions shaded in white denote the absence of extreme events during the respective season.

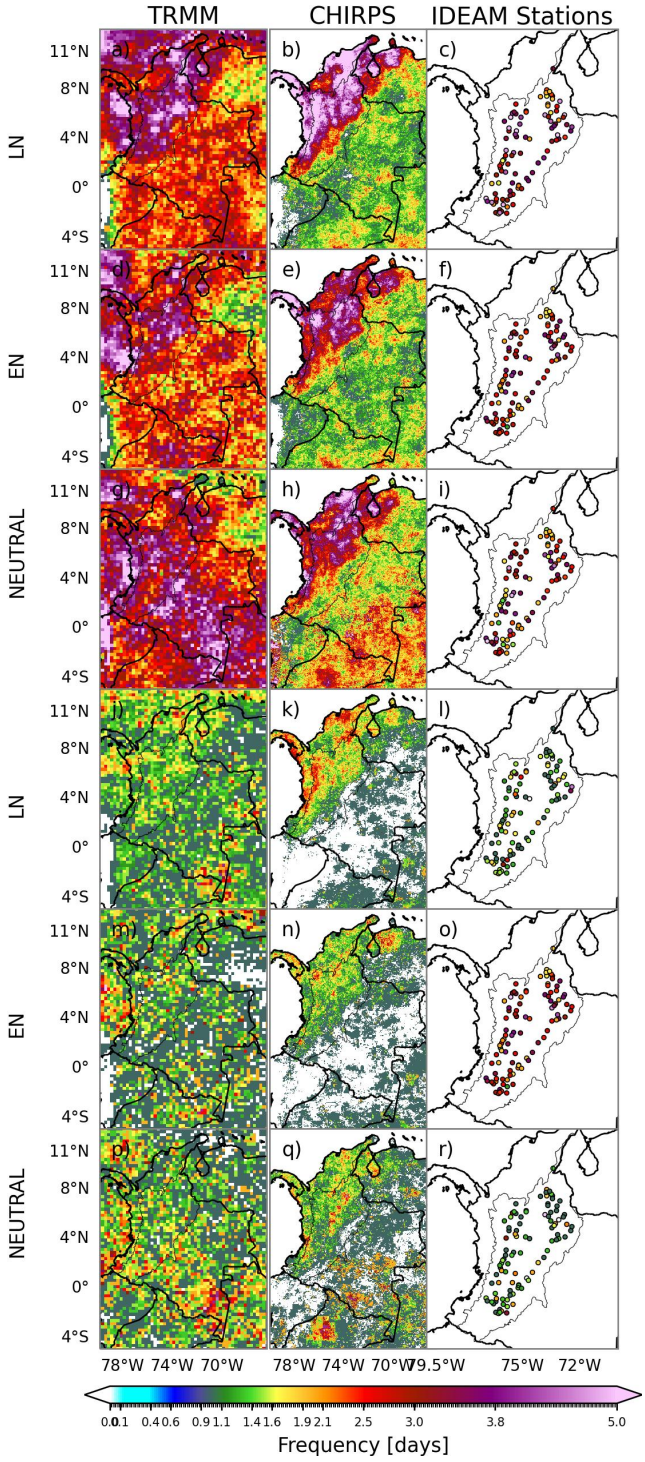

Figure **2-13**.: Characterization of extreme precipitation events, categorized by the frequency at the 95th (top three rows) and 99th percentiles (bottom three rows), during SON. Data is sourced from TRMM at the 95th (a, d, g) and 99th percentiles (j, m, p), CHIRPS at the 95th (b, e, h) and 99th percentiles (k, n, q), and IDEAM stations at the 95th (c, f, i) and 99th percentiles (l, o, r). The labels in each row signify the phases of the ENSO, encapsulating LN years, EN years, and neutral years. Regions shaded in white denote the absence of extreme events during the respective season.

of ENSO (Aguilar et al., 2005; Araujo et al., 2020; Cerón et al., 2022; Giraldo-Osorio et al., 2022; Hoyos et al., 2013a; Poveda et al., 2020; Rodríguez et al., 2019). However, they are not focused on studying the influence of ENSO in isolation, which also generates a bias in the impact that natural variability can have on EPEs.

ETCCDI indices have been the methodology for characterizing these events. These studies have revealed a significant relationship between ENSO and the frequency of extreme precipitation events, particularly in cases where events exceed the 20 or 30 mm thresholds. Interestingly, the results show that during the LN phase, the frequency of these events is higher compared to EN and neutral years, as Giraldo-Osorio et al. (2022) discovered. Additionally, during LN, annual wet spells are much longer than during El Niño (Pabón-Caicedo, 2012; Rodríguez et al., 2019).

In the Colombian Andes, there has been an increase in the understanding of EPEs through different approaches. For example, some have focused on looking at EPEs in relation to flooding in the Cauca and how it can be influenced by ENSO (Ávila et al., 2019). Thus, other research has focused on studying Colombia's whole country or more specific regions. However, no complete information on the characterization of EPEs in the Andes is unrelated to climate change.

When examining the influence of ENSO in the Caribbean, Pacific, and Andean regions are impacted by the average precipitation regime and extreme weather events compared to Colombia's eastern and southern regions. Cerón et al. (2022) findings confirm that extreme weather events play a crucial role in the natural variability of precipitation. However, the contribution of extreme events cannot be solely attributed to ENSO, as other high and low-frequency phenomena can also have a significant impact; this suggests external factors that play a role regarding precipitation extremes in Colombia (Builes-Jaramillo et al., 2022), inclusive of another phenomenon to large-scale (Jones and Carvalho, 2018; Kayano and Capistrano, 2014).

2.2.3 Comparison between ENSO and neutral years

The difference between LN – Neutral years, EN – Neutral years, and LN – EN years were calculated to find an increase or decrease of the EPE in the 95th and 99th percentile in intensity and frequency. Also, we observe the evolution of the differences in the seasonal climatology and its spacial variability, specifically in the Colombia Andes. T-tests were used for statistical search significance in the results.

DJF

During the DJF season, the distribution in the space of the differences in intensity at the 95th percentile is not homogeneous (Figure **2-14**). In TRMM, the number of statistically significant values is limited. However, considerable values are observed mainly in the north of the Colombian and Venezuelan territories. Generally, positive values indicate more intense magnitudes in LN than in neutral years (12 mm/day). In the Andes, the significant values are less localized in the region, with positive magnitudes in the center and negative magnitudes in the west and east. This distribution prevents any clear pattern from being discerned (Figure **2-14**). No significant difference is exhibited between EN and neutral years (Figure **2-14**). However, significant differences are highlighted in the Andes between LN - EN years, particularly in the northern and central regions. These differences include positive and negative values, with a gradient in the central area. Significant values are also shown in Panama, the northern Pacific Ocean, and the Caribbean Sea (Figure **2-14**).

Despite the similarities between the TRMM and CHIRPS datasets, the latter reveals some intriguing differences in extreme precipitation events across Colombia during different ENSO phases. In particular, CHIRPS data highlights significant increases in extreme precipitation intensity during LN years in the northern Pacific coast, west, and east of the Colombian Andes. These findings indicate that EPEs are more intense during LN years (Figure **2-14**b, e, and h). In contrast, during EN years, significant increases in extreme precipitation intensity were less common, with only a few areas showing substantial differences, primarily in the Panama region and some isolated points in the Andes (Figure **2-14**b, e, and h). Surprisingly, the differences in precipitation intensity between LN and EN years were more diverse, with a significant positive difference observed in the Andes and the Pacific coast. Again, however, there was a mix of positive and negative differences, with many positive values located in the west and east of the Andes and the northern Pacific coast and negative values in the southern Pacific coast (Figure **2-14**).

A limited number of stations show significant differences between LN and neutral years, mainly located west of the Andes, where positive and negative values are observed (Figure **2-14**c, f, and i). These findings suggest that both LN and neutral years predominate in the 95th percentile in EPEs. In the central region, some stations demonstrate positive values, indicating that LN has more pronounced EPEs than neutral years. In contrast, stations located in the eastern Andes display larger magnitudes during neutral years, as evidenced by positive values (Figure **2-14**). Regarding LN-EN, some rain gauges reflected positive values in certain Andean areas (Figure **2-14**).

Figure **2-14**j, m, and p indicate a low significant difference between ENSO and neutral years in the intensity at the 99th percentile. TRMM data shows some important values in the Andes, as well as in the Pacific Ocean and the northern of the study region in LN-neutral years. Still, the positive or negative differences are inconclusive (Figure **2-14**). In addition,

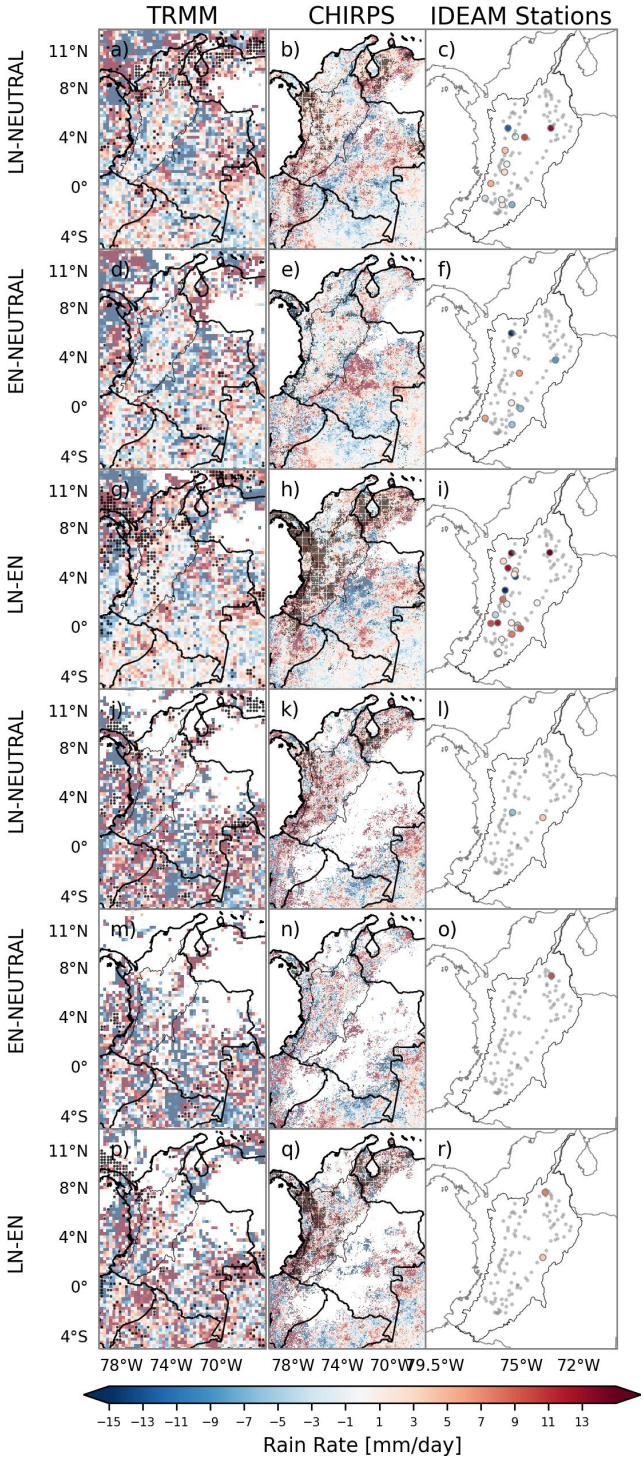

Figure **2-14**.: Difference between ENSO and neutral years by the intensity at the 95th (top three rows) and 99th percentiles (bottom three rows), during DJF. Data is sourced from TRMM at the 95th (a, d, g) and 99th percentiles (j, m, p), CHIRPS at the 95th (b, e, h) and 99th percentiles (k, n, q), and IDEAM stations at the 95th (c, f, i) and 99th percentiles (l, o, r). The labels in each row signify the phases of the ENSO, encapsulating LN-Neutral years, EN-Neutral years, and LN-EN. Grid points signify significant differences at a 95% confidence level.

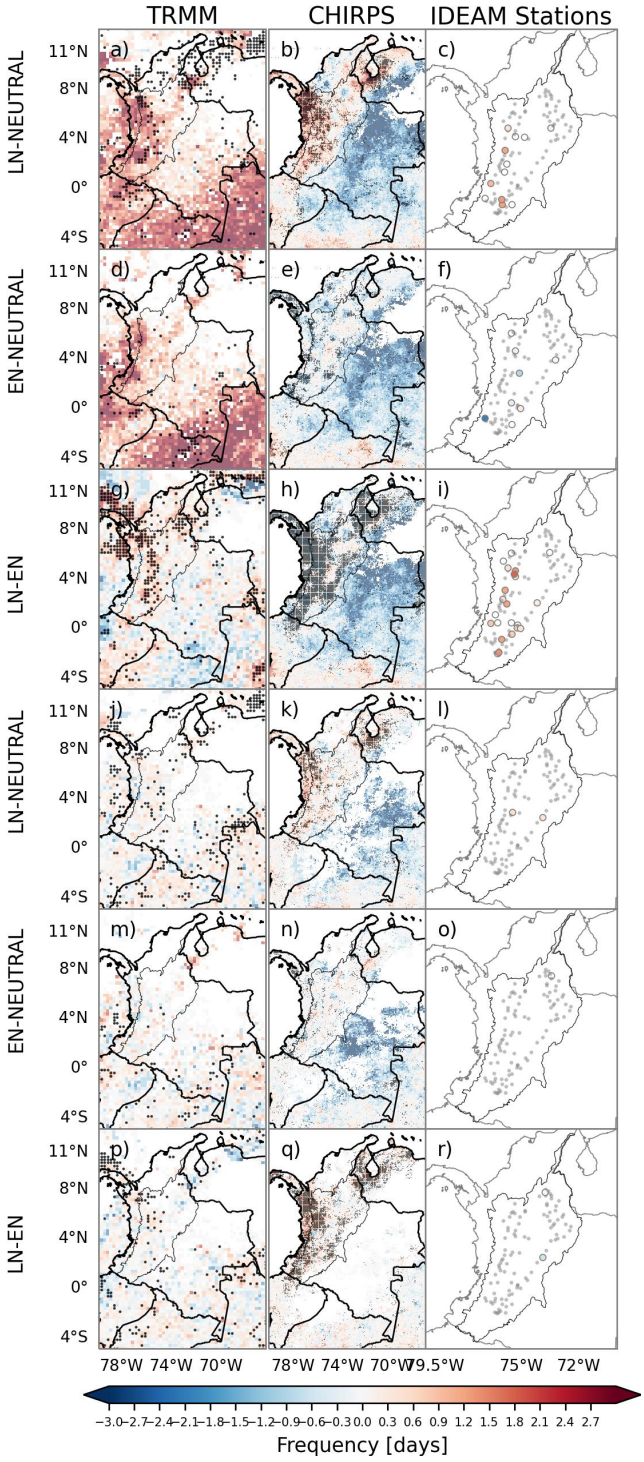

Figure **2-15**.: Difference between ENSO and neutral years by the frequency at the 95th (top three rows) and 99th percentiles (bottom three rows), during DJF. Data is sourced from TRMM at the 95th (a, d, g) and 99th percentiles (j, m, p), CHIRPS at the 95th (b, e, h) and 99th percentiles (k, n, q), and IDEAM stations at the 95th (c, f, i) and 99th percentiles (l, o, r). The labels in each row signify the phases of the ENSO, encapsulating LN-Neutral years, EN-Neutral years, and LN-EN. Grid points signify significant differences at a 95% confidence level.

the comparison between EN - neutral years and LN - EN does not show significant values (Figure **2-14**m and p). It is important to note that no extreme events exist in the eastern and northern regions, as illustrated in Figure **2-14**.

On the other hand, CHIRPS reveals significant intensities at the 99th percentile, mainly on the west flank of the western branch of the Andes, with primarily positive values, indicating that precipitation extremes during LN are more intense than in neutral years (Figure **2-14**k, n, and q). Similarly, significant magnitudes were found at the 95th percentile on the Pacific coast and north of Venezuela, with primarily positive values. Meanwhile, significant differences were observed between EN and neutral years north of the Pacific coast (Figure **2-14**n). Finally, Figure **2-14**q shows significant differences between LN and EN, with positive and negative magnitudes, on the west of the Andes, Pacific coast, and north of the territory.

Only two stations meet the significance criterion and have opposite magnitudes between LN and neutral years (Figure **2-14**l). However, the overall pattern remains unchanged mainly between EN and neutral years and between LN and neutral years (Figure **2-14**o). Specifically, only one and two significant stations displayed positive magnitudes, indicating limited variations in the observed phenomenon.

The characterization of the frequency of EPEs did not show whether there was an increase or decrease in the composite of LN, EN, and neutral years. However, the influence of ENSO on the EPEs appears to be shown in the difference in the frequency. During the DJF season at the 95th percentile in TRMM, there are positive values throughout the region in the LN-neutral years' difference; only significant magnitudes are found in the west and north of the Andes and are very localized to the north region (Figure **2-15**a, d, g). Although most of the values are positive between EN and neutral years, there are few areas with significance (Figure **2-15**a, d, g); solely between LN and EN are their larger areas with significant and positive values (west and north of the Andes, Panama, and east of the Caribbean Sea) (Figure **2-15**g and h).

The results are similar in CHIRPS in the Andes, with positive and significant values to the west and north, Pacific coast, and northern Venezuela in LN-neutral years (Figure **2-15**b). On the other hand, there are no significant values between EN and neutral years (Figure **2-15**e), similar to what is described in TRMM. However, both databases differ in the magnitudes in the eastern plains region. While in TRMM, the differences are positive, in CHIRPS, the differences are negative, in LN - neutral years and EN - neutral years. LN and EN's significance differs from CHIRPS and TRMM, where CHIRPS has a larger extension with significant values (Figure **2-15**h). However, its magnitudes present a gradient between positive and negative values.

Figure **2-15**c, f and i highlight the statistically significant rainfall stations. Positive and significant values are found in LN and neutral years and LN-EN (Figure **2-15**c and i), while negative values are seen between EN and neutral years (Figure **2-15**f). Overall, TRMM and

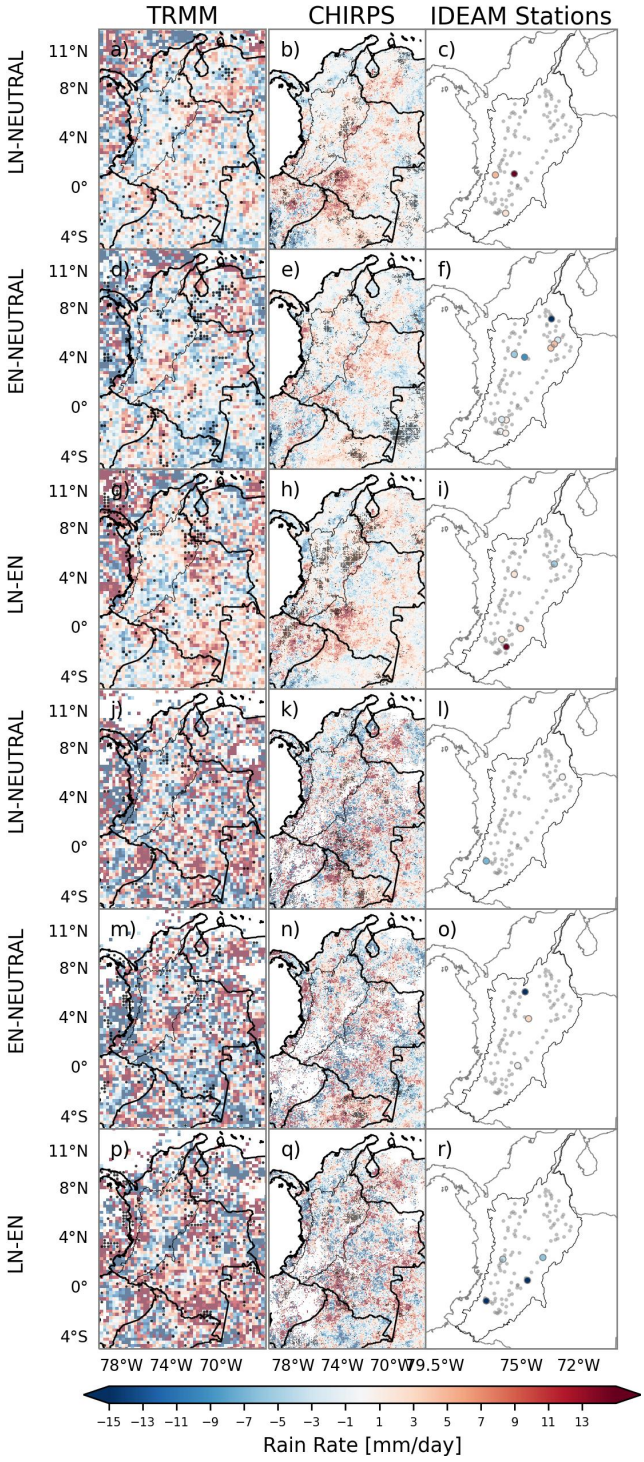

Figure **2-16**.: Difference between ENSO and neutral years by the intensity at the 95th (top three rows) and 99th percentiles (bottom three rows), during MAM. Data is sourced from TRMM at the 95th (a, d, g) and 99th percentiles (j, m, p), CHIRPS at the 95th (b, e, h) and 99th percentiles (k, n, q), and IDEAM stations at the 95th (c, f, i) and 99th percentiles (l, o, r). The labels in each row signify the phases of the ENSO, encapsulating LN-Neutral years, EN-Neutral years, and LN-EN. Grid points signify significant differences at a 95% confidence level.

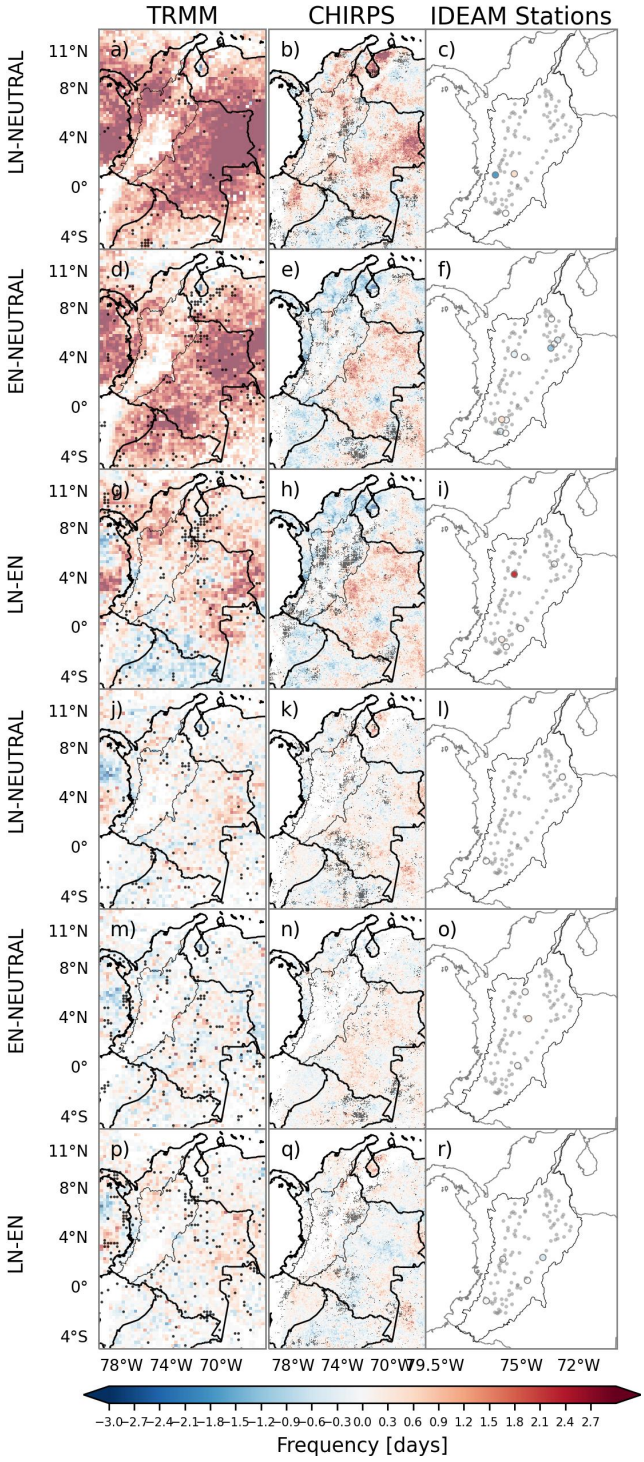

Figure **2-17**.: Difference between ENSO and neutral years by the frequency at the 95th (top three rows) and 99th percentiles (bottom three rows), during MAM. Data is sourced from TRMM at the 95th (a, d, g) and 99th percentiles (j, m, p), CHIRPS at the 95th (b, e, h) and 99th percentiles (k, n, q), and IDEAM stations at the 95th (c, f, i) and 99th percentiles (l, o, r). The labels in each row signify the phases of the ENSO, encapsulating LN-Neutral years, EN-Neutral years, and LN-EN. Grid points signify significant differences at a 95% confidence level.

CHIRPS have similar differences to those shown at the stations. However, only TRMM does not show similarities in some regions with CHIRPS and the stations, and in both satellite databases, they do not agree with what is shown in the stations in EN-neutral years.

Finally, with positive values reduction in significant differences observed at the 99th percentile in frequency, showing about 1.2 events and CHIRPS showing -1.2 events, consistent with the findings at the 95th percentile showing about 2.1 events and CHIRPS showing -2.1 events. In TRMM, the differences between LN - neutral years and LN - EN are significant in the Andes. At the same time, there are more significant values in CHIRPS data for the Andes region in LN - EN (Figure **2-15**j, m, and p).

In contrast, in CHIRPS, some positive and significant values are observed northwest of the Andes and the Pacific region in LN and neutral years (Figure **2-15**k, n and q). In EN and neutral years, only positive values were in the Andes (Figure **2-15**n). Figure **2-15**l, o, and r in DJF show negative values in stations in eastern Colombia. Similarly, in LN - EN comparison, significant positive values are concentrated in the west of the Andes, along the Pacific coast, and the northeast of the study region, consistent with what was observed at the 95th percentile.

MAM

As previously mentioned, the first rainy season occurs during the MAM period, primarily in the Colombian Andes, and is intensified during LN events, with increased precipitation leading to severe flooding (Cerón et al., 2022; Poveda et al., 2011). However, both TRMM and CHIRPS show no significance in intensities at the 95th percentile. The signal between the differences between ENSO and neutral years is mixed. TRMM data indicates a higher frequency of extreme events during LN in the eastern Andes (Figure **2-17**) and EN to the south (Figure **2-17**). In contrast, Figure **2-17** displays a higher number of extreme events during LN compared to EN.

Conversely, CHIRPS presents positive and significant values to the west and east of the Andes in LN events as opposed to EN events (Figure **2-16**b, e, and h). Furthermore, the eastern region of Colombia exhibits more extensive areas of positive values in CHIRPS (Figure **2-16**b, e, and h) and TRMM (Figure **2-16**a, d, and g). The observed patterns from station data differ from those in the other databases. More intense and significant events are detected in the southern regions during LN compared to neutral years. At the same Figure **2-16**c, f and i, time, both positive and negative values are found in the south and northern regions between EN and neutral years (Figure **2-16**c, f and i). Additionally, higher magnitudes are recorded during LN events as opposed to EN events west of the Andes (Figure **2-16**c, f, and i).

The pattern observed in the difference in intensities at the 99th percentile is also evident

at the 99th percentile within the Andes region, as depicted by TRMM (Figure **2-16**j, m and p). However, CHIRPS does not maintain this consistency, exhibiting high variability in intensity across the Andes with positive and negative values. This makes it challenging to discern a definitive pattern between ENSO and neutral years. Even so, in Figure **2-16**k, n, and q, a small area east of the Andes is preserved with significant and positive values, indicating an intensity of the events in LN than EN. Regions demonstrating similar patterns at the 95th and 99th percentiles include eastern Colombia, Venezuela, and northern Ecuador. These areas exhibit positive values during both LN (Figure **2-16**k) and EN (Figure **2-16**q), potentially indicating a significant influence of ENSO in these regions. Other local circulation phenomena may further amplify this effect. On the other hand, 4% of the stations presented a significant value and did not coincide with the stations illustrated in the 95th percentile. Additionally, the magnitudes recorded spanned both positive and negative values. Notably, Figure **2-16**n and q, show stations in the south and north, respectively, with negative values and magnitudes lower than -20 mm/day. Figure **2-16**n is primarily influenced by neutral years, while Figure **2-16**q is characterized by more extreme events during EN than LN periods.

In the Andes, there is spatial coherence and a clear position in the impact of LN and EN episodes on the frequency of extreme events during the peak rainy season (MAM) compared to the preceding months in TRMM (Figure **2-17**a, d, and g). In TRMM, significant values are predominantly found in the eastern Andes for LN-EN differences, in the same way as CHIRPS (Figure **2-17**b, e, and h). However, the latter display significant differences in more extensive eastern and western Andes areas. Additionally, CHIRPS exhibits contrasting values in EN-neutral years with negative values (Figure **2-17**e); Figures **2-17**b and e have areas highlighted with negative values. Moreover, the number of stations does not differ significantly from DJF, despite expectations of a lower count compared to the MAM season. The rain gauges with significant values in Figure **2-17**c, f, and i are primarily located in the eastern Andes. Only in Figure **2-17**f are more stations spatially distributed. All results are mixed in positive and negative values.

There is no discernible influence of ENSO or neutral years on frequency EPE in the Andes region at the percentile 99. Figure **2-17** do not show extreme events in this area. Only some values are concentrated far north of the Andean region. The databases are consistent with rain gauges in LN-neutral years and LN-EN (Figure **2-17**l and r) but not EN-neutral years. Surprisingly, most stations exhibit positive and significant results, indicating a more prominent contribution of events during EN years than neutral years (Figure **2-17**o).

JJA

During JJA, both satellite databases showed different values in the Andes in the intensities at the 95th percentile. TRMM displays positive values across most Andes regions (Figure **2-**

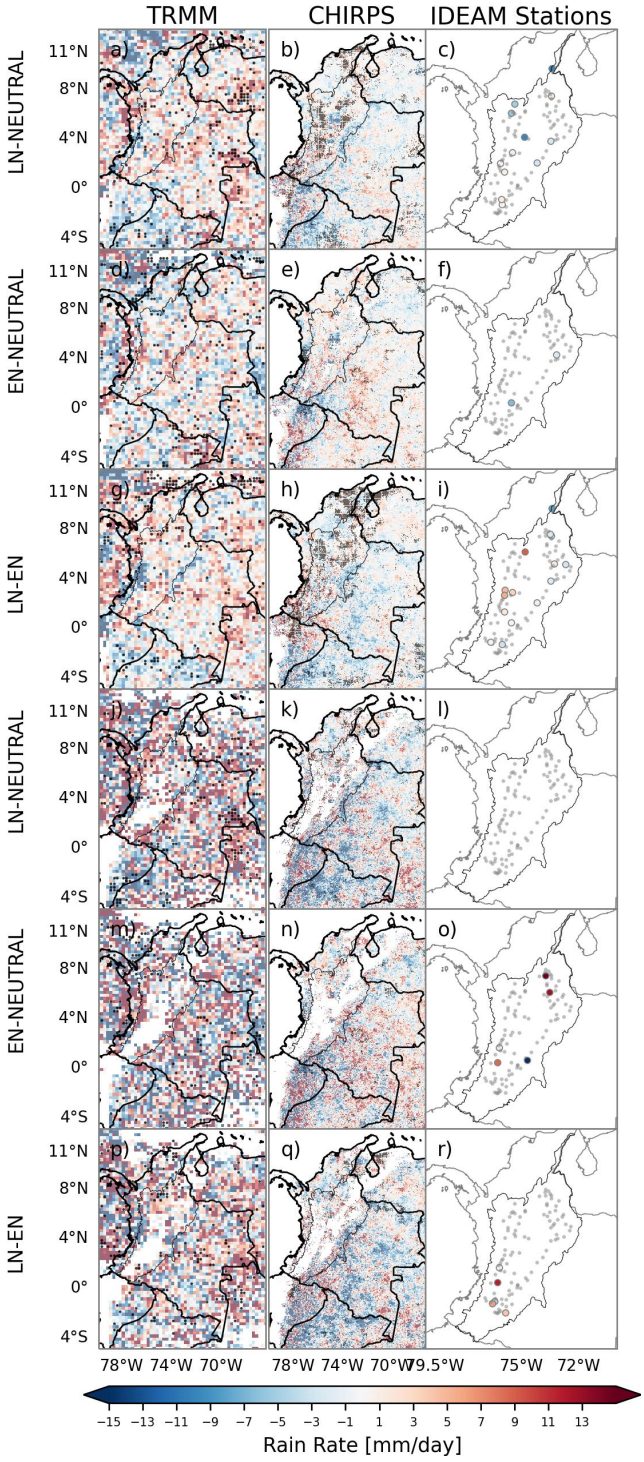

Figure **2-18**.: Difference between ENSO and neutral years by the intensity at the 95th (top three rows) and 99th percentiles (bottom three rows), during JJA. Data is sourced from TRMM at the 95th (a, d, g) and 99th percentiles (j, m, p), CHIRPS at the 95th (b, e, h) and 99th percentiles (k, n, q), and IDEAM stations at the 95th (c, f, i) and 99th percentiles (l, o, r). The labels in each row signify the phases of the ENSO, encapsulating LN-Neutral years, EN-Neutral years, and LN-EN. Grid points signify significant differences at a 95% confidence level.

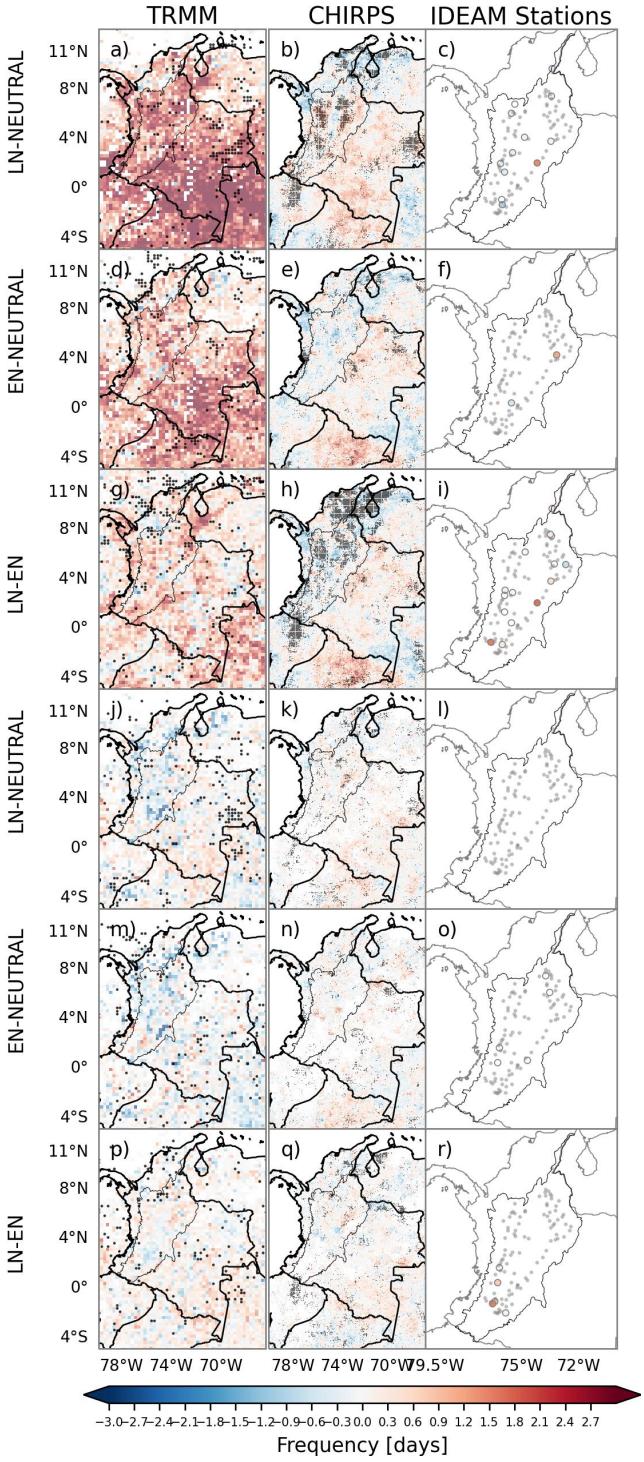

Figure **2-19**.: Difference between ENSO and neutral years by the frequency at the 95th (top three rows) and 99th percentiles (bottom three rows), during JJA. Data is sourced from TRMM at the 95th (a, d, g) and 99th percentiles (j, m, p), CHIRPS at the 95th (b, e, h) and 99th percentiles (k, n, q), and IDEAM stations at the 95th (c, f, i) and 99th percentiles (l, o, r). The labels in each row signify the phases of the ENSO, encapsulating LN-Neutral years, EN-Neutral years, and LN-EN. Grid points signify significant differences at a 95% confidence level.

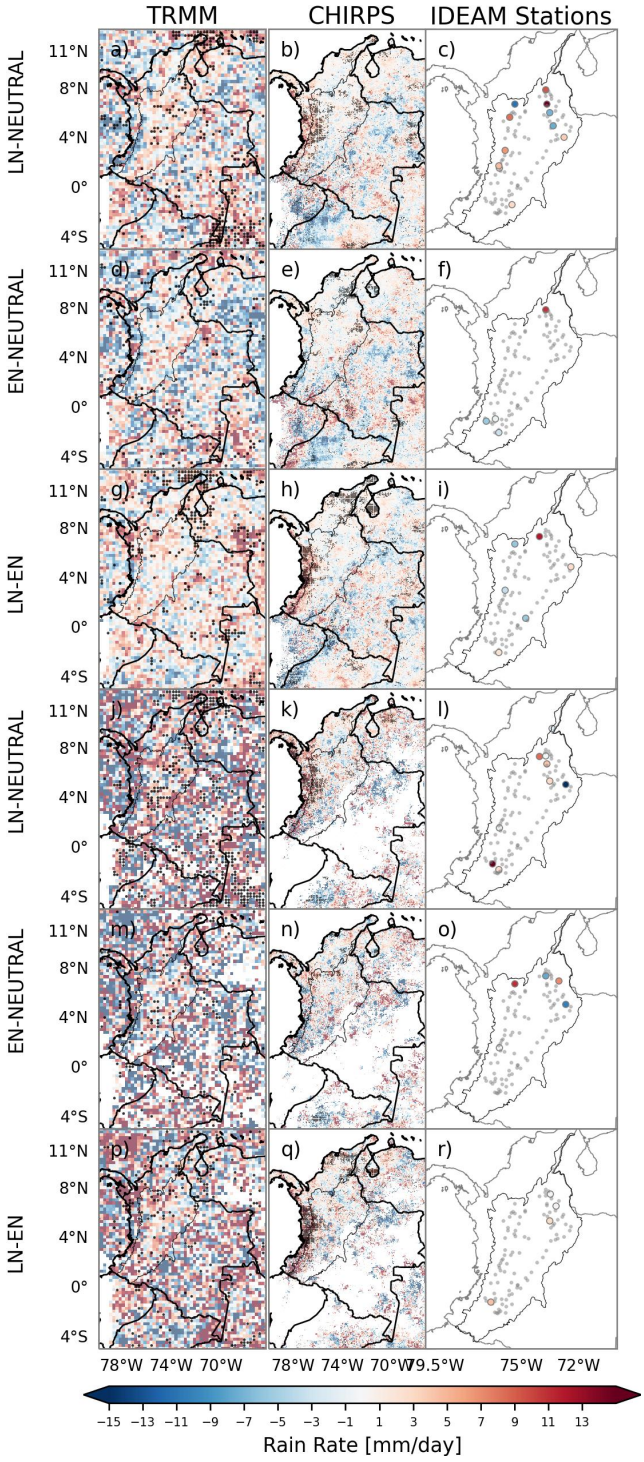

Figure **2-20**.: Difference between ENSO and neutral years by the intensity at the 95th (top three rows) and 99th percentiles (bottom three rows), during SON. Data is sourced from TRMM at the 95th (a, d, g) and 99th percentiles (j, m, p), CHIRPS at the 95th (b, e, h) and 99th percentiles (k, n, q), and IDEAM stations at the 95th (c, f, i) and 99th percentiles (l, o, r). The labels in each row signify the phases of the ENSO, encapsulating LN-Neutral years, EN-Neutral years, and LN-EN. Grid points signify significant differences at a 95% confidence level.

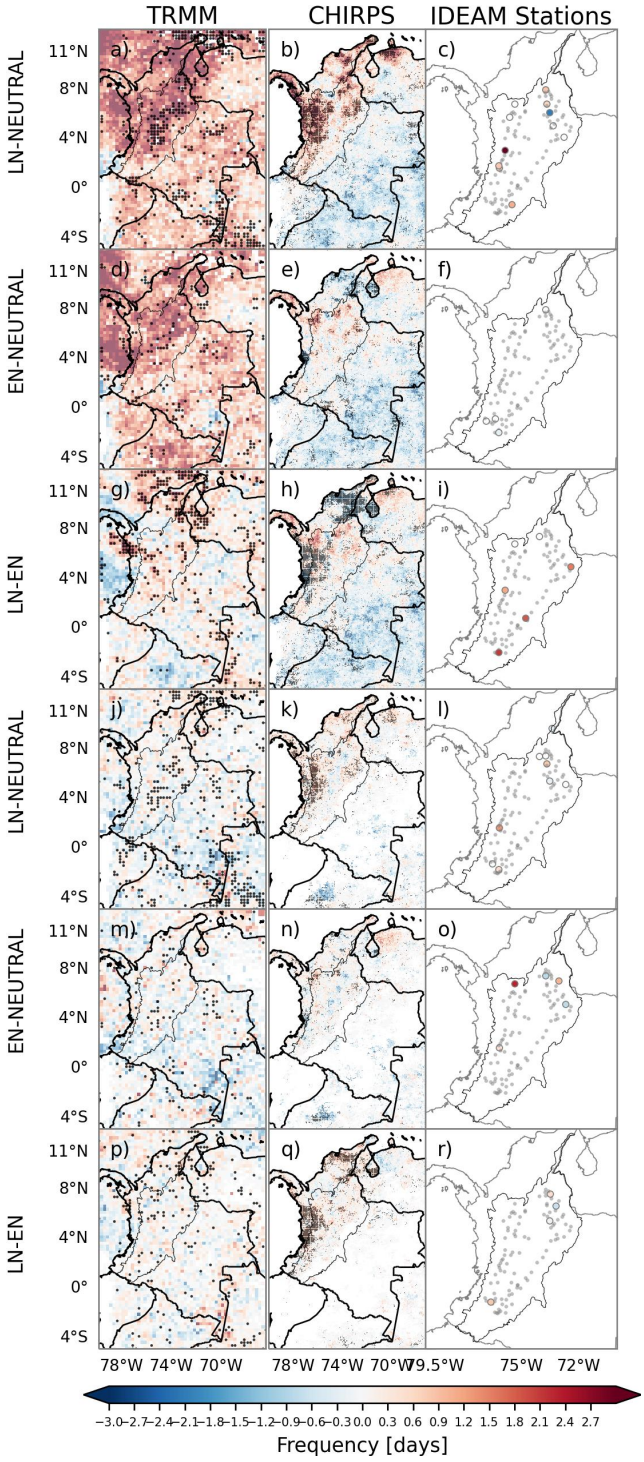

Figure **2-21**.: Difference between ENSO and neutral years by the frequency at the 95th (top three rows) and 99th percentiles (bottom three rows), during SON. Data is sourced from TRMM at the 95th (a, d, g) and 99th percentiles (j, m, p), CHIRPS at the 95th (b, e, h) and 99th percentiles (k, n, q), and IDEAM stations at the 95th (c, f, i) and 99th percentiles (l, o, r). The labels in each row signify the phases of the ENSO, encapsulating LN-Neutral years, EN-Neutral years, and LN-EN. Grid points signify significant differences at a 95% confidence level.

18a, b, c, d, e, f, g, h, and i), while CHIRPS differ in TRMM, presenting negative values in Figures 19a and 19c. Notably, CHIRPS demonstrated high significance during this season, indicating an arid period. On the other hand, the station data revealed negative values during both LN-neutral and EN-neutral years (Figure **2-18**c and f). Additionally, the LN-EN analysis highlighted increased intensity events in the western Andes during LN years and higher intensities in the eastern regions during neutral years (Figure **2-18**i).

Figure **2-18**j, m, and p illustrate no significant events in the Andes at the 99th percentile when comparing the differences between ENSO phases according to TRMM. This finding is consistent with the observations from both CHIRPS (Figure **2-18**k, n, and q) and rain gauges (Figure **2-18**l, o, and r). It is important to note that CHIRPS maintains the same pattern in the eastern portion of the study region. Meanwhile, the values in TRMM display a mixed pattern, and ultimately, no statistically significant values are identified at the 99th percentile.

The frequency of composite events at the 95th percentile, as illustrated in Figure **2-11** for TRMM and CHIRPS, reveals a notable difference in events within the Andes. TRMM values are higher than CHIRPS in the Andes region, which can explain the difference in Figure **2-19**a, d, and g. On the other hand, in JJA, results presented by TRMM and CHIRPS are similar to the previous season, highlighting the extensive significance magnitudes in the difference between LN-neutral and LN-EN in almost the entire Andes in CHIRPS (Figure **2-19**b and h). Nonetheless, the stations display a positive difference in the northeast of the Andes and are distributed throughout the Andes, in LN-neutral and LN-neutral, respectively (Figure **2-19**c and i). Consequently, during LN, the events are more frequent.

Similarly, at both the 95th and 99th percentiles, the TRMM and CHIRPS datasets do not align spatially. TRMM exhibits negative values in all Andes in LN-neutral and EN-neutral years while presenting positive values during LN-EN events. In contrast, CHIRPS displays positive values in all cases, as shown in Figure **2-19**k, n and q. Only some stations present positive values for the difference between LN-EN, as illustrated in Figure **2-19**l, o and r.

SON

In the SON season of LN episodes, the intensity of EPE increases in the easternmost part of the Andes, as depicted in TRMM (Figure **2-20**a, d and g). Conversely, CHIRPS exhibits a special effect during LN, with negative values (Figure **2-20**b and h). Seasonally extreme events increase in EN compared to neutral years in TRMM (Figure **2-20**d) but decrease in CHIRPS (Figure **2-20**e). The same pattern occurs in the westernmost Andes but with an inverse relationship between TRMM and CHIRPS (FFigure **2-20**). It should be noted that significant values are present in CHIRPS in LN-neutral the west Andes region. Few stations have values significant in LN-neutral, with positive values in the western Andes and negative values to the north (Figure **2-20**c). For EN-neutral, negative values are situated in

the south, while mixed values are present in LN-EN (Figure **2-20**f).

During the second rainy season in the eastern plains of Colombia, there is a noticeable lack of intense events in LN, EN, and neutral years, as evidenced by the 99th percentile of CHIRPS data (Figure **2-20**k, n and q). The impact of ENSO or neutral years on the Andes is less clear, with higher variability of magnitudes observed in both TRMM and CHIRPS datasets. Moreover, significant differences can be found in the east-central region of the Andes and the Eastern Caribbean during LN-neutral years, according to TRMM data (Figure **2-20**j). In contrast, CHIRPS data reveals significant values to the west of the Andes and along the Pacific Coast during LN-neutral and LN-EN years (Figure **2-20**l and r). However, the available station data does not provide a conclusive understanding of the contribution of ENSO and neutral years to these patterns (Figure **2-20**k and q).

An outstanding contribution from Rainfall occurs in SON in the Colombian Andes due to the double passage of the ITCZ. Therefore, it has been demonstrated that the precipitation increase or decrease during ENSO activation. LN generally has increased precipitation, and the EPE would be expected to be more intense. Previous results have shown that it does not happen, but the contribution to the increase or decrease in the occurrence of events is higher in the ENSO.

In Figure **2-21**a, d and g in TRMM, during LN and EN, there are more frequent events than in neutral years, with significant regions in the Andes, eastern Caribbean, and south of the territory at the 95th percentile. Figure **2-21**g shows that events are higher in LN than EN in almost all of the Andes, and significant values are distributed throughout the region. However, negative values surround the ocean, Pacific coast, Caribbean, and eastern Colombia. Likewise, in JJA, CHIRPS agrees with TRMM with positive values in the Andes; the significance values are more extensive in the west of the Andes, Pacific coast, and north of Colombia and Venezuela in LN-neutral and LN-EN (Figure **2-21**b and e). However, the results differ to the east and south of the territory. The values are negative, indicating contribution from the neutral years (Figure **2-21**b and e) and EN years (Figure **2-21**e). The stations present the same pattern. Positive and significant values are in LN-neutral and LN-EN (Figure **2-21**c and i), e.g., in LN hay, more occurrences of an event than in neutral years and EN episodes.

The frequency of extreme events decreases at the 99th percentile, accompanied by a reduction in significant differences. TRMM data shows these events are higher north of the Andes during both LN and EN events and even greater in the south and during neutral years (Figure **2-20**j, m and p). The significant values found in the western Andes in LN–neutral (Figure **2-20**j). The pattern change in LN-EN with opposite signs in the Andes and est Colombia only determines small areas where LN and EN events increase or decrease. The frequency change of extreme rainfall observed in SON over northern South America in CHIRPS extends over a large Andes region. In this season, LN and EN have increased in frequency

events (Figure **2-20**k, n and q), but no events are displayed over a larger region to the east and south. The positive and significant values are concentrated in Colombia's westernmost part of the Andes and the northernmost regions (Figure **2-20**k and q). The extreme event signal displays highly significant values in nearly all rain gauges during EN-neutral years, with differences between -1 and 1. The magnitudes vary, making it difficult to determine whether the increase in events is predominantly driven by EN or neutral years. Research conducted by Grimm and Tedeschi (2009) about extreme precipitation events in South America found specifically for Colombia in August and September that the number of extreme events significantly decreased during EN and increased in LN. They also mention that the magnitudes of intensities of extreme events in EN, LN, and neutral years are variable in smaller areas. Finally, it should be noted that the differences in all seasons in response to the EPEs in EN and LN are not necessarily the opposite, i.e., despite the reduction of precipitation in the Andes during EN, this does not mean the absence of events. On the contrary, the contribution may be higher than in neutral years in some months.

2.2.4 Cluster analysis

To analyze the spatial distribution characteristics of EPEs, the commonly used k-means clustering algorithm was employed for Colombia Andes. Figure **2-22** illustrates the five regions classified by the method in the database TRMM and CHIRPS the variations, indicating that each area has similar behavior in intensity of EPEs in center-north, center-south, southernmost, west, and east Andes. Both sources of information classify the EPEs similarly to those shown in Figure **2-2**, which shows the 95th and 99th percentile thresholds, and particularly, the regions obtained from the cluster analysis describe a similar pattern to the station thresholds. Clusters 2 and 3 have large areas in CHIRPS with coverage near the Pacific coast in cluster 2 and wide extension in the center Andes in cluster 3 compared with respective regions in TRMM.

Figure **2-23**, on the other hand, shows the classification of EPEs daily intensity at the 99th percentile highlights two aspects; the first is the similitude with the 95th percentile in TRMM, but the area changes slightly at the 99th percentile, and Second, is the difference between CHIRPS and TRMM in cluster 1 at the 99th percentile (Figure **2-23** a and b). It was to be expected that the regions would differ in extent and position since the 99th percentile represents very extreme precipitation. Therefore it is more difficult to exceed this threshold. Each cluster has a different geographical distribution; thus, the atmospheric dynamic varies.

We found that the k-means method adequately classified regions with similar intensities at the 95th and 99th percentile in the Andes due to the results obtained initially in the characterization of intensities of the EPEs (Figures **2-6**, **2-8**, **2-9**, **2-11**, **2-13**). There it can be observed that in the IDEAM stations, TRMM and CHIRPS contours draw similar

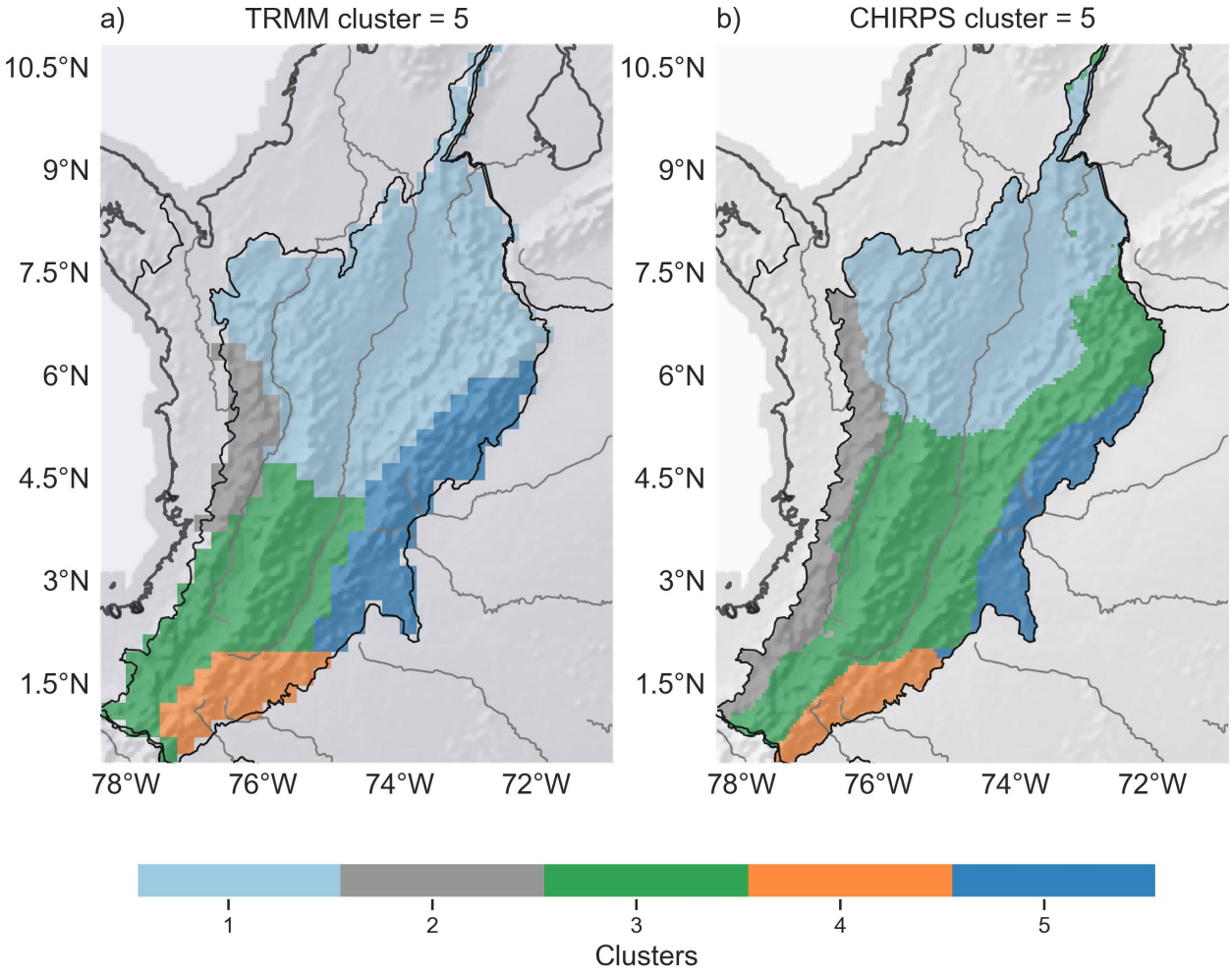

Figure **2-22**.: Cluster classification in the Colombian Andes in the 95th percentile. a) TRMM and b) CHIRPS.

magnitudes in broad regions such as east, west, and north of the Andes, regions that agree with the clustering (Figure **A-1**).

Figure **2-24** presents the annual rainfall cycle of each cluster. IDEAM stations were selected only with the delimitation of the clusters obtained in the 95th percentile in TRMM and CHIRPS (Figure **A-1**). Thus, each cluster has a number of stations for averaging the annual cycle.

Figure **2-24** a-e show that TRMM and CHIRPS can capture the bimodal precipitation pattern in the Andes, but there may be insufficiencies in the accuracy of the data stations. Figure **2-1**a, shows the behavior for cluster one in the Andes region, where stations are located mainly at low altitudes and where the most significant number of stations are recorded. TRMM and CHIRPS databases capture bimodal precipitation regimes, two wet and two dry

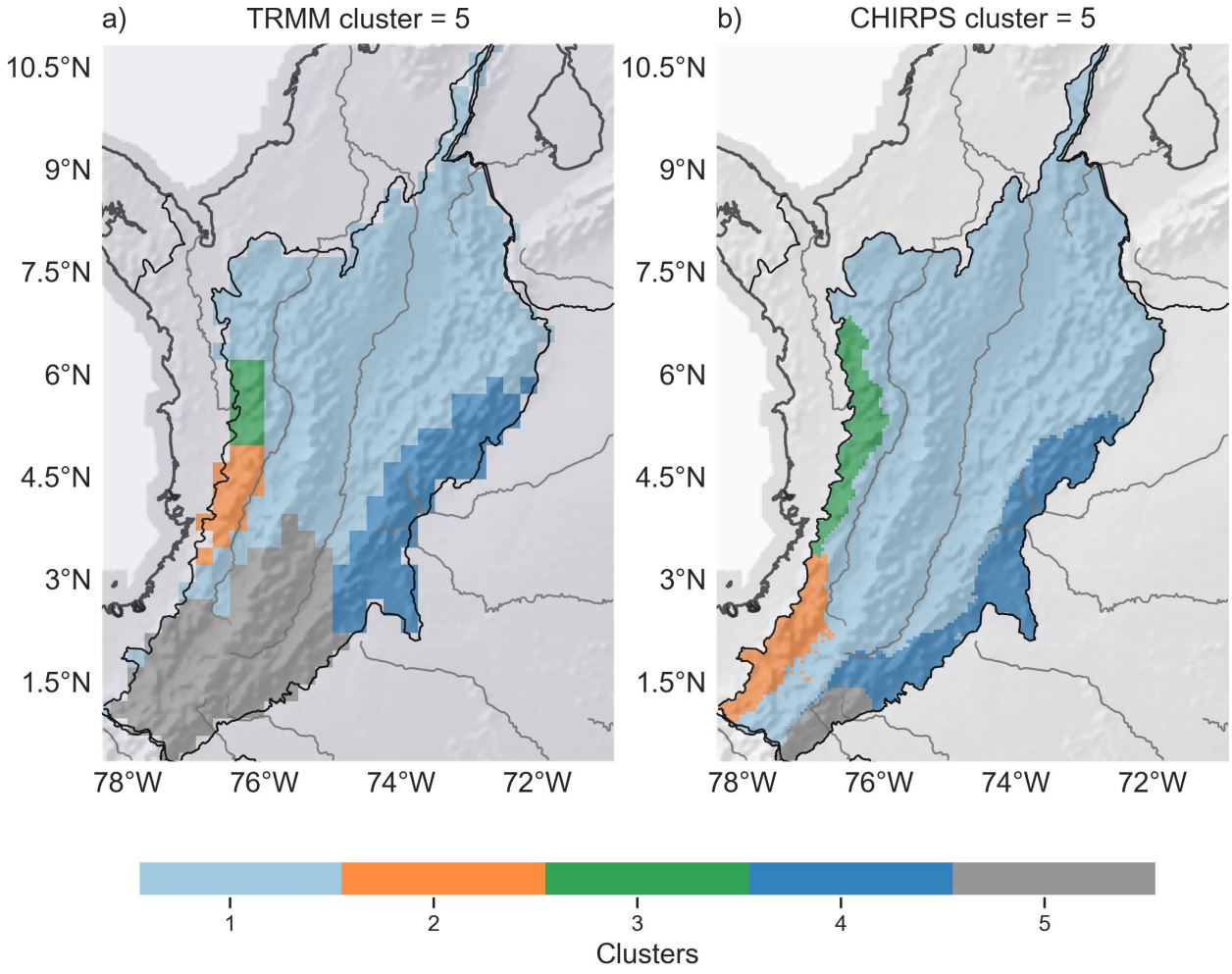

Figure **2-23**.: Cluster classification in the Colombian Andes in the 99th percentile. a) TRMM and b) CHIRPS.

seasons, and the performance is good in amplitude. However, TRMM and CHIRPS data differences are observed in Figure **2-24** b, c, d, and e. The highest values are observed in Figure **2-24** b, corresponding to the westernmost part of the Andes, with an overestimation in both databases and higher TRMM values. It is important to note that the cycle rainfall mean in TRMM and CHIRPS differ because of the number of stations in each cluster.

In Figure **2-24** c, which covers the south-central Andes, and TRMM and CHIRPS record similar magnitudes to those recorded by the stations, the bimodal pattern of TRMM tends to be less coherent and with higher values. For regions represented in Figure **2-24** d and e, no rain gauges are inside the cluster described for CHIRPS. Both information data have a discrepancy in the amplitude of the annual precipitation cycle, in general, with overestimation; however, TRMM and CHIRPS have a good representation of the bimodal cycle

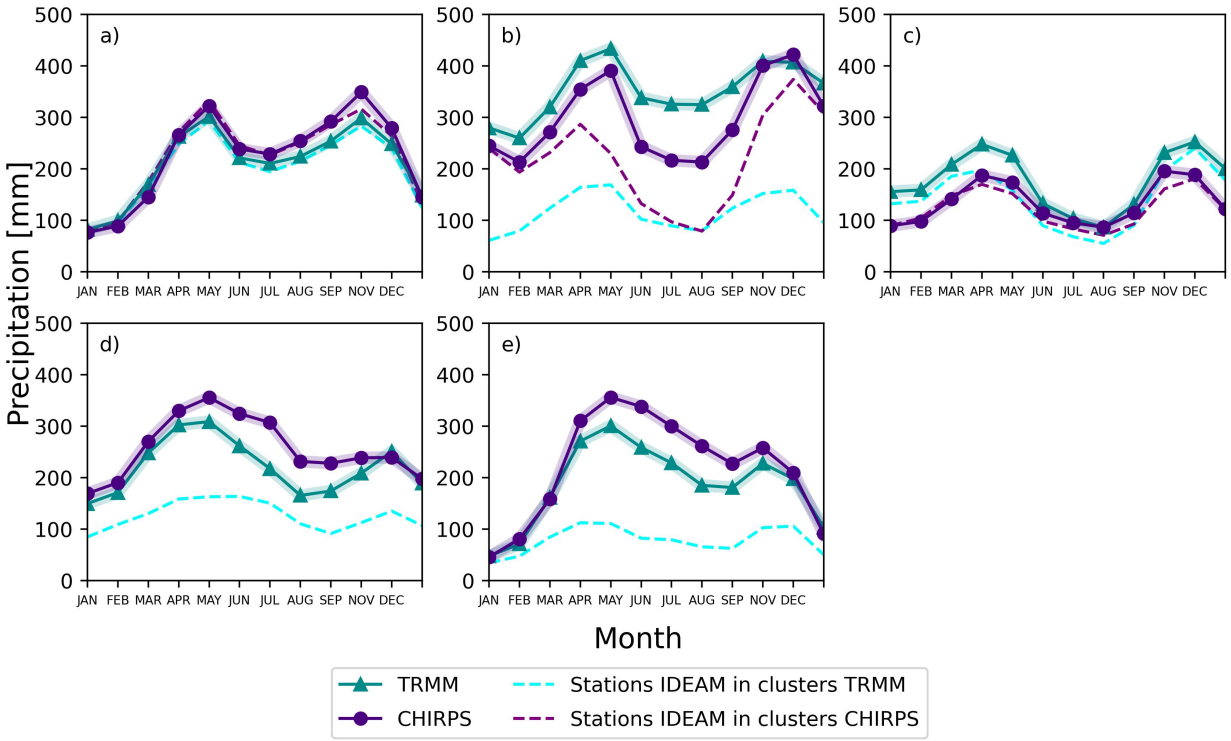

Figure **2-24**.: Annual rainfall cycle for the Andes of Colombia comparing average spatial data from TRMM and CHIRPS satellite sources with mean measurements from IDEAM stations. a) Cluster 1, b) Cluster 2, c) Cluster 3, c) Cluster 4, d) Cluster 4.

(Vallejo-Bernal et al., 2021).

The annual precipitation cycle in each region shows a broad view of rainfall variability in the Andes because of the complex topography that divides the area into mountainous zones and valleys of varying sizes. However, the stations' locations in each cluster are generally located inside the central Andes (not shown), which generates uncertainty about the behavior of the regions further east and west of the Andes. It is known, for example, that west of the Andes bordering the Pacific is the area with the highest accumulated rainfall in Colombia and worldwide (Poveda and Mesa, 2000), and its variability is not registered for stations. And to the east, bordering the eastern plains, circulation phenomena such as the Orinoco low-level jet affect precipitation behavior in that region (Builes-Jaramillo et al., 2022).

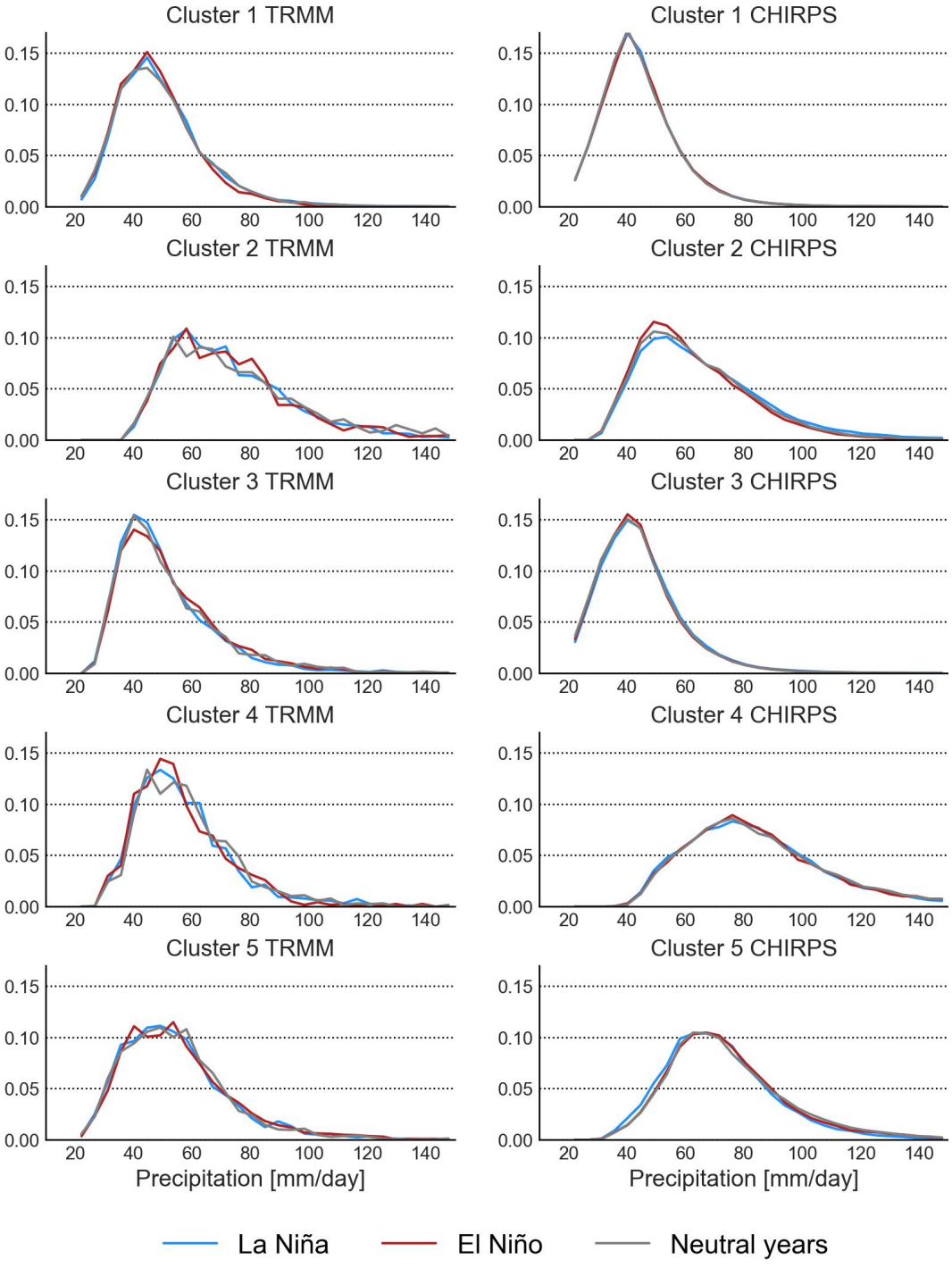

Figure **2-25**.: Histograms of monthly EPEs intensities distribution were found at the 95th percentile for each cluster and discretized by LN, EN, and neutral years. The first column corresponds to the groups found in TRMM and the second in CHIRPS.

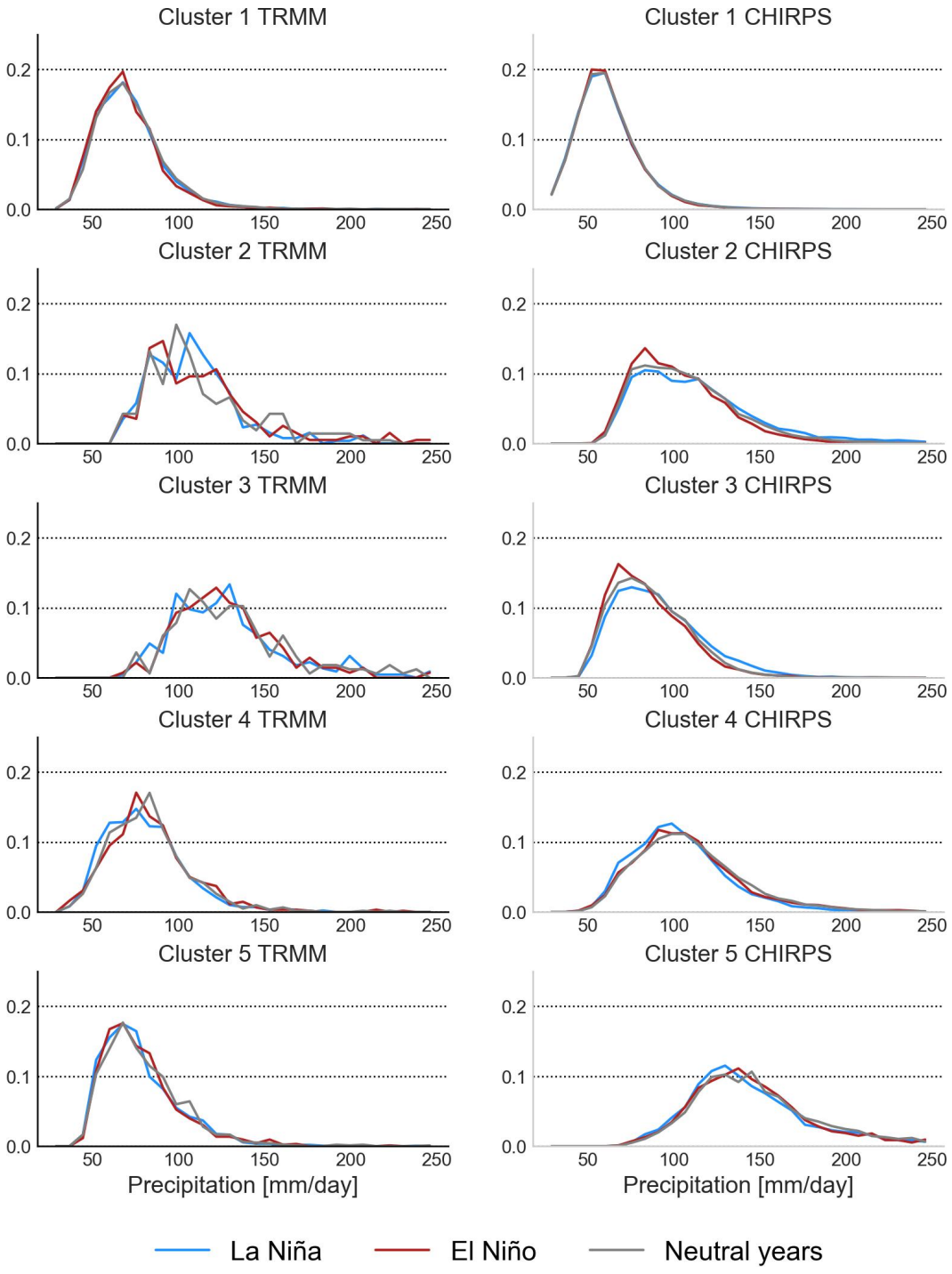

Figure **2-26**.: Histograms of monthly EPEs intensities distribution were found at the 99th percentile for each cluster and discretized by LN, EN, and neutral years. The first column corresponds to the groups found in TRMM and the second in CHIRPS.

For further analysis in the areas of the region classified by clusters, the histogram between

	Intensity 95th percentile									
	TRMM					CHIRPS				
	R1	R2	R3	R4	R5	R1	R2	R3	R4	R5
LN-Neu	0,42	0,11	0,04*	0,09	0,27	0,79	0,38	0,54	0,13	0,04*
EN-Neu	0,03*	0,23	0,73	0,09	0,64	0,70	0,09	0,69	0,58	0,95
LN-EN	6×10^{-4}*	0,80	0,01*	0,76	0,78	0,53	0,02*	0,79	0,32	0,04*
	Intensity 99th percentile									
	TRMM					CHIRPS				
	R1	R2	R3	R4	R5	R1	R2	R3	R4	R5
LN-Neu	0,47	1×10^{-3}*	0,55	0,17	0,82	0,17	0,42	0,67	0,15	0,09*
EN-Neu	0,12	0,53	0,93	0,31	0,69	0,92	0,68	0,01*	0,20	0,73
LN-EN	0,21	0,03	0,52	0,76	0,44	0,24	0,24	0,04*	0,93	0,06*

Table **2-1**.: The p-values were obtained from the U-test in each cluster classification in TRMM and CHIRPS. Values with an asterisk (*) are statistically significant.

ENSO and neutral years and LN-EN was calculated over the study period (from now on, we will refer to the clusters as a region). The distributions represent daily events' monthly intensity and frequency at the 95th and 99th percentile. Furthermore, to ensure the comparison between TRMM and CHIRPS, the events' frequency was standardized by dividing by the number of pixels corresponding Andean region in each database. Finally, to determine the significance of the stations and compare them with other data, the U-test was conducted based on the number of stations present in the TRMM and CHIRPS clusters.

The distribution of intensity of the EPE in the 95th percentile in Figure **2-25** highlights several aspects. First, the frequency of the intensities is similar during LN, EN, and neutral years, as shown in the maps of characterization temporal and spatial (Figures **2-14**, **2-15**, **2-16**, **2-17**). Second, the difference between the regions. For example, Regions 1 and 3 correspond in their totality to the central mountains Andes; i.e., high frequencies are low intensities, and the maximum magnitude is approximately 80 mm/day.

On the other hand, in clusters 2, 4, and 5, the events in ENSO phases and neutral years start at higher intensities than in clusters 1 and 3. In low frequencies, the intensity of events can be higher compared to regions 1 and 3, with values around 120 mm/day. The database results agree that in TRMM and CHIRPS, in TRMM, neutral years tend to have a slightly higher frequency than LN and EN, while in CHIRPS, intensities EPEs in LN are higher frequencies (Figure **2-25**).

TRMM showed differences in the distribution in the 99th percentile (Figure **2-26**). Although the EPEs are more intensities in neutral years than in LN and EN in clusters 1, 2, 3, and 4, the frequency is high at low intensities in LN and EN compared to neutral years, e.g.,

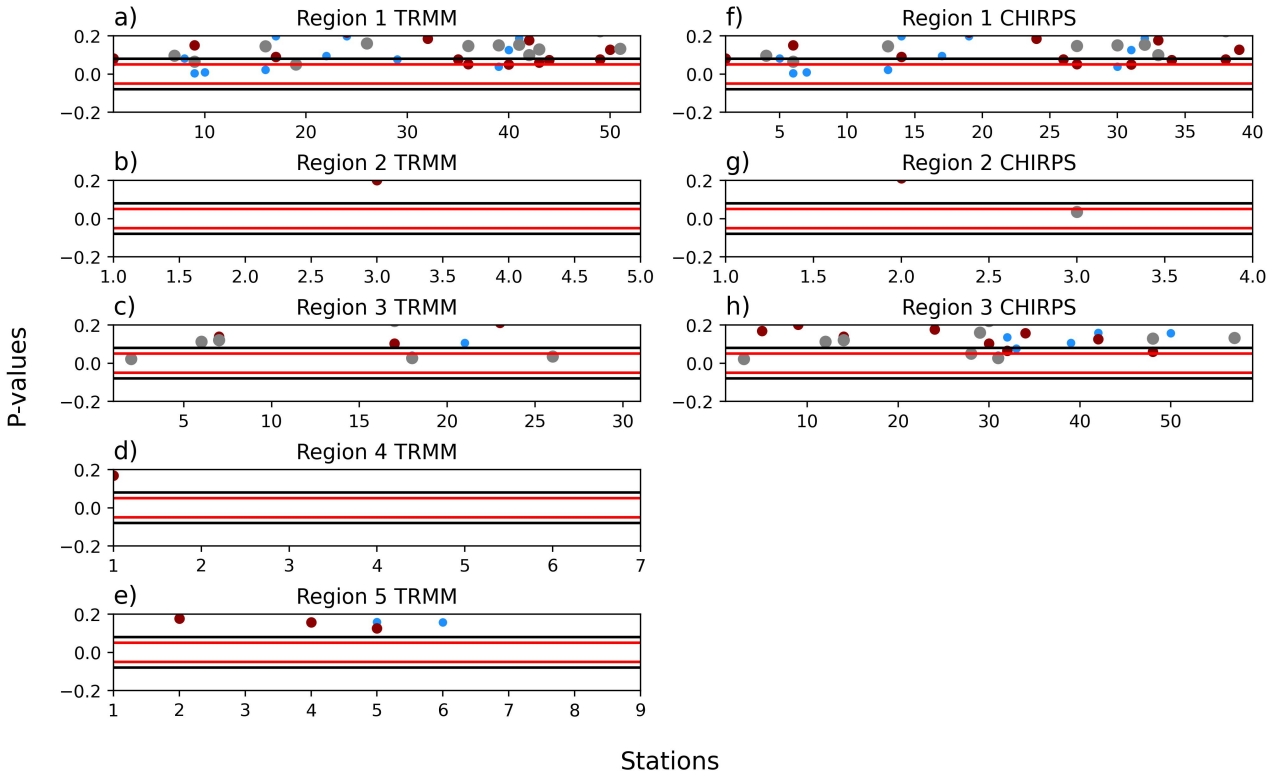

Figure **2-27**.: The p-values of the stations were obtained from the U-test conducted by the EPEs intensity series at the 95th percentile, LN-neutral years (blue), En-neutral years (red), and LN-EN (gray). The number of stations corresponds to those found in each cluster in TRMM or CHIRPS. The red line has the value of -0.05 and 0.05, and the black line of -0.08 and 0.08. Stations with p-value < 0.05 fall in the range of the red line values. CHIRPS regions 4 and 5 are not plotted because there are no stations within these zones.

extreme events with lower intensity are highlighted when one of the ENSO phases is active. In Region 5, the magnitudes higher are in EN in TRMM, even with high values that are not reached in LN and neutral years. However, the distribution and analysis in CHIRPS are analogous to the 95th percentile, where the difference between LN, EN, and neutral years is minimum.

Mann Whitney test or U-test was used to determine whether the influence of ENSO is significant, so the null hypothesis is to test whether the median in the ENSO is equal to the median in the neutral years or between both ENSO phases. If the null hypothesis is rejected, the medians are different; therefore, the magnitudes for ENSO events and neutral years differ in amplitude. Unfortunately, few regions were statistically significant; in TRMM, cluster 1 was significant in EN-neutral years and LN-EN, and cluster 3 in LN-neutral years and LN-EN at the 95th percentile, in CHRIPS in LN-EN in clusters 1 and 5 during LN-neutral years

and LN-EN, which is difficult to determine the impact of ENSO in the Andes (Table **2-1**).

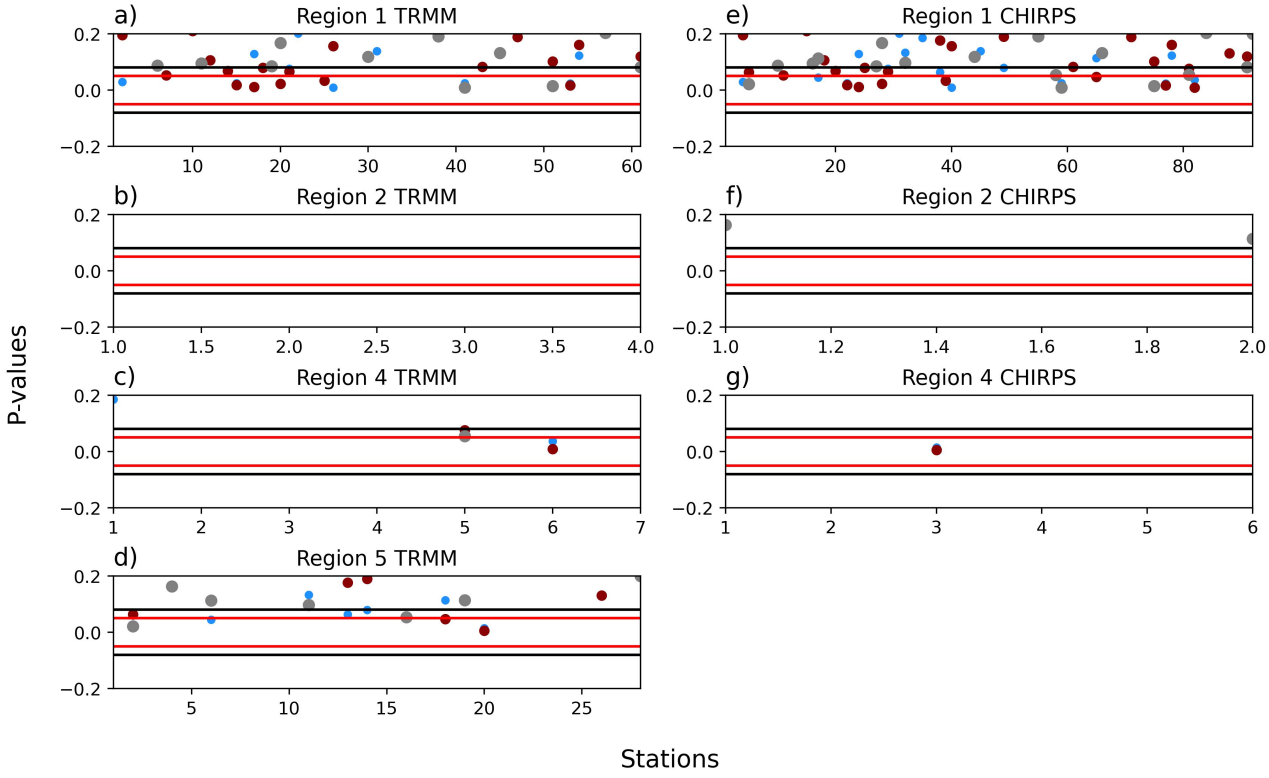

Figure **2-28**.: The p-values of the stations were obtained from the U-test conducted by the EPEs intensity series at the 99th percentile, LN-neutral years (blue), En-neutral years (red), and LN-EN (gray). The number of stations corresponds to those found in each cluster in TRMM or CHIRPS. The red line has the value of -0.05 and 0.05, and the black line of -0.08 and 0.08. Stations with p-value < 0.05 fall in the range of the red line values. CHIRPS regions 4 and 5 are not plotted because there are no stations within these zones.

Nevertheless, TRMM has better agreement with the stations, with more significant stations in clusters 1 and 3, in Region 1 with LN-neutral years and cluster 3 with LN-EN (Figure **2-27**). The intensities at the 99th percentile are shown in the cluster 2 significance in LN-neutral years and CHIRPS the clusters 3 and 5, the first in EN-neutral years and LN-EN, and second in LN-neutral years and LN-EN.

Figure **2-28** shows that the number of events is high in TRMM and CHIRPS in cluster 1, particularly the events that are predominant during LN in TRMM. Conversely, the frequency of events decreases in clusters 2, 3, and 4; likewise being the LN phase where most EPEs occur; while in cluster 4, the events are more frequent during EN in TRMM, and magnitudes similar in EN and neutral years in CHIRPS.

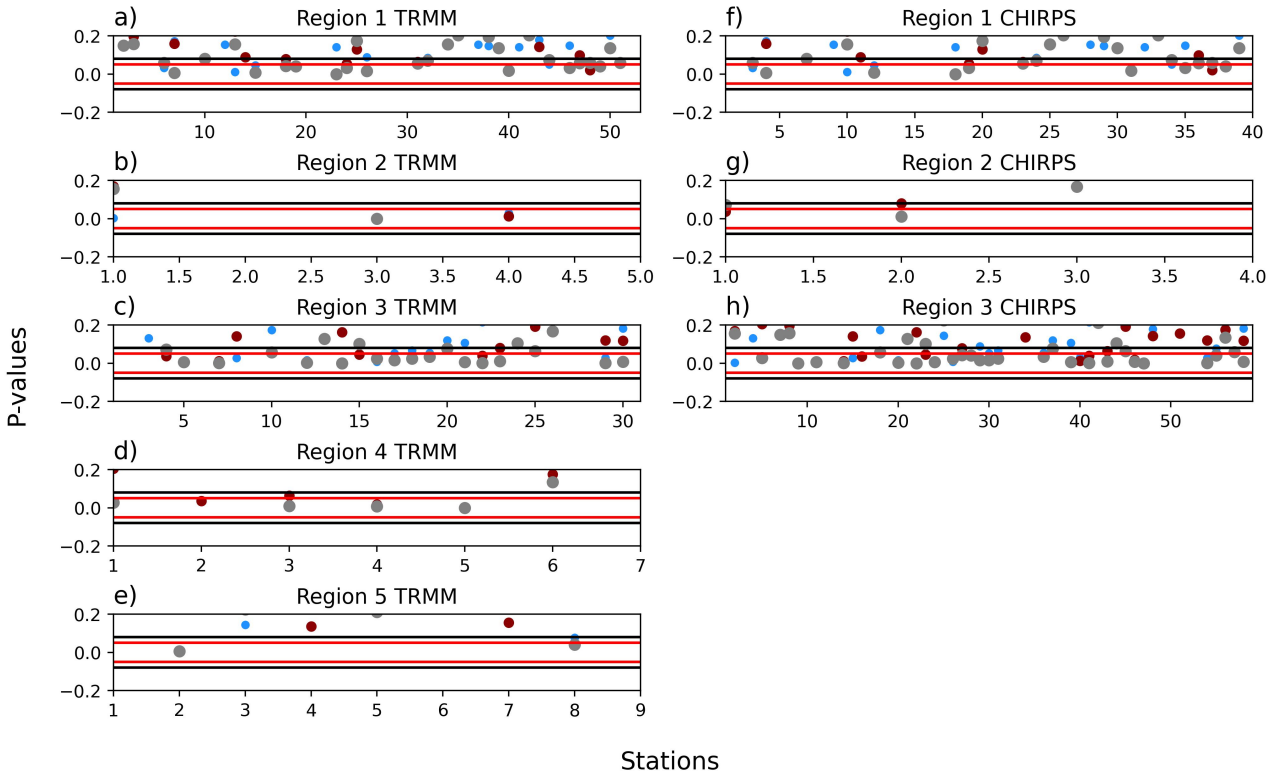

Figure **2-29**.: The p-values of the stations were obtained from the U-test conducted by the EPE frequency series at the 95th percentile, LN-neutral years (blue), En-neutral years (red), and LN-EN (gray). The number of stations corresponds to those found in each cluster in TRMM or CHIRPS. The red line has the value of -0.05 and 0.05, and the black line of -0.08 and 0.08. Stations with p-value < 0.05 fall in the range of the red line values. CHIRPS regions 4 and 5 are not plotted because there are no stations within these zones.

IDEAM's stations obtain significance between LN and EN. In the 95th percentile, 10% of stations located in cluster 1 in TRMM were significant, and 13% in cluster 3. Clusters 1 and 3 of CHIRPS were significant at 75% and 22%, respectively. It should be recalled that the number of stations within each region is not homogeneous, and Regions 1 and 3 are where the stations are concentrated (Figure **2-29**).

Moreover, in the 99th percentile, clusters 1 and 5 have 6% and 5% of stations with significant differences between LN and EN, respectively. Only cluster 1 in CHIRPS 9% of stations were significant of 92 stations, which is deficient in significance (Figure **2-30**).

The black lines in Figures **2-27**, **2-28**, **2-29**, and **2-30** are intended to show that although the stations are not within the zone of significance, they were not far away. Therefore the effects of ENSO or neutral years on the frequency and intensity of extreme precipitation

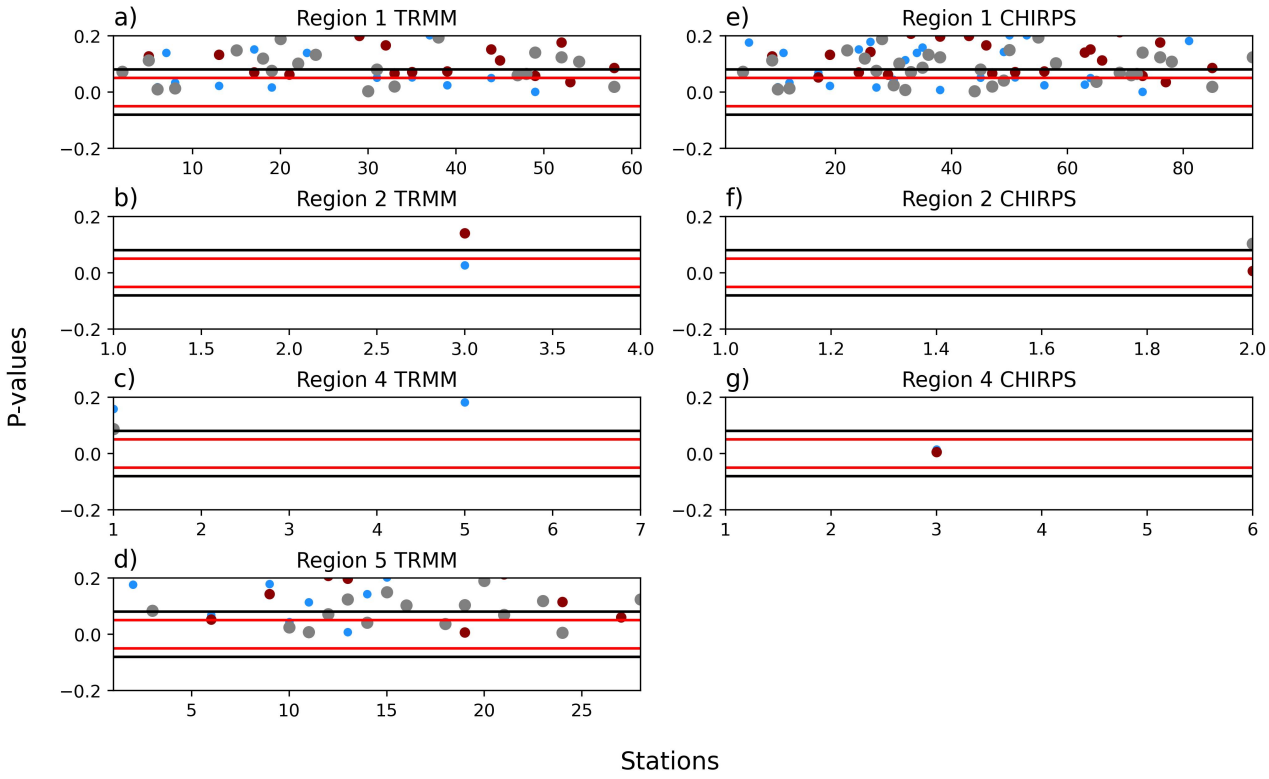

Figure **2-30**.: The p-values of the stations were obtained from the U-test conducted by the EPE frequency series at the 99th percentile, LN-neutral years (blue), En-neutral years (red), and LN-EN (gray). The number of stations corresponds to those found in each cluster in TRMM or CHIRPS. The red line has the value of -0.05 and 0.05, and the black line of -0.08 and 0.08. Stations with p-value < 0.05 fall in the range of the red line values. CHIRPS regions 4 and 5 are not plotted because there are no stations within these zones.

events should not be underestimated.

2.3. Conclusions

We study the intensity and frequency of extreme precipitation events in the Colombian Andes. For this purpose, we performed a characterization with *in-situ* information from 100 stations from IDEAM and two satellite databases (TRMM and CHIRPS). Here, we define extreme events as the daily precipitation value that exceeds a threshold obtained from the 95th and 99th percentiles for extreme and very extreme events, respectively. In addition, for regions with complex topography like the Andes, a threshold value was established for each station and each pixel in the database to reflect the precipitation variability.

Our results indicate that the intensity in the EPEs at both percentiles does not differ in magnitude between ENSO and neutral years and is in agreement in all three databases. EPEs values are lower east and west of the Andes, and higher magnitudes are found north and around the center in TRMM and CHIRPS. The stations differ slightly in magnitudes west of the Andes, where values are moderate. For the surroundings of the Colombian Andes, the values in both percentiles are high on the Pacific coast, southern Colombia, at the border of the Ecuadorian territory, and lower intensities are observed in the eastern Colombian plains and the north of the territory on the Caribbean coast (Figure **2-2**).

The MAM and SON seasons have the highest extreme events during the year for both percentiles. The heatmaps clearly show this pattern with databases TRMM and CHIRPS and agree with those indicated by the station averages (Figures **2-3** and **2-4**). Although the intensities do not reveal a specific pattern between months, the data provided by CHIRPS have the highest intensities in June-July-August, which can suggest that the database possibly presents problems in representing precipitation intensities in the tail of the distribution. Araujo et al. (2020) also found that CHIRPS underestimates extreme events at the 99th percentile, while TRMM overestimates. Estimating EPEs depends on the geographical location and the large-scale precipitation regime, and it must be taken into account that satellite databases present uncertainties at both low and high altitudes.

Based on the analysis of the EPEs, it can be inferred that the event intensities remain relatively consistent throughout the year and do not exhibit significant differences in magnitude between LN, EN, and neutral years for both the 95th and 99th percentile. Remarkably, the magnitudes of the *in situ* station intensities are much larger west of the Andes at the 95th percentile and over the entire area at the 99th percentile (Figures **2-6**, **2-8**, **2-10** and **2-12**) compared to TRMM and CHIRPS. On the other hand, CHIRPS mainly shows some differences during LN at the 99th percentile, with no events in the Andes and higher magnitudes to the south, specifically at the Ecuadorian border and in the eastern plains.

The frequency-based analysis of EPE characterization reveals the following: i) Events occur year-round, but their frequency varies in different seasons, both in the Andes region and the rest of the territory, specifically at the 95th percentile (Figures **2-7**, **2-9**, **2-11** and **2-13**). In DJF, the databases show that the events are higher west of the Andes and north of the study region and have moderate frequencies in the rest of the area. In CHIRPS, during this season, there are important events to the east near Venezuela, which TRMM does not record. Then in MAM, the frequencies are higher to the north and east of the Andes. During JJA, increased magnitudes are observed throughout the Andes and south of the study region. Finally, in SON, the most critical events are concentrated north of the Andes and Colombia. ii) It appears that EPEs are more frequent during LN compared to EN and neutral years, and iii) The pattern in the 99th percentile is similar in the 95th percentile. However, the frequency decrease due to the unlikelihood of getting events in this threshold (Figures **2-7**, **2-9**, **2-11** and **2-13**).

The results of the ENSO and neutral years comparison vary between information provided by the databases, mainly in the frequency of events. The intensity at the 95th and 99th percentile was not conclusive, i.e., it was not observed whether extreme events (LN, EN, and neutral years) predominate in any ENSO phase (Figures **2-6**, **2-8**, **2-10** and **2-12**). However, The difference in frequencies was significant mainly in the Andes, and between LN-neutral years and LN-EN, CHIRPS showed larger areas with significance. On the other hand, the frequencies highlight more events during LN than in neutral years and EN. TRMM and CHIRPS had differences in the frequency comparison between EN and neutral years at the 95th percentile and at the stations. In TRMM, it was observed that EN events might be more frequent than in neutral years, but CHIRPS showed in some places in the Andes the opposite. In the 99th percentile, the same may be true, even if one of the databases records EPEs in the Andes and the other does not. Although the results in CHIRPS for the Andes are congruent with TRMM, it also differs in other regions where it clearly shows the impact of neutral years and EN compared to LN (Figures **2-6**, **2-8**, **2-10** and **2-12**). It is relevant to mention that few stations were significant in this comparison and therefore did not show a pattern.

To complement the characterization of EPEs in the Andes, we used k-means cluster analysis to identify if there are regions that share the same characteristics in the intensity of an extreme event. In this sense, to perform the clustering, we analyzed the daily precipitation extremes, and there we found five 95th and 99th percentile regions that possibly present homogeneity due to their characteristics. Additionally, we compared the areas with the monthly intensity, the daily information did not provide sufficient information. The monthly distribution of the EPEs showed differences in intensity and frequency between the regions; in some frequencies, some of the intensities are high, for example, in clusters 1 and 3 (Figures **2-25**, **2-26**). As in the spatial and temporal analysis, the intensity of the events does not differ in magnitude between LN, EN, and neutral years in the 95th percentile.

In the U-test, all clusters exhibited a surprising predominance of a single phase of ENSO or neutral years; however, this predominance was statistically significant in a few clusters.

In summary, the increase in average precipitation during LN may increase the EPEs in the Andes region. It was found throughout this work that the intensity of the events may not present high differences when the active phase of LN, EN, or neutral conditions are present. In the Andes, some regions have similar event intensities. Additionally, LN years have a higher event occurrence rate than neutral years, even though events still occur during neutral years and should not be disregarded.

3. Characterization and comparison of extreme temperature events

Abstract

The El Niño Southern Oscillation (ENSO) is a critical climate modulator in northern South America, and its El Niño (EN) and La Niña (LN) phases cause anomalies in hydroclimatic variables, including surface temperature and its extreme values. This study characterizes extreme temperature events (ETEs) during ENSO and neutral years, specifically in the Colombian Andes, eliminating the temperature trend using linear regression to minimize the influence of climate change. Extreme temperature events are characterized by their intensity and frequency in diurnal and nocturnal periods. We use the 90th percentile indices for daily maximum temperature extremes (TXx) and the 10th percentile for daily minimum temperature extremes (TNn). The results indicate that sea surface temperature (SST) is correlated and has a significant relationship with TXx and TNn extremes. In addition, diurnal and nocturnal TXx and TNn extremes were found to be more intense during EN. On the other hand, TXx extreme events are more frequent during EN, while TNn extremes are more frequent during LN, both in diurnal and nocturnal periods. In summary, it is observed that warmer days and nights are more frequent and intense during EN, while cold days and nights are less intense and more frequent in LN.

Keywords

Extreme temperature events; El Niño-Southern Oscillation (ENSO); maximum temperature, mínimum temperature, Andes, intensity; frequency; trend.

3.1. Data and methods

We used hourly data of air temperature at 2 meters with a horizontal resolution of 0.25° taken from the product of ERA5 reanalysis of The European Center for Medium-Range Weather Forecast (ECMWF) (Hersbach et al., 2020) for the period 1979-2019. Since the last century, a steady temperature increase has been observed worldwide with a positive trend in minimum, mean, and maximum temperature (Alexander, 2016; Dunn et al., 2020; IPCC, 2021). In South America, this has been evidenced in several works (Aguilar et al.,

2005; Meseguer-Ruiz et al., 2018; Pabón-Caicedo, 2012; Rodríguez et al., 2019; Rusticucci et al., 2017; Salvador and de Brito, 2018; Skansi et al., 2013). Therefore, to corroborate the existence of a trend in the region, we used the non-parametric Mann-Kendall test. Additionally, to examine how the ENSO impacts ETEs, the trend was removed to rule out any climate change effects, i.e., the increasing trend in temperature. For this purpose, we used linear regression to remove the hourly trend in the time series (Foster and Rahmstorf, 2011).

Subsequently, ETEs were characterized for daytime and nighttime periods and then aggregated into daily intervals. In each period and pixel, two indices were used; the extreme of daily maximum temperature (TXx) and the extreme of daily minimum temperature (TNn). These indices were estimated for the 90th and the 10th percentiles, respectively. The threshold calculated per pixel allows for studying the spatial variability of temperature extremes because the Andes have altitudinal gradients with steep orography and valleys. To explore the relationship between the time series of sea surface temperature anomalies of the Niño 3.4 region and the extreme indices for the 90th and 10th percentiles, we calculated the correlation between these variables. Then, we performed a Spearman correlation analysis to determine the strength and direction of the relationship between the two time series.

The ETEs were characterized as EN, LN, and neutral years. To identify ENSO and neutral events, we used the Oceanic Niño Index (ONI), which is calculated from a 3-month running mean of SSTs in a central Pacific region defined as Niño-3.4 (5°N-5°S, 120°-170°W). This index is estimated based on centered 30-year base periods updated every five years. An EN (LN) event occurs if the ONI remains at or exceeds 0.5°C (-0.5°C) for a period of at least five consecutive months.

Finally, to compare ETEs between El Niño, La Niña, and neutral years, we calculated differences for extreme event characterizations between ENSO phases and neutral years. Then, to verify if extreme events prevail in intensity or frequency statistically, we used the t-test. In addition, we plotted specific histograms for the Colombian Andes region, and we used a non-parametric U-test to compare the distribution of extreme events between ENSO years and neutral years in this region.

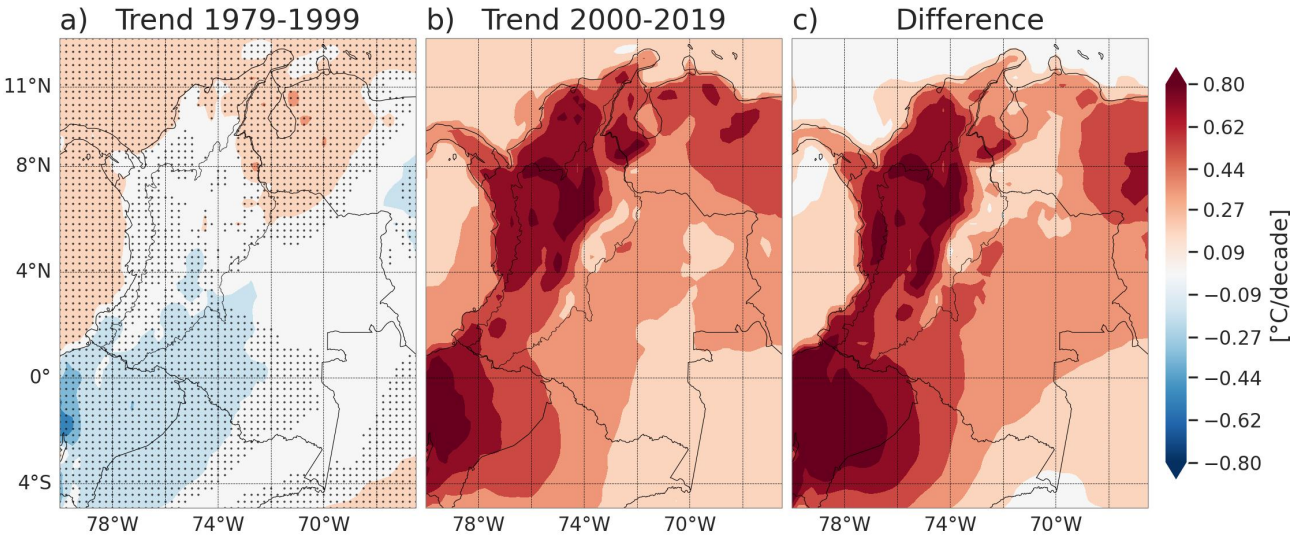

Figure **3-1**.: Linear trends for daily temperature in two periods: a) 1979-1999, b) 2000-2019, and c) difference between both periods. In a) hatched areas show significant trends with a confidence level of 95%, while in b) the whole shaded area corresponds to statistically significant temperature trends.

3.2. Results and discussion

3.2.1 The impact of ENSO on extreme temperature events

Figure **3-1** compares trends between two periods, before and after the 2000s. Various statistical techniques have been implemented to find robust results on surface temperature trends. This research used the non-parametric Mann-Kendall test, which has proven to be equally stringent. The positive trends after the pre-industrial era are irrefutable, and scientific knowledge has increased the reliability of such results (IPCC, 2021). Between 1979 and 1999, low positive values trends were observed in the Caribbean Sea, and some negative trends are shown to the south (Figure **3-1**a) between Ecuador and Colombia, indicating the impact of a possible external forcing. Then, in the period 2000-2019, there was an increase in positive and significant trends throughout the study area, particularly in the Colombian Andes (Figure **3-1**b). The differences between the two periods show positive magnitudes throughout the area and equally high in the Andes region (Figure **3-1**c), suggesting a much more marked and significant trend after 2000, when temperatures began to increase more drastically (Foster and Rahmstorf, 2011).

Similar results have been found in South America (de Barros Soares et al., 2017), with high and significant positive trends in Brazil and in a few regions, including Colombia. However,

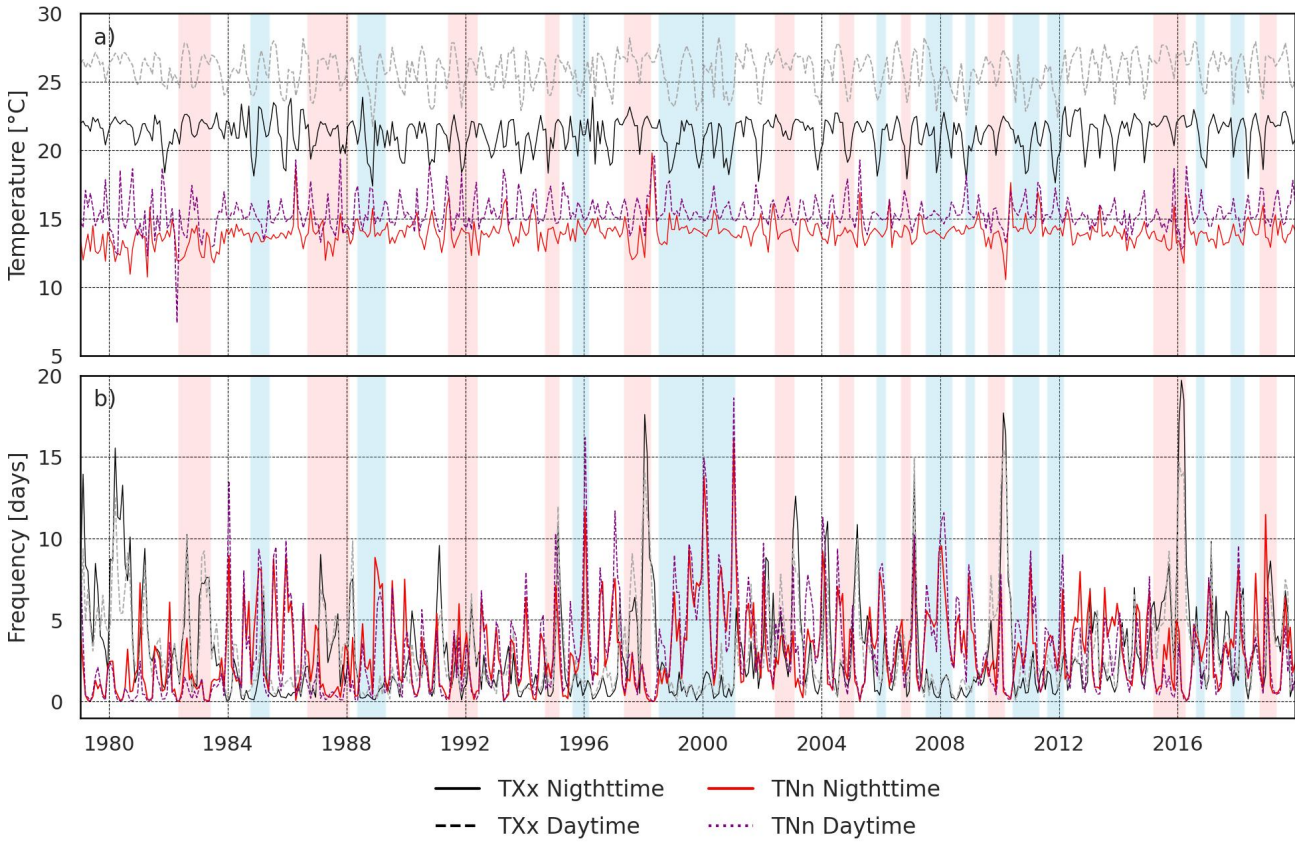

Figure **3-2**.: Time series of extreme values indices: daily TXx 90th percentile and daily TNn 10th percentile in daytime and nighttime. a) Intensity and b) Frequency. The blue shading refers to LN events, and the red shading to EN events.

it should be noted that they used another methodology to find trends in the data. Many studies focus on the change in TXx and TNn due to their importance in extremes (Aguilar et al., 2005; Arblaster and Alexander, 2012; Alexander, 2016), because the observed and simulated data have agreed with positive trends and indicate an increase in warm days at the 90th percentile. In contrast, the frequency of cold nights (10th percentile) has decreased, consistent with the observed warming in global surface temperature and trends in TXx and TNn in South America (Aguilar et al., 2005; Alexander, 2016; Dunn et al., 2020; IPCC, 2021; Rusticucci, 2012; Salvador and de Brito, 2018). But the change has been more rapid related to daily minimum temperature extremes than those daily maximum temperature extremes. Regarding daily temperature extremes in regions with complex topography, it has been studied that altitude strongly affects the minimum temperature extremes more than the maximum ones; however, these results are not conclusive due to the scarcity of information in regions with high altitudes and the bias that can present the databases as reanalysis (Meseguer-Ruiz et al., 2018).

In Figure **3-1**, we wanted to show that the positive trend in temperature is a fact. We analyzed the trend in different time scales and found positive and significant slopes. For the characterization of the ETEs, we removed the trend from the hourly resolution.

Once the trend was removed, daily diurnal and nocturnal ETEs were calculated for the indices TXx at the 90th percentile and TNn at the 10th percentile. Figure **3-2** shows the Colombian Andes' time series and the ETEs evolution in intensity and frequency. The series shows no trend pattern to mitigate the effects of climate change as far as possible. On the other hand, there is a marked seasonality in the indices, which indicates the influence of insolation cycles during the year for this tropical region. As for the events of the TXx extremes, they fluctuate more during the day than the TNn extremes. (Figure **3-2**).

Figure **3-2**a shows a difference in the magnitudes of the intensity of the TXx extremes at day and night and almost similar magnitudes at the TNn extremes. However, the intensity of both indices is not different between EN, LN and neutral years. The most remarkable feature in Figure **3-2**b is the high occurrence of ETEs; during LN, the TNn extremes are higher in both periods (diurnal and nocturnal) compared to EN or neutral years. The opposite happens with the TXx extremes, being higher during EN. In Figure **3-2**, it is possible to highlight the highest peaks of ETEs in intense and prolonged ENSO events.

During EN, the Colombian Andes experience warmer and drier conditions than usual; due to changes in atmospheric circulation patterns caused by the warming of the Pacific Ocean, which lead to a decrease in rainfall and an increase in temperature. Decreased precipitation, soil humidity, and water flow directly affect temperature, which explains changes in its extreme values, in this case, in the maximum and minimum temperatures (Espinoza et al., 2020; Poveda et al., 2005, 2011).

The ENSO index is correlated with extreme temperatures. Figures **3-3**a and **3-3**b show

positive and significant correlation coefficient values between sea surface temperature (SST) anomalies and the intensity of TXx extremes in the daytime and nighttime time series in several regions, including the Pacific Ocean, the Colombian Andes, Ecuador, and east of territory. It has been observed that significant correlations are present in the Pacific Ocean, although the influence of ENSO in the Andes has also been highlighted (Bedoya-Soto et al., 2019; Poveda et al., 2001; Waylen and Poveda, 2002). Positive and significant correlations persist for the extremes of TNn (Figures **3-3**c and d), which extend from the Pacific Ocean to the Caribbean Sea, concentrating mainly in the central and northern Andes. However, these significant correlations decrease in the daytime series and become more localized north and south of the Andes. The results indicate a clear relationship between temperature extremes and the geography of the region studied.

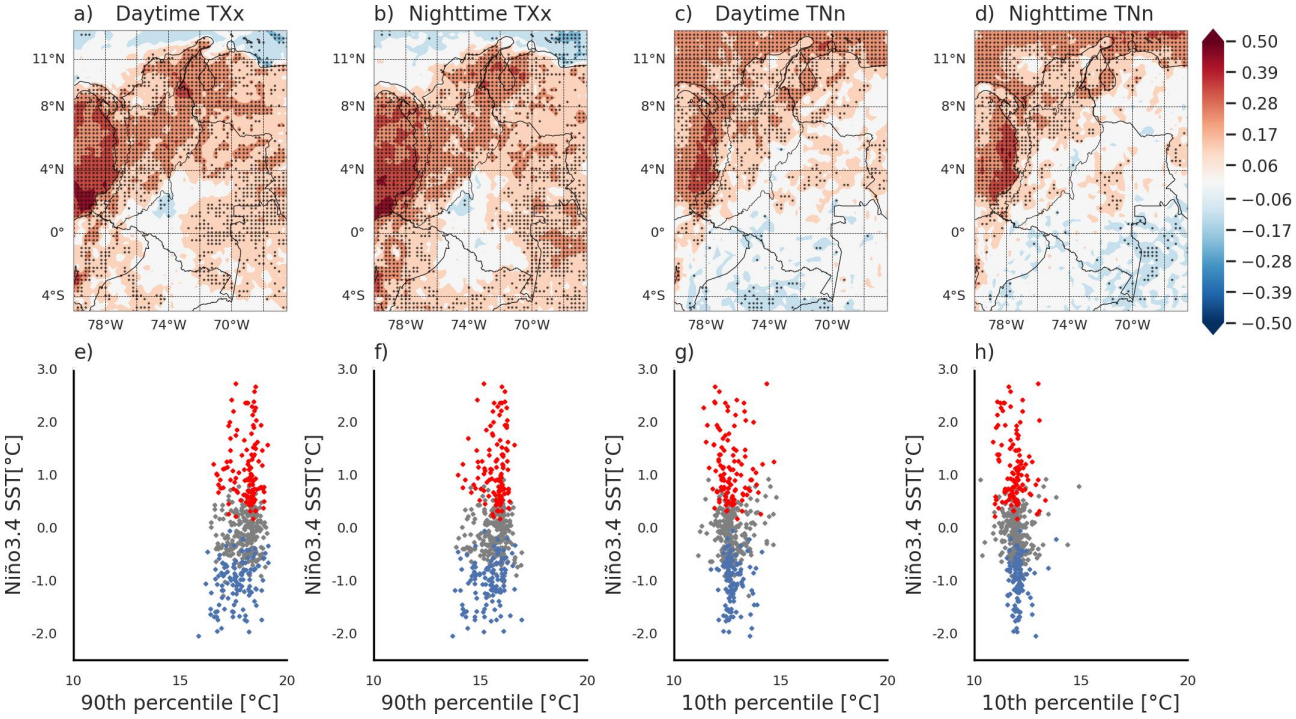

Figure **3-3**.: Correlation between sea surface temperature (SST) anomalies of the Niño 3.4 region and the frequency of the ETEs indices. a) Daytime TXx extremes, b) Nighttime TXx extremes, c) Daytime TNn extremes, and d) Nighttime TNn extremes. Panels a) to d) depict the correlation, with hatched regions indicating significant associations at a 0.05 p-value. The second row represents the scatter plot only for the Andes between the same variables; the points are discriminated in the values corresponding to LN (blue), EN (red), and neutral (gray). e) Daytime TXx extremes, f) Nighttime TXx extremes, g) Daytime TNn extremes, and h) Nighttime TNn extremes.

We also wanted to show the relationship between ENSO and the indices using a scat-

ter plot, highlighting which periods corresponded to EN, LN, and neutral years for both databases. The results show that SST anomalies are related to the indices of temperature extremes. Positive SST anomalies in EN and the negative SST anomalies during LN are about high intensities at the TXx extremes and low at TNn, respectively. The values of the SST anomalies and the indices have a directly proportional relationship, i.e., the warmer the Pacific Ocean, the greater the intensity of the TXx extremes. But if the ocean is colder than normal conditions, the extremes are more minimal (TNn). In neutral years, this relationship is in the middle, indicating the strong correlation with ENSO and ETEs indices (Figures **3-3**e, f, g, and h).

The frequency of extreme temperature events and their relationship with SST anomalies is remarkable. In general, it is observed that when SST anomalies are positive, the frequency of extreme TXx events is higher. In contrast, when SST anomalies are negative, there is a higher frequency of extreme TNn events. Furthermore, a significant correlation was found for extreme events TXx and TNn in almost the entire region, except in a portion of the plains region in TXx (Figures **3-3**a, b, c, and d).

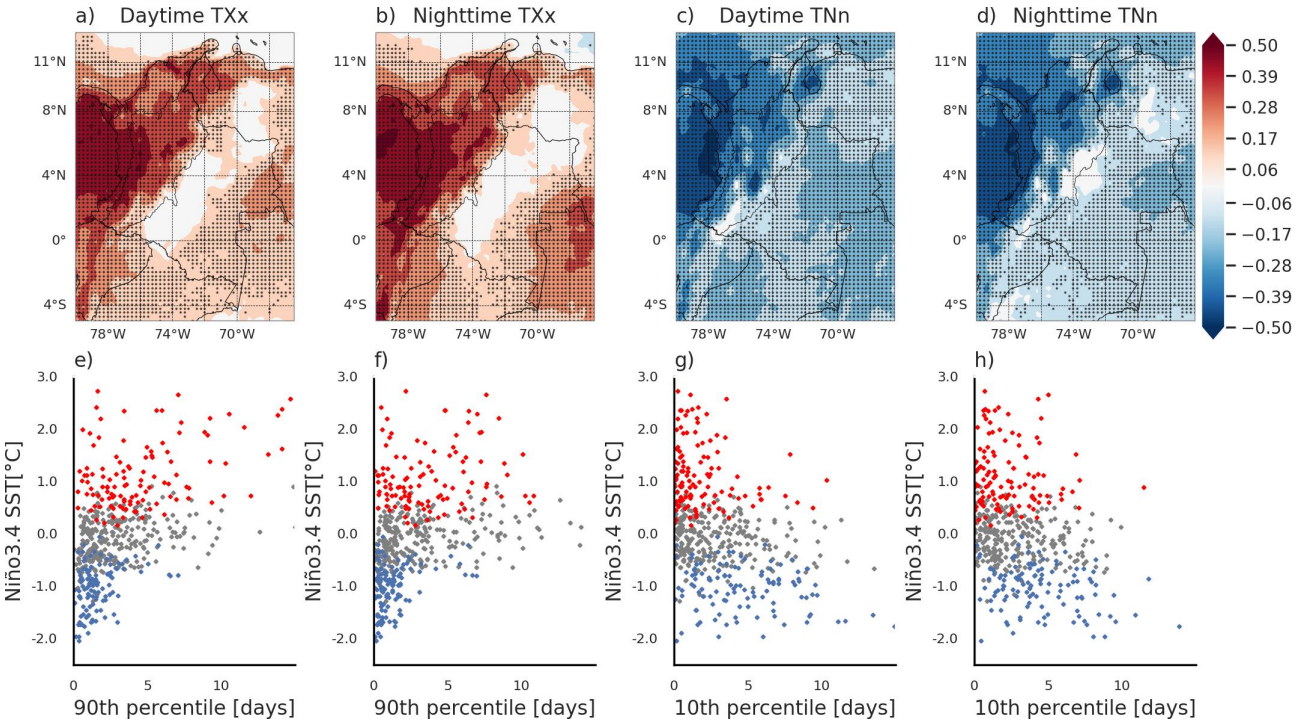

Figure **3-4**.: Correlation between sea surface temperature (SST) anomalies of the Niño 3.4 region and the frequency of the ETEs indices. a) Daytime TXx extremes, b) Nighttime TXx extremes, c) Daytime TNn extremes, and d) Nighttime TNn extremes. The second row represents the scatter plot only for the Andes between the same variables; the points are discriminated in the values corresponding to LN (blue), EN (red), and neutral (gray). e) Daytime TXx extremes, f) Nighttime TXx extremes, g) Daytime TNn extremes, and h) Nighttime TNn extremes.

Figures **3-3**e, f, g, and h show that TXx extremes occur more frequently during EN years and when SST anomalies are positive, while for LN, extreme events are less frequent when the anomalies are negative. On the other hand, for TNn extremes, the opposite is true: negative values in SST anomalies indicate a higher frequency of these events, and warmer temperatures are associated with a lower occurrence of events in this index. During neutral years, when SST anomalies are between LN and EN, the frequency of TXx extremes can be as high as during EN events, and the occurrence of TNn extremes can be as high as in periods when LN occurs.

Bedoya-Soto et al. (2019) demonstrated from the correlation between SST anomalies in the El Niño 3.4 region with the singular value decomposition (SVD) that there is a positive correlation between EN and surface temperature throughout northern South America. According to the results found in this work, the surface temperature is strongly influenced by ENSO.

3.2.2 Characterization and comparison of ETEs

Characterization of extreme temperature events was carried out in a broad area to show their distribution in the Andes and its surroundings. The results were analyzed and presented for the December-January-February (DJF) and June-July-August (JJA) seasons since these are the seasons that show the most relevant differences.

Figures **3-5**a and b show that the intensity values of diurnal TXx in DJF are lower in the Andes because of higher altitudes. The intensity of extremes is high in the Magdalena basin and around the Andes, where elevations are low. During JJA, no extreme values are observed in the plains between Colombia and Venezuela in any of the ENSO periods or neutral years. There are a few differences in the intensities of the events between ENSO and neutral years, and there are regions where there is no presence of ETEs, for example, during LN in the Caribbean Sea. In contrast, in that same region, there are events during EN.

In the Andes region, TNn extremes are lower in areas with higher altitudes, while moderate indice intensities are observed in the inter-Andean valleys. It is also observed that extreme TNn's intensity is more minimal in EN than in Ln and neutral years during the daytime (Figures **3-5**c and d). Outside the Andes, indice intensities may be slightly higher. During the nighttime, the intensities of TXx extremes are marginally reduced in the Andes, whereas very high-intensity values are observed in DJF in Venezuela during ENSO active phases and neutral periods, except for JJA in LN (Figures **3-6**a and b). Results do not show TXx events in the plains of Colombia and Venezuela in DJF. TNn extremes tend to extend further eastward in the region at night, covering other mountains like the Sierra Nevada in Santa Marta or the mountain range in Venezuela. EN often experiences the lowest TNn values compared to LN and neutral years.

The impact of ENSO on ETE is reflected in the frequency of these events. DJF shows less recurrence of TXx extremes in LN years but is more frequent in EN and neutral years, with EN having the highest values (Figure **3-7**a). The frequency of such events is higher from south to east of the territory, with the eastern plains of Colombia experiencing the highest values in EN and neutral years, along with northern Colombia and the Pacific region. Extreme TXx events in JJA are less prominent. During EN and neutral years, high frequencies occur in the Andes, northern Colombia, the Caribbean Sea, and the Pacific Ocean, while few events happen to the territory's east. LN shows an average of 6 to 7 events throughout the Andes, lower than during EN and neutral years (Figure **3-7**b).

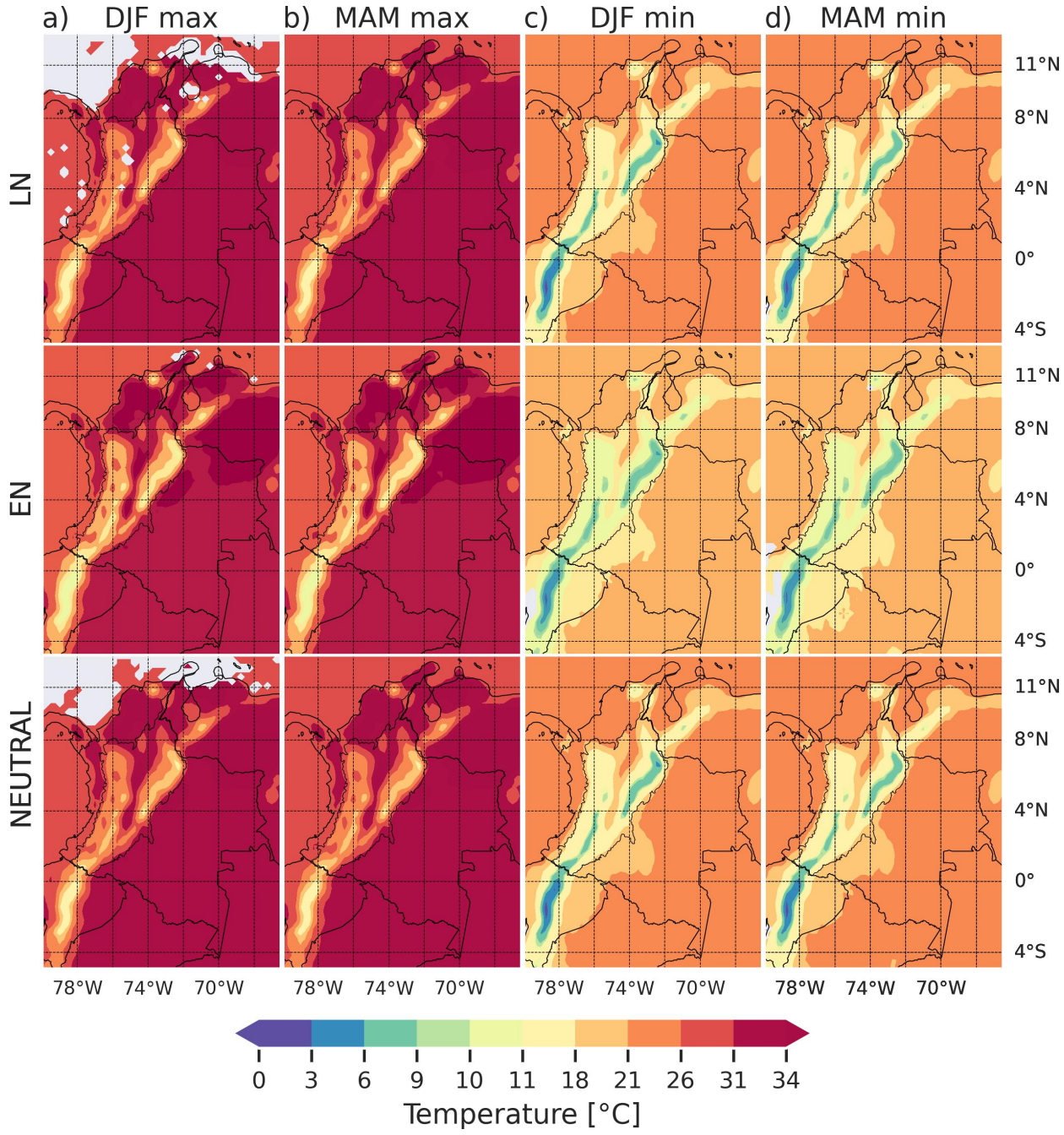

Figure **3-5**.: The index indicates the intensity of extreme events that occur during the daytime. These events include a) TXx in DJF, b) TXx in JJA, c) TNn in DJF, and d) TNn in JJA. Furthermore, the extreme events are categorized in the first row as occurring during LN years, in the second row as occurring during EN years, and in the third row as occurring during neutral years.

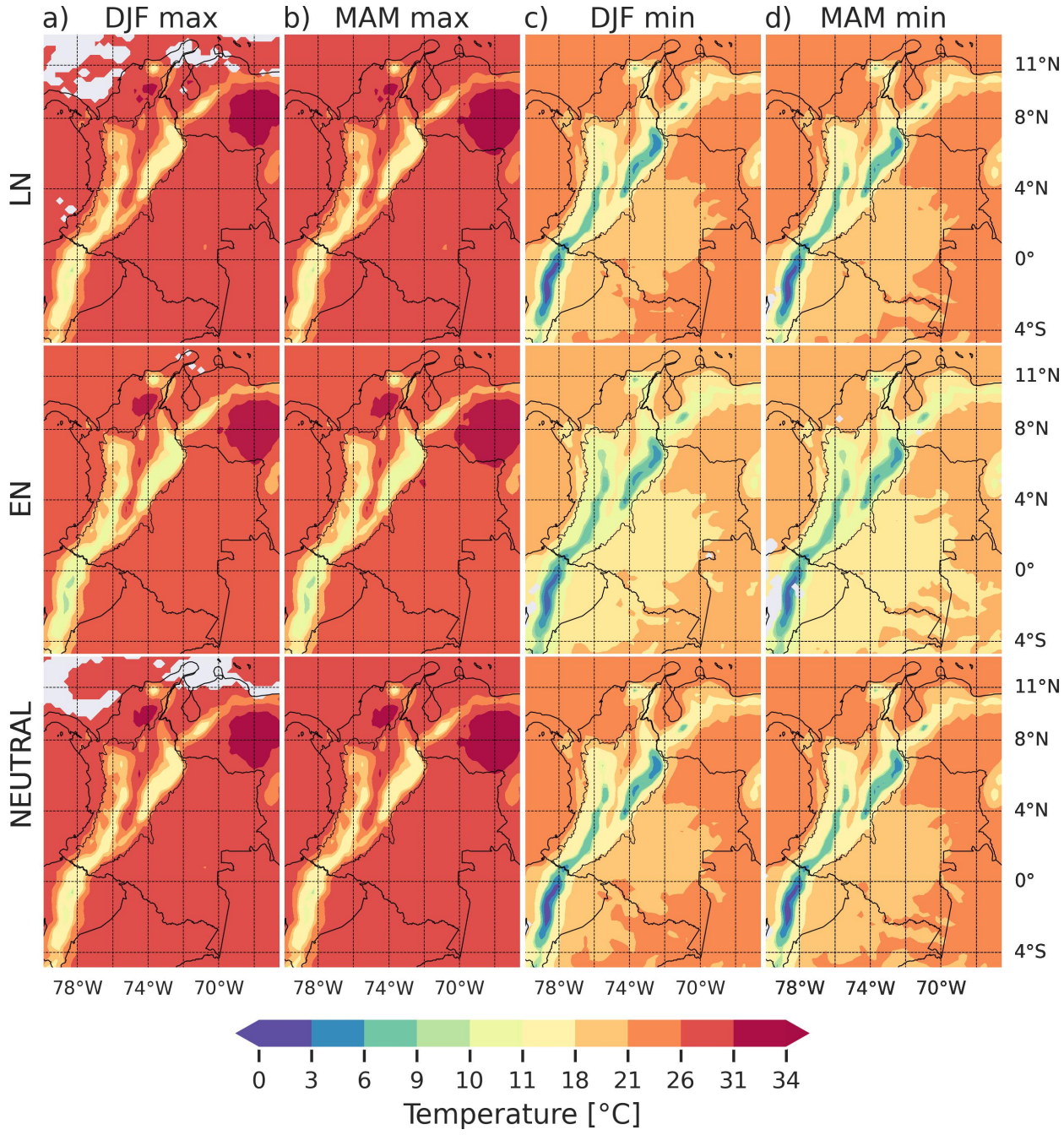

Figure **3-6**.: The index indicates the intensity of extreme events that occur during the nighttime. These events include a) TXx in DJF, b) TXx in JJA, c) TNn in DJF, and d) TNn in JJA. Furthermore, the extreme events are categorized in the first row as occurring during LN years, in the second row as occurring during EN years, and in the third row as occurring during neutral years.

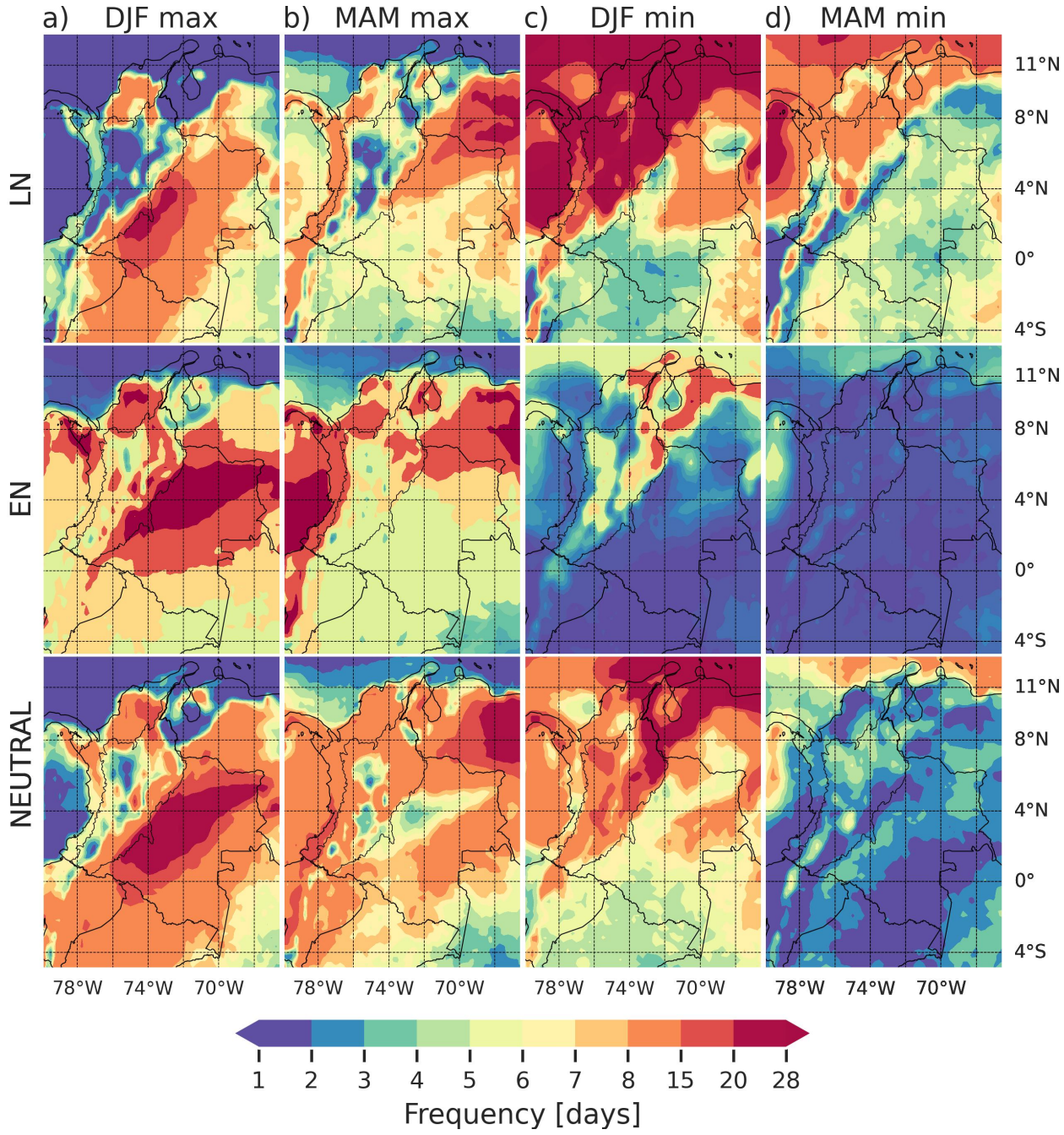

Figure **3-7**.: The index indicates the frequency of extreme events that occur during the daytime. These events include a) TXx in DJF, b) TXx in JJA, c) TNn in DJF, and d) TNn in JJA. Furthermore, the extreme events are categorized in the first row as occurring during LN years, in the second row as occurring during EN years, and in the third row as occurring during neutral years.

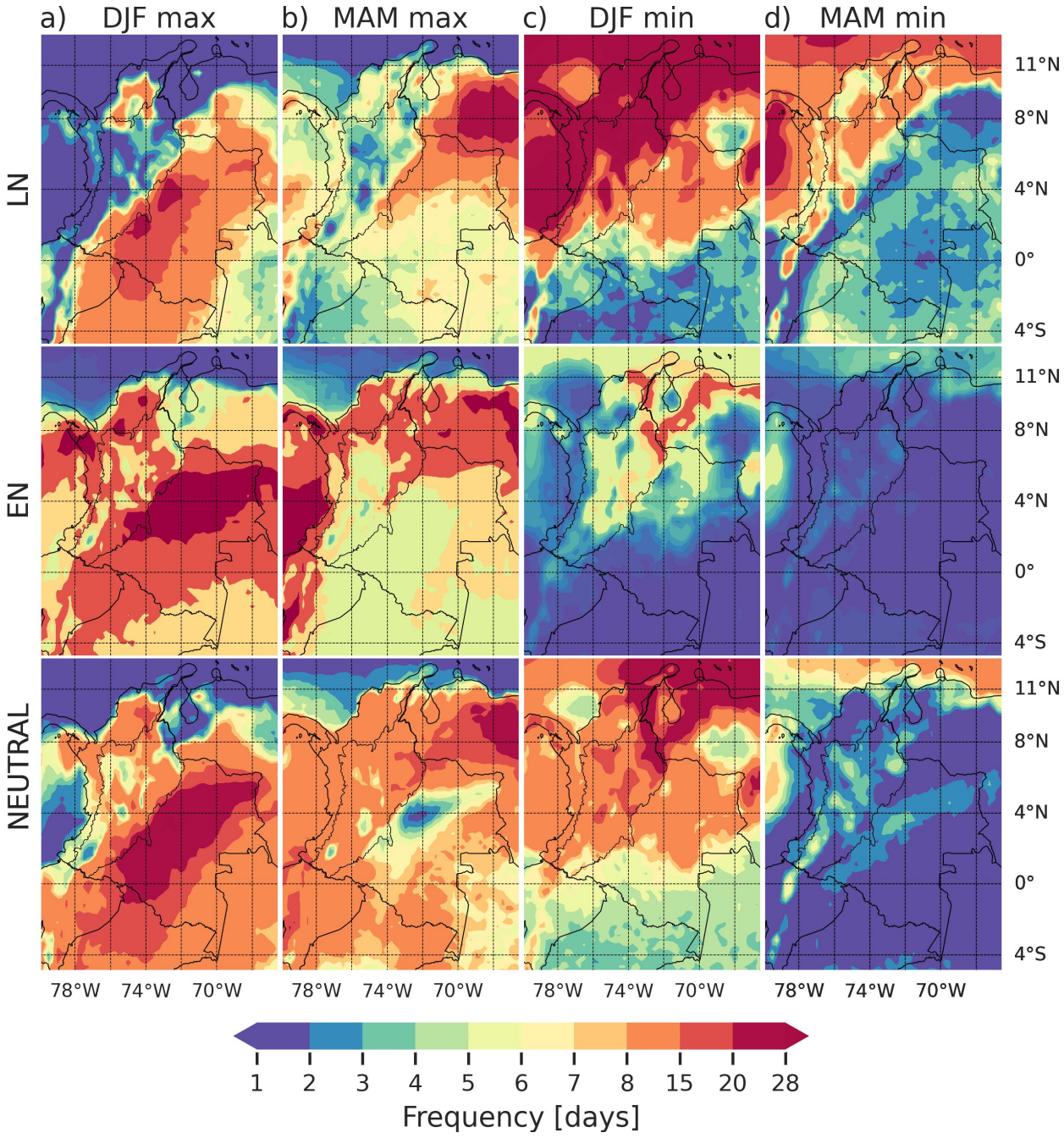

Figure **3-8**.: The index indicates the frequency of extreme events that occur during the nighttime. These events include a) TXx in DJF, b) TXx in JJA, c) TNn in DJF, and d) TNn in JJA. Furthermore, the extreme events are categorized in the first row as occurring during LN years, in the second row as occurring during EN years, and in the third row as occurring during neutral years.

During the DJF season in LN, over 28 extreme TNn events occur on average, with the

highest occurrence being in the Andes region towards the west and north. Even in neutral years, the frequency of TNn events remains high, although lower than during LN and higher than during EN. It is worth noting that in EN, LN, and neutral years studied, the north of Colombia experiences more frequent events than the south during DJF. However, during the JJA season, TNn occurrences are higher in the south and lower in the north, with the Andes region experiencing high occurrences during LN compared to EN and neutral years. Figures **3-7**c and d illustrate this behavior.

Extreme TXx events are expected to occur less frequently during nighttime (Vincent et al., 2005). However, the pattern of these events is not entirely consistent. While there are similarities between nocturnal and diurnal extremes, there are also some differences. For instance, in the eastern region of Colombia, the frequency of nocturnal TXx extremes is slightly higher during DJF in LN, EN, and neutral years. Additionally, EN and neutral years tend to have more frequencies of nocturnal TXx extremes compared to diurnal ones in the Andes (as shown in Figure **3-8**a).

On the other hand, TXx events tend to decrease during ENSO phases and neutral years in JJA (as shown in Figure **3-8**b). This is not the case for nocturnal TNn extremes during DJF and JJA, as the pattern is similar to diurnal extremes with minor differences. In DJF, TNn occurrence is higher in the north and lower in the south, while the opposite is observed in JJA (as depicted in Figures **3-8**c and d).

Figures **3-9**a and b depict the variation in the intensity of diurnal TXx extremes. Significant differences are present in the Andes region during DJF and JJA, as well as on the coast and the Pacific Ocean during DJF in LN-neutral years. The intensity of extremes is higher in EN and neutral years compared to LN, with EN having higher intensity values than neutral years. This pattern is predominant in the Andes in DJF and milder in JJA.

In the Andes, diurnal TNn extremes have a high significance in LN-neutral and LN-EN years and are less significant and localized in EN-neutral years. There, TNn extremes were found to be less minimal in neutral years and EN than in LN. (see Figures **3-9**c and d).

Significant differences between ENSO and neutral years continue in the Andes in DJF and JJA in nighttime TXx extremes, except JJA in EN-neutral years. The TXx extremes are more intense during EN and neutral years than during LN (Figures **3-10**a and b). The patterns of difference TNn in DJF and JJA show a decrease in significance in the Andes region compared to the TXx index (as seen in Figures **3-10**c and d). The difference between LN-EN in the Andes is significant throughout the region, indicating that during LN, the nighttime TNn extremes are lower in magnitude than EN.

In Figure **3-11**, we can see the notable impact of ENSO and neutral years in the occurrence of ETEs. Specifically, in DJF, the magnitudes are consistently higher in EN, LN and neutral years at diurnal extremes. In LN-neutral years, there are negative values throughout the territory, which indicates a high frequency of TXx extremes during neutral years compared

to LN.

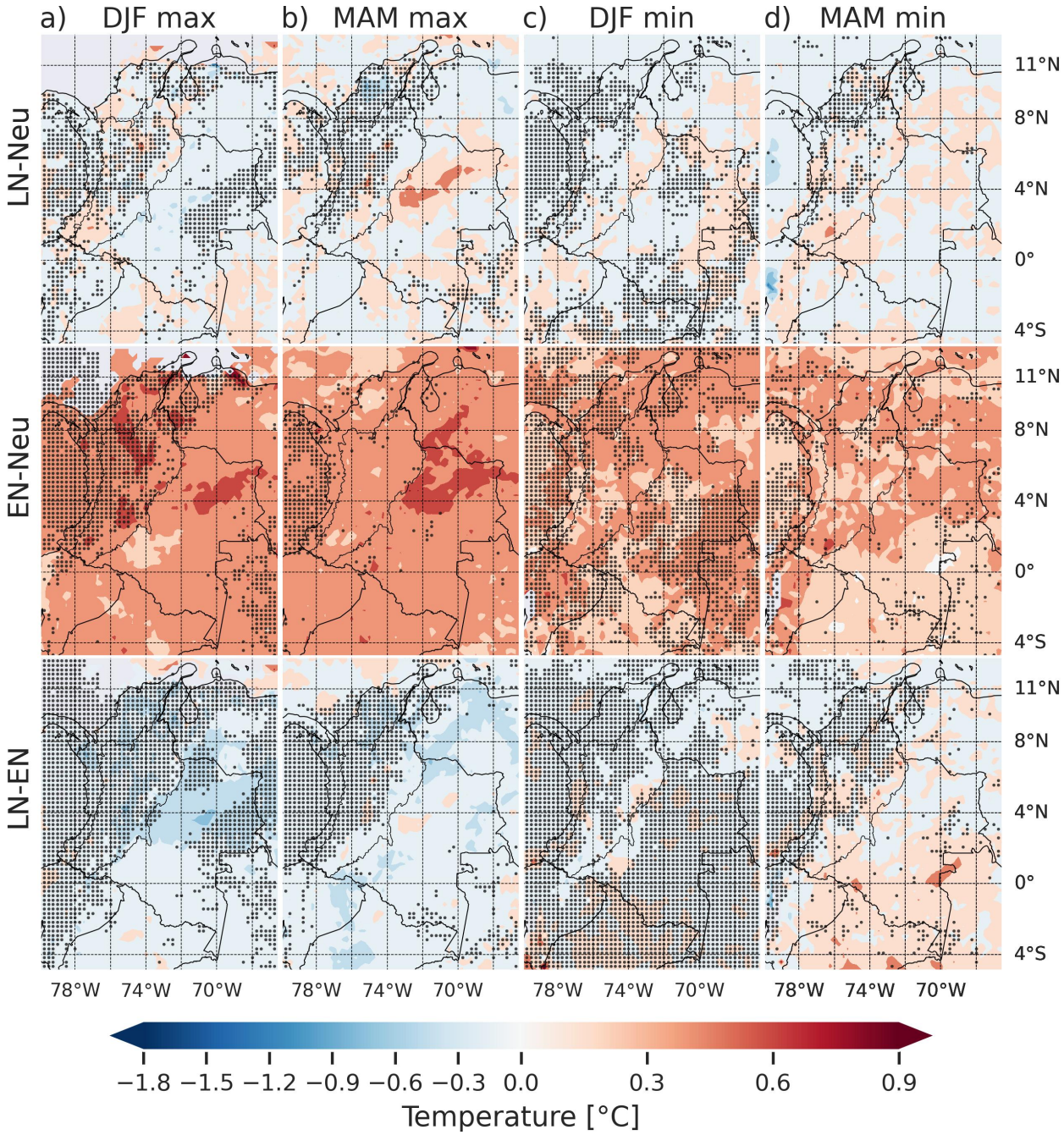

Figure **3-9**.: Comparative analysis of daytime ETEs Index intensity during different ENSO Phases and Neutral years. The first row shows the difference between LN and EN, the second row shows the difference between EN and Neutral years, and the third row shows the difference between LN and EN. The events analyze a) TXx in DJF, b) TXx in JJA, c) TNn in DJF, and d) TNn in JJA. Grid points signify significant differences at a 95% confidence level.

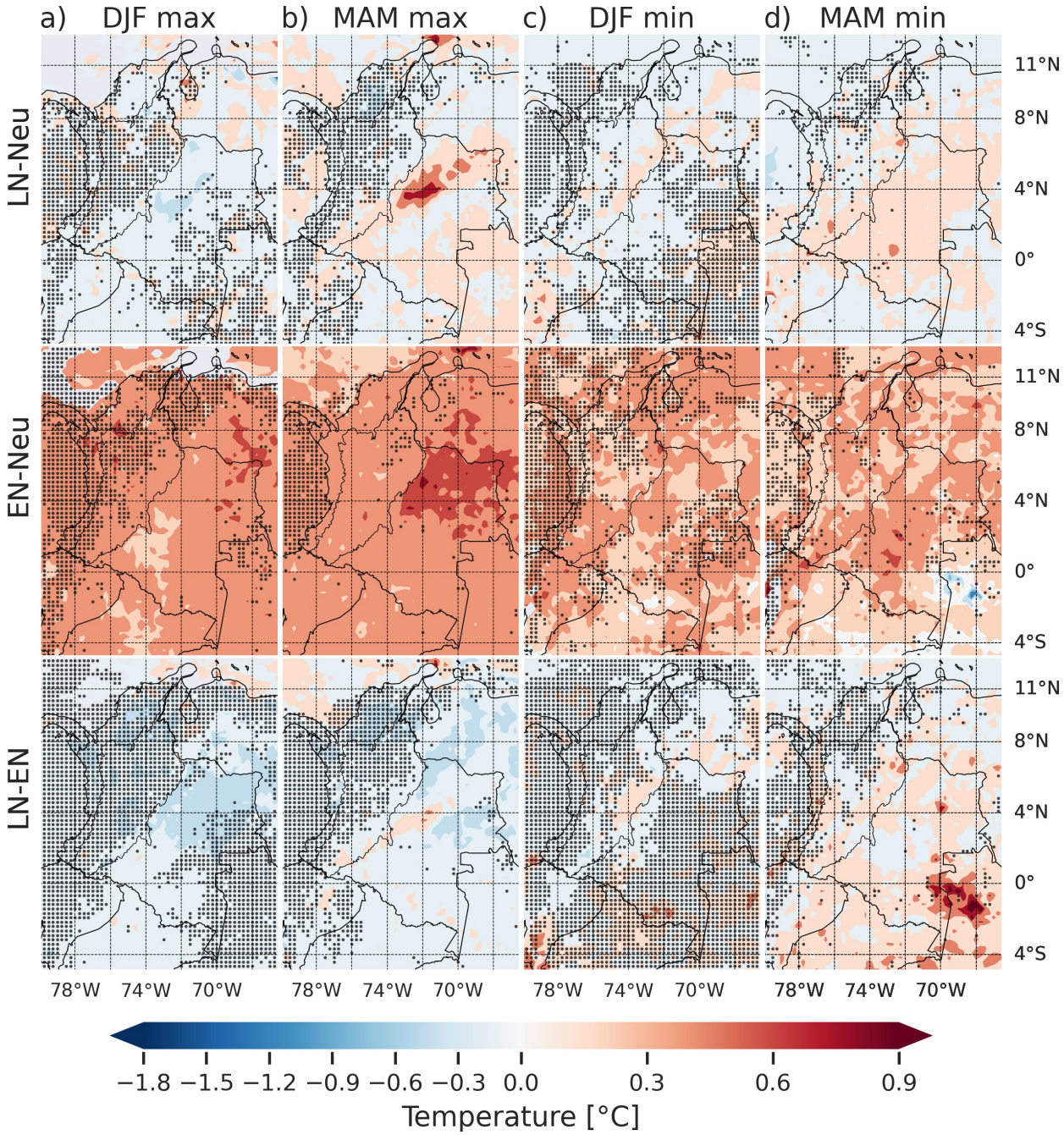

Figure **3-10**.: Comparative analysis of nighttime ETEs Index intensity during different ENSO Phases and Neutral years. The first row shows the difference between LN and EN, the second row shows the difference between EN and Neutral years, and the third row shows the difference between LN and EN. The events analyze a) TXx in DJF, b) TXx in JJA, c) TNn in DJF, and d) TNn in JJA. Grid points signify significant differences at a 95% confidence level.

Additionally, it is worth noting that EN years have more frequent TXx extremes than LN and neutral years (as illustrated in Figure **3-11**a). Moving to JJA, we see that the magnitudes of the differences are lower between ENSO and neutral years, but the same pattern follows in the tropical Pacific and the Andes. In these two seasons, the differences were significant in the Andes and during EN-neutral years and LN-EN (Figure **3-11**b).

During TNn nighttime extremes in DJF, frequencies are higher and more significant in LN compared to EN and neutral years. The Andes, northern Colombia, and the Caribbean Sea specifically show this trend (Figure **3-11**c). However, EN-neutral years exhibit little spatial significance, whereas, in neutral years, TNn extremes occur more frequently; that behavior was observed in Figure **3-8**. In JJA, the differences remain significant only in the Andes for LN-neutral years and LN-EN, but with lower event occurrence than DJF. In LN-neutral years, only a few regions show that there is more frequent nocturnal extreme TNn in LN. In EN-neutral years, the pattern is similar to those observed in TXx (Figure **3-11**d).

The nighttime TXx and TNn extremes have shown that their intensity and frequency pattern depends on the active ENSO phase. During the DJF period, the Andes region experiences a persistence of significant magnitudes. Neutral years depict more events than LN, but the differences are small; although tend to converge to zero show that they are significant. On the other hand, EN results in higher frequency events with high magnitude and significant values detected from the Andes to the north of Colombia, as shown in Figure **3-12**a. However, during JJA, no significant differences are noted between EN and neutral years in the Andes, although positive values persist, indicating a higher occurrence of extreme events during EN. Comparing LN with EN and neutral years, significant negative values are concentrated primarily in the western and northern regions of the study area, as seen in Figure **3-12**b.

During events of LN, there are more extreme nocturnal TNn events compared to neutral years and EN, as evidenced by positive and significant values found in the west and north of the Andes in DJF, as well as north of the study region (Figure **3-12**c). The EN-neutral years difference show much less significant values during DJF. In JJA, positive magnitudes in the frequency are maintained in the Andes in extreme TXx nighttime in LN-neutral years and LN-EN, although the significance decreases (Figure **3-12**d). The pattern observed in EN-neutral years is similar to that seen in DJF.

We compared ENSO phases and neutral years in the Andes through the histograms of daytime and nighttime TXx and TNn indices. In Figure **3-13**a, the low-intensity values of the TXx end correspond to high frequencies. In LN, lower intensity extremes are more frequent in the daytime and nighttime TXx extremes, which is consistent with what is seen in the maps in Figure **3-13**b. Similarly, during EN and neutral years, more events occur in the highest TXx intensity values; however, the frequency decreases the higher the magnitude of the ETEs, i.e., they are less likely to occur.

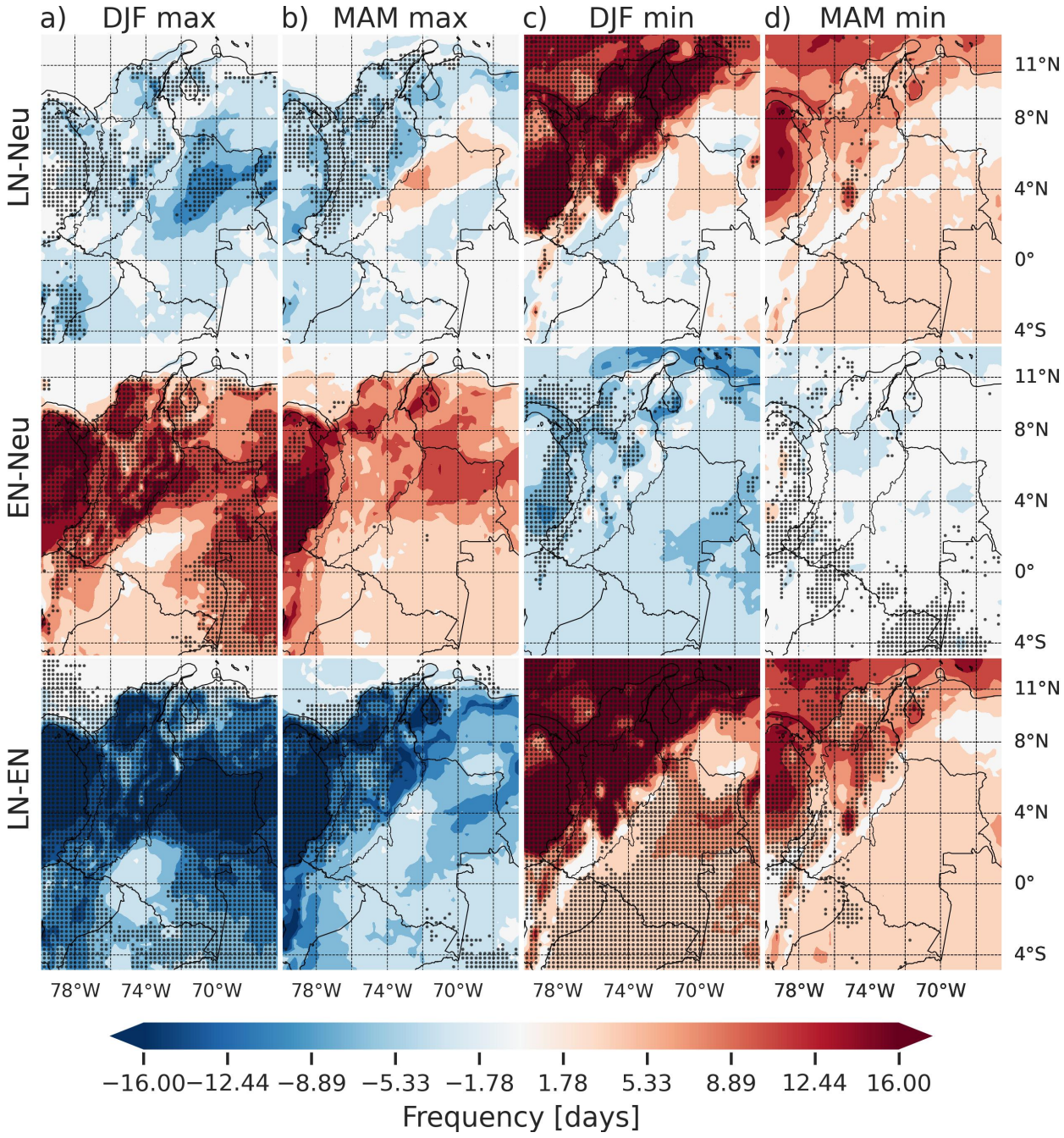

Figure **3-11**.: Comparative analysis of daytime ETE Index frequency during different ENSO Phases and Neutral years. The first row shows the difference between La Niña and El Niño, the second row shows the difference between El Niño and Neutral years, and the third row shows the difference between La Niña and El Niño. The events analyze a) TXx in DJF, b) TXx in JJA, c) TNn in DJF, and d) TNn in JJA. Grid points signify significant differences at a 95% confidence level.

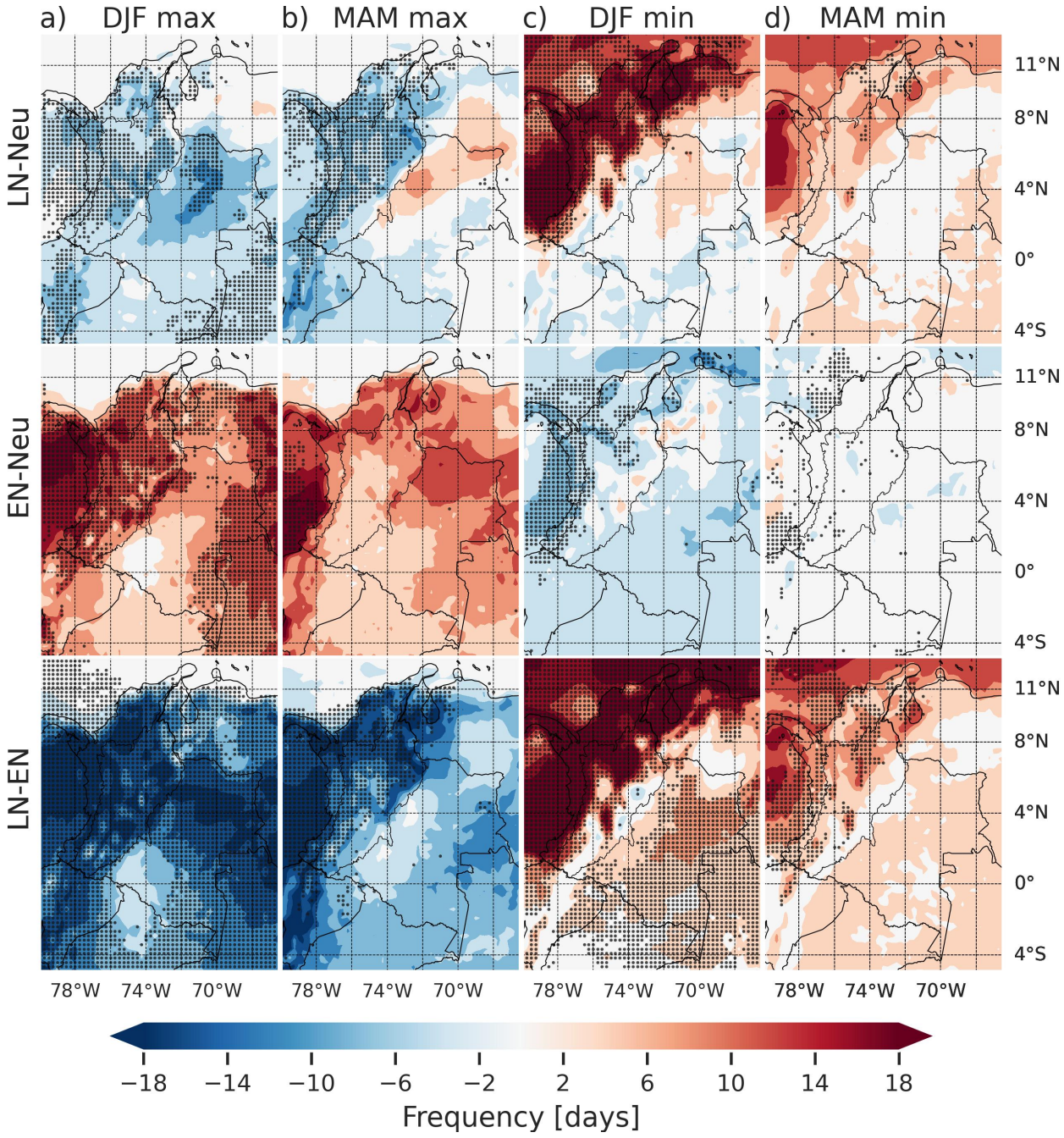

Figure **3-12**.: Comparative analysis of nighttime ETEs Index frequency during different ENSO Phases and Neutral years. The first row shows the difference between La Niña and El Niño, the second row shows the difference between El Niño and Neutral years, and the third row shows the difference between La Niña and El Niño. The events analyze a) TXx in DJF, b) TXx in JJA, c) TNn in DJF, and d) TNn in JJA. Grid points signify significant differences at a 95% confidence level.

The U-test applied between LN-neutral years and EN-neutral years indicated the significant distribution of TXx extremes in the Andes, except for LN-EN nighttime, where the test was almost significant with a p-value of 0.05 (Table **3-1**).

Figure **3-13**c and Figure **3-13**d show the intensity distribution of the TNn extremes during the day and night. At both times of the day, the extremes maintain similar intensities. The frequency of events does not differ between ENSO events and neutral years, i.e., the histogram shows that the intensities at the TNn extremes in daytime and nighttime can occur in almost equal frequency. The results are consistent with the time series in the TNn ETEs (Figure **3-2**), which exhibited that the magnitudes differed little between daytime and nighttime, and between EN, LN, and neutral years. This differs in the TXx ETEs, which showed a wide range of value differences. On the other hand, compared with the maps (Figures **3-9**, **3-10**, **3-11**, **3-12**), it is possible to observe that at night, the intensities of the ETEs TNn present high values in EN, while in LN, the magnitudes may be lower.

Furthermore, the differences were not significant in the nocturnal extremes between EN-neutral and EN-neutral years, indicating no difference in their magnitudes (Table **3-1**). However, the graph suggests that some daytime extremes and neutral LN-years in the nighttime extremes may be more intense. Nonetheless, the difference is not substantial.

As mentioned, the ENSO has been extensively studied in northern South America to understand its impact on regional hydroclimatology. The influence of surface temperature varies seasonally and is governed by different processes (Cai et al., 2015). It is widely known that during EN, the SST anomaly in the central and eastern Pacific leads to positive temperature anomalies. Poveda (2004) has summarized several mechanisms for the hydrological deficit, including the weakening of the Choco low-level jet stream at 700 hpa, reduction in the number and intensity of tropical easterly waves over the northern tropical Atlantic, displacement of the ITCZ to the southwest of its normal position due to the establishment of an anomalous Hadley cell over the American tropics. In addition, alteration of the atmospheric moisture balance in the lower levels of the atmosphere, and positive feedback between land-atmosphere processes, due to deficits in soil moisture and evapotranspiration, and therefore the recycled precipitation of local origin tends to decrease as a result of lower water availability in the soil and in the atmosphere.

The change in atmospheric conditions described above suggests that not only the average climate patterns are affected during EN but also the extreme conditions. While the connection between ENSO and ETE has been well-documented in southern South America (Renom et al., 2011; Tencer et al., 2016), this relationship has only been studied during strong or extreme ENSO events in northern South America (Bedoya-Soto et al., 2019; Poveda et al., 2011). Therefore, it is crucial to focus research on understanding the impact of ENSO on ETE in the region and identify other mechanisms contributing to extreme weather events caused by natural variability or climate change. In addition, it is worth noting that changes

in the insolation cycle throughout the year and other phenomena at different temporal and spatial scales can also affect extreme events such as TXx and TNn, whether during ENSO or neutral years.

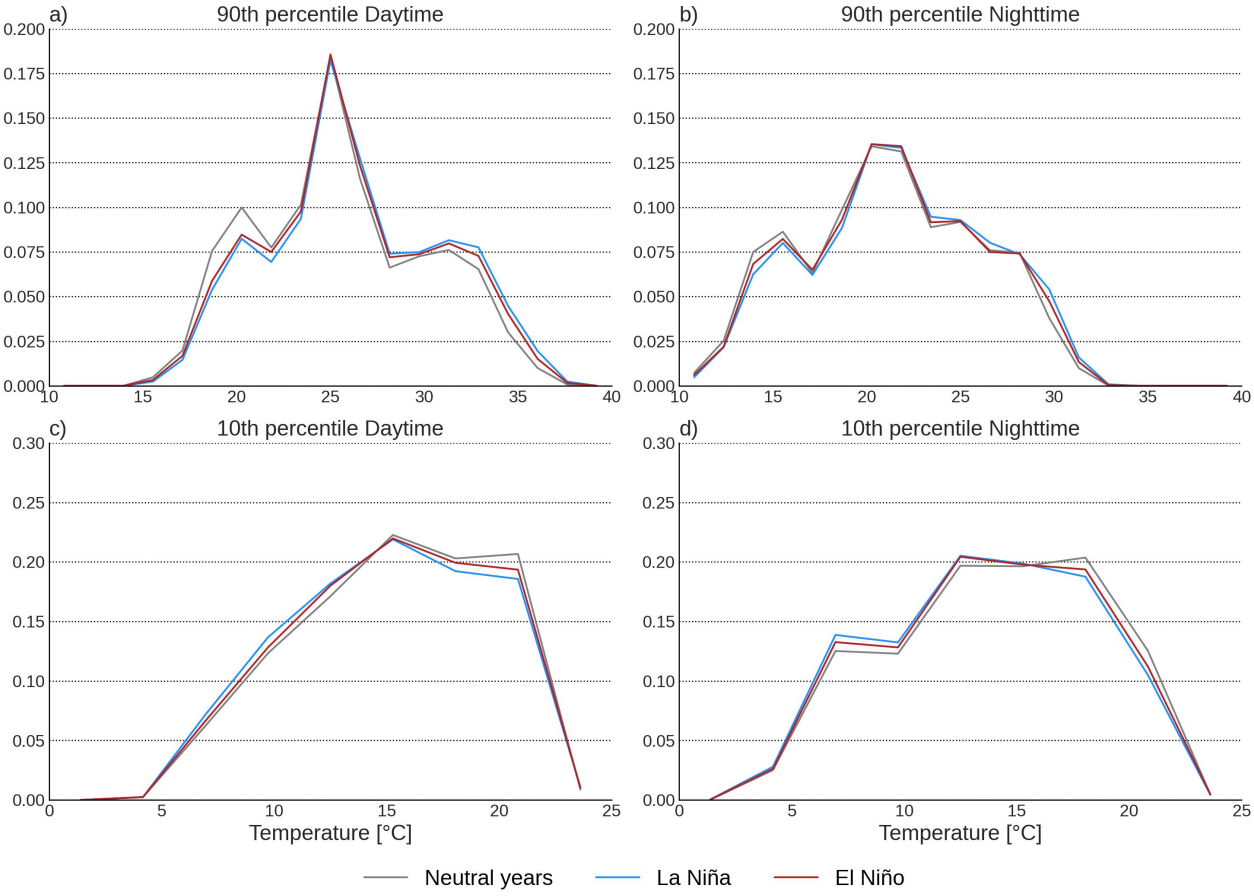

Figure **3-13**.: Comparative distribution of monthly intensity of ETEs indices during EN (Red), LN (Blue), and Neutral Years (Light Gray) in the Andes: a) TXx daytime, b) TXx nighttime, c) TNn daytime, and d) TNn nighttime.

	Intensity		
	LN-NEUTRAL	EN-NEUTRAL	LN-EN
TXx Daytime	1.04×10^{-4}	1.54×10^{-2}	9.3×10^{-9}
TXx Nighttime	7.9×10^{-6}	0.02	0.05*
TNn Daytime	0.035	1.73×10^{-3}	1.17×10^{-3}
TNn Nighttime	3.20×10^{-6}	0.09*	0.05*

Table **3-1**.: Differences between the distributions at a 5% significance level (sig. < 0.05) by U-test. Values associated with an asterisk indicate that they are not statistically significant.

3.3. Conclusions

This chapter aimed to characterize extreme temperature events in the Colombian Andes during ENSO and neutral years. A trend analysis was conducted to consider the impact of natural variability. Both daily maximum (TXx) and minimum (TNn) temperature extremes were assessed during diurnal and nocturnal periods. The outcomes revealed that temperature extremes during both day and night were more common during strong ENSO events, showing high peaks in frequency, as depicted in Figure **3-2**b.

A significant correlation was found between SST anomalies and each temperature index over the study region (Figures **3-3** and **3-4**),. In addition, Figures **3-3**e, f, g, and h, and **3-4**e, f, g, and h showed a precise classification of SST anomalies when LN, EN, and neutral years occur in the Andes. In general, it was observed that positive (negative) EN (LN) SST anomalies indicate more intense events at daytime and nighttime TXx extremes, while TNn extremes are less intense. On the other hand, positive SST anomalies during ENSO were also found to increase the frequency of extreme daytime and nighttime TXx events, while the frequency is moderate in neutral years and low in LN. In contrast, TNn extremes are more frequent during LN and less frequent during EN.

The most relevant results of this chapter were observed in the frequency of extremes for both TXx and TNn indices. Diurnal and nocturnal events were observed to be high in the Andes during the DJF and JJA seasons. Moreover, it was found that diurnal and nocturnal TXx extremes were more frequent during EN and neutral years, while TNn extremes were more common during LN and less frequent during EN. Regarding location, diurnal and nocturnal TXx extremes were more frequent in the Andes towards the south during the DJF season and towards the north during the JJA season. Conversely, TNn extremes were more frequent in the Andes towards the north during the JJA season and towards the south during the DJF season (refer to Figures **3-7** and **3-8**).

In summary, the comparison between different phases (LN-neutral years, EN-neutral years, and LN-EN) shows that extreme temperature events (TXx and TNn) are more significant and intense during neutral and EN years compared to LN periods, except in the case of EN-neutral years where the significant values decrease in the diurnal and nocturnal extremes (Figures **3-9** and **3-10**). Furthermore, the distribution of indices between ENSO and neutral years confirms these results, but the probabilities of more intense events may be higher for neutral years (Figure **3-13**a and b). The daytime and nighttime TNn extremes show no difference in frequency and magnitude between the periods. Figures **3-11** and **3-12** indicate that extreme TXx temperature events are more frequent during EN than in neutral and LN years, while daytime and nighttime TNn extremes are more frequent during LN compared to neutral and EN years. Therefore, LN, EN, and neutral years impact ETEs, and their effect varies in daytime and nighttime. That is, days and nights are warmer and more frequent during EN, while they are cooler and more frequent during LN.

4. Atmospheric circulation patterns related to EPEs

Abstract

The weather conditions in the Colombian Andes can vary greatly depending on extreme precipitation events, and it has been shown that during El Niño – Southern Oscillation (ENSO), there is a pattern in the increase or decrease of precipitation. We explored the atmospheric circulation pattern affecting precipitation over northern South America during La Niña (LN), El Niño (EN), and neutral years. Specifically, we wanted to observe if it is possible to find similarities between the strong 2010 LN event and its composite and how it differs from the EN composite and neutral years. The anomalies revealed similarities in the evolution of LN, characterized by weak convective development in the eastern tropical Pacific and deep convection in northern South America, driven by available moisture, strengthened uplift of air masses, and upper-level divergence. EN and neutral years showed an opposite (similar) pattern to LN. However, cross-section analysis revealed differences between October 2010 and the climatological October of LN, with weakening in a vertical motion and limited availability in the upper level during the particular event. These differences may be related to moisture transport and convergence, the sources of which may vary due to other atmospheric phenomena or features. In addition, it was found that during EN, moisture transport and convergence tend to be high, a key factor for extreme precipitation.

Keywords

El Niño-Southern Oscillation (ENSO); Northern South America, Colombian Andes, Precipitation, Pattern Circulation.

4.1. Methodology

For this chapter, monthly data of specific humidity, omega (vertical velocity), geopotential height, vertically integrated moisture flux (zonal and meridional), wind (zonal and meridional), and wind divergence at various pressure levels were used. These data were taken at a horizontal resolution of 0.25°x 0.25° of product ERA5 from the European Center for Medium-Range Weather Forecast (ECMWF, Hersbach et al., 2020) from 1979 to 2019. The

analysis concentrated on a geographical area delineated by longitudes 130°W to 10°W and latitudes 20°S to 30°N, with a particular emphasis on understanding the influences external phenomena might have on the northern regions of South America.

EPEs occur from the sub-daily to the daily scale. Notwithstanding the analysis in Chapter 1, we wanted to observe seasonal variations, so to follow the evolution of seasonal extremes, the analysis in this chapter will be on a monthly scale.

Additionally, the velocity potential was calculated using spherical harmonics from the meridional and zonal wind fields. A crucial point of emphasis is that this variable was estimated using data from the entire globe rather than being restricted to the study area. This approach was adopted to avert potential boundary-related computational issues (Li et al., 2006). Finally, from the vertically integrated moisture flux variable field, humidity convergence was determined.

Chapter 2 noted a pronounced increase in the frequency of extreme events during September, October, and November, particularly during LN episodes. The investigation aimed to discern whether there exist consistent atmospheric conditions that could potentially influence precipitation in the Colombian Andes across diverse LN events, compared to the composite ENSO phase evolution. As a case study, the LN event of 2010-2011, categorized as an intense phase, was selected, with an explicit focus on October 2010 — a month associated with a high incidence of extreme weather events. Consequently, the research sought to scrutinize the evolution of the anomaly field of related variables two months prior to and subsequent to October. The composite of EN events and neutral years occurring within the stipulated period were also incorporated into the study for a comprehensive understanding.

Finally, an exploration of vertical circulation was conducted through a cross-sectional analysis encompassing variables such as specific humidity, omega (vertical velocity), and geopotential height. This analysis spanned between longitudes 80°W - 60°W and latitudes 10°S - 15°N, thereby predominantly covering the Colombian Andes. Correspondingly, an evaluation of these variables was undertaken from August to December for the events occurring in 2010. This included an examination of composite data from LN, EN, and neutral years, to generate a comprehensive understanding of their distinctive patterns.

4.2. Results and discussion

This section will discuss the potential large-scale mechanisms contributing to extreme precipitation events during ENSO. Findings from the preceding chapter indicate that these extreme events manifest more frequently during the September-October-November (SON) season in LN years, although their intensity may not necessarily be heightened. To investigate this phenomenon more thoroughly, our study focused on the strong La Niña event that

occurred from 2010 to 2012, which significantly impacted the designated region. This event was compared with a composite analysis of LN years to discern similarities. We also examined the composite of EN and neutral years to scrutinize their contrasting effects and understand the common climatic conditions.

To gain deeper insights into the evolution of the horizontal atmospheric structure concerning hydroclimatological variables, we have concentrated our analysis on the period of September-October-November. This season has a high frequency of extreme events according to literature findings and the outcomes detailed in Chapter 2. Our study focuses on the month of October, enabling us to conduct a retrospective analysis of conditions. By examining the two months prior to October, we can determine the antecedent conditions of the variables. Additionally, we look two months ahead to determine if the conditions will sustain an increase in the frequency of these events or extremes or facilitate their attenuation. This allows us to gain a better understanding of the factors that contribute to these occurrences.

Figure **4-1** shows the evolution of the geopotential variable at 200 hPa during the 2010 event. In August 2010, positive anomalies were observed throughout the territory. Then, in September 2010, negative anomalies appeared in the eastern Pacific, but positive anomalies persisted in the rest of the region. In October 2010, these negative anomalies extended from the southern to the northern eastern Pacific. These anomalies extend to the mainland by November and attain higher magnitudes in December. A similar pattern is shown in the LN composite, although with lower magnitudes. During EN, on the other hand, positive anomalies persist from August to December, being more intense in December. In neutral years, anomalies are mainly negative and close to zero in northern South America between August and October. These results are consistent with what is expected during the negative and positive phases of ENSO. In addition, they agree with previous studies that have shown anomalies in surface air temperature and sea level pressure (Shinker and Bartlein, 2009). The EN events are characterized by warm temperatures, higher mean sea level pressure, and higher 200 hPa geopotential height values compared to the average. In contrast, the LN conditions are cold, with lower mean sea level pressure and lower 200 hPa geopotential heights. It is worth noting that the pattern observed during LN lacks the uniformity seen in either EN or neutral years when comparing the LN event and LN composite.

To better understand how precipitation responds, especially during extreme events, it is essential to consider other factors that affect vertical motion and moisture fluxes. Assessing the patterns of vertical motions is crucial, primarily due to the significant impact that large-scale upward and downward motions have on precipitation. Rising motions enhance precipitation, while sinking motions suppress it. Figure **4-2** displays the omega variable (vertical velocity) at 500 hPa; climatology shows that negative values of omega are predominantly situated over the low-pressure band of the Intertropical Convergence Zone (ITCZ), suggesting rising air masses. Conversely, positive values indicate downward air masses in the extratropical regions.

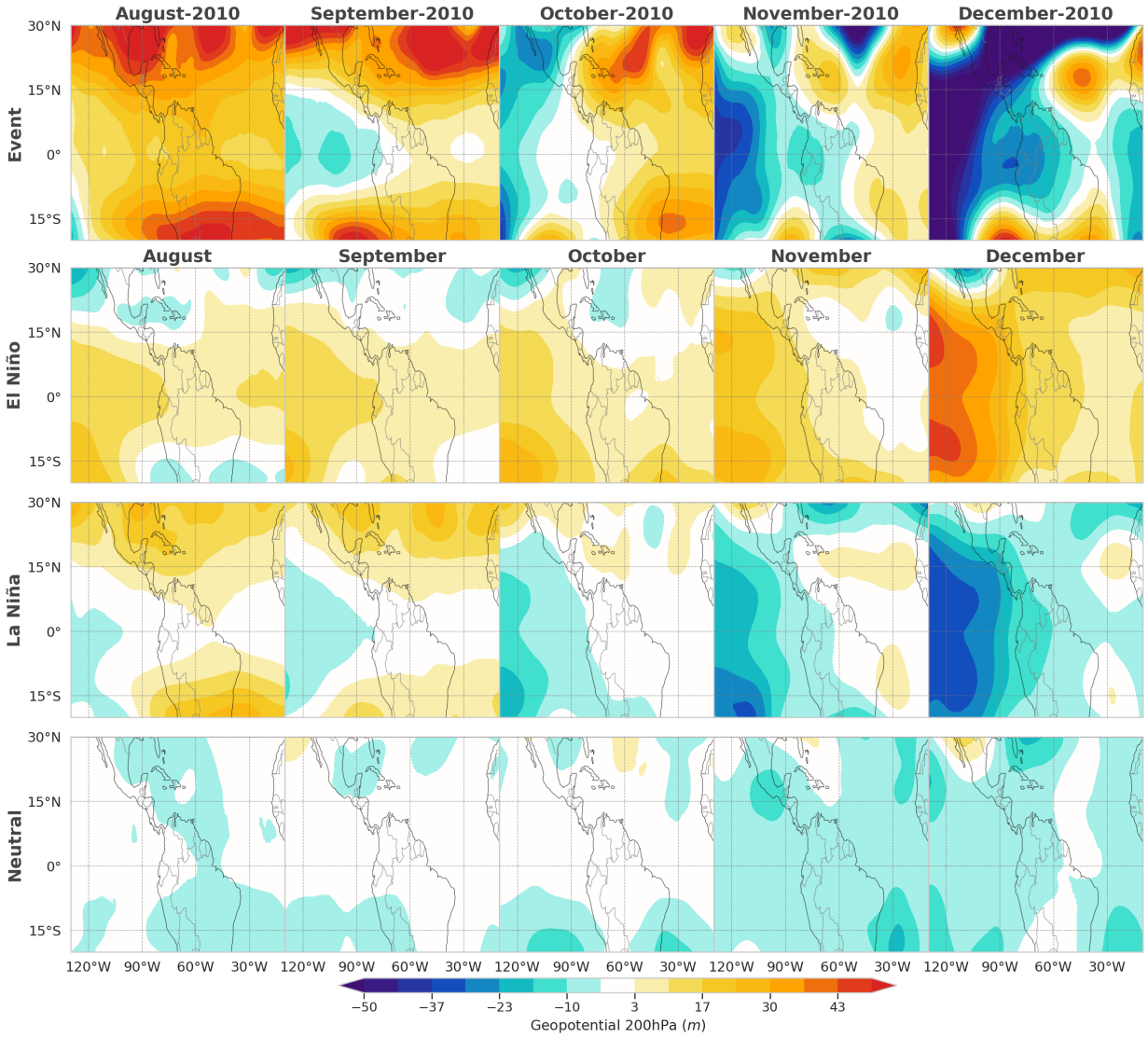

Figure **4-1**.: 200 hPa geopotential height anomalies from August to December, in the 2010 LN event (first row), EN composite (second row), LN composite (third row), and neutral years composite (fourth row).

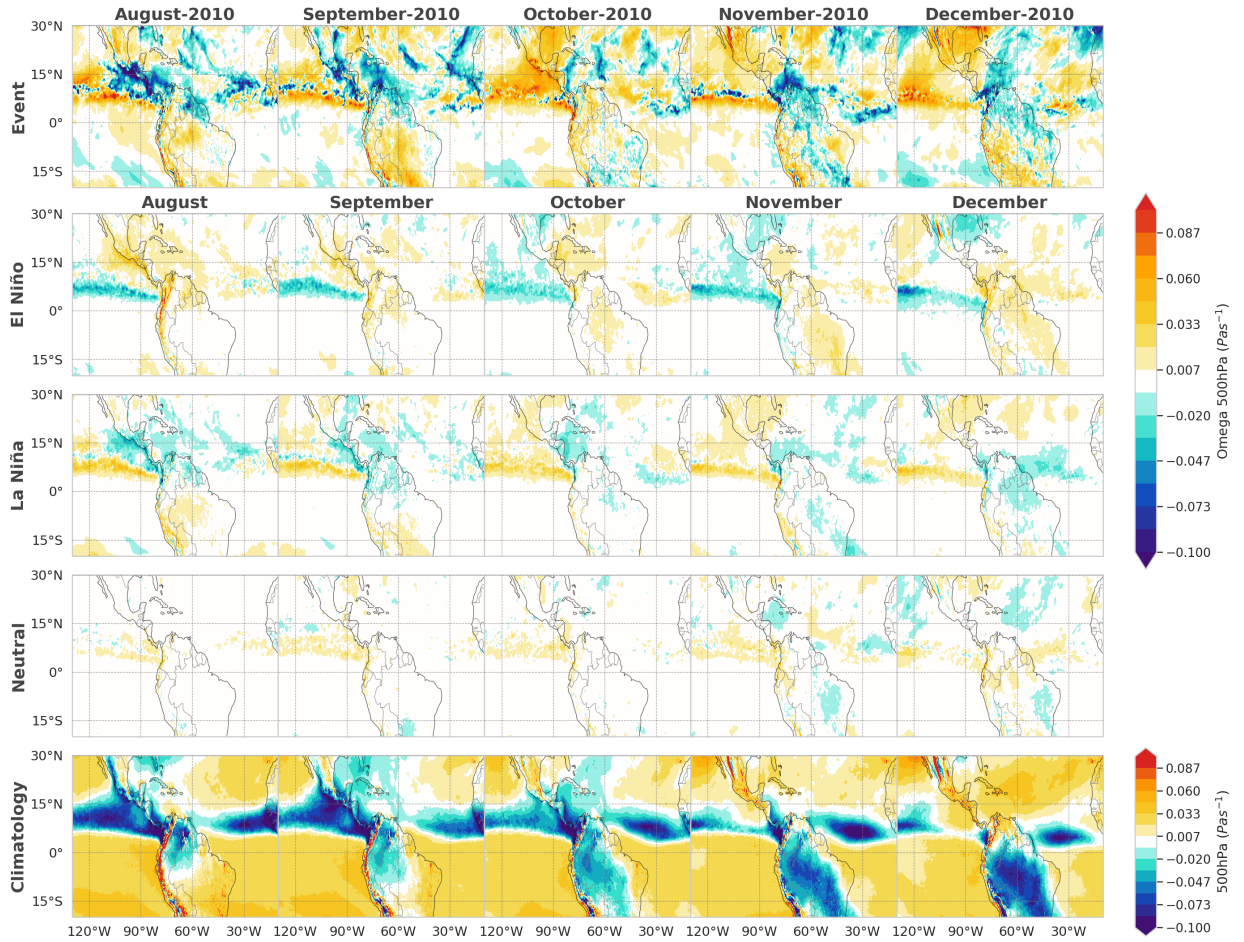

Figure **4-2**.: 500 hPa omega anomalies from August to December, in the 2010 LN event (first row), EN composite (second row), LN composite (third row), neutral years composite (fourth row), and climatology (fifth row).

When studying the 2010 LN event, it was observed that the convective uplift was weakening due to persistent positive omega anomalies over the eastern tropical Pacific from August to December. These anomalies were particularly intense in October, which is the month that experiences the highest frequency of extreme precipitation events. However, negative values indicating a strengthening of the uplift were noted over the Andes and a significant portion of the northern territory of South America in the preceding and subsequent months. This pattern was also observed in the LN composite, with positive anomalies in the tropical Pacific and negative values in the continent. In contrast, positive anomalies were found over northern South America during EN. At the same time, negative values predominated in the eastern Pacific, where the convergence of low-level winds and warm sea surface temperature caused stronger atmospheric ascension, signifying a more dynamic interaction between

oceanic and atmospheric processes.

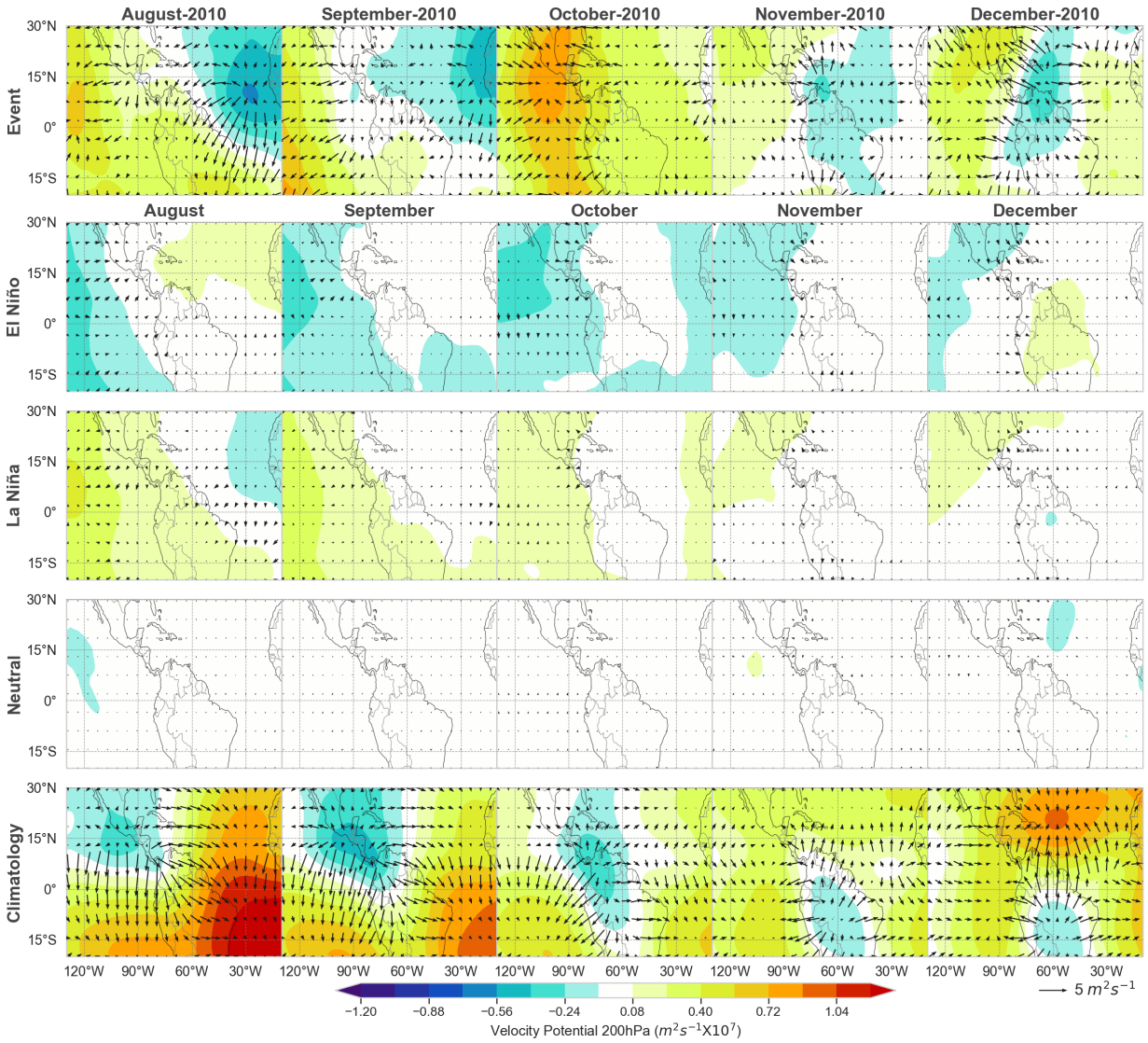

Figure **4-3**.: 200 hPa velocity potential (shades) and divergence (vectors) anomalies from August to December, in the 2010 LN event (first row), EN composite (second row), LN composite (third row), neutral years composite (fourth row), and climatology (fifth row).

The current anomalies observed in the omega pattern align with the documented alterations found in the Walker cell during occurrences of EN or LN (Cai et al., 2020; Chen et al., 2019; Trenberth, 2019). EN event causes a rise in the air over the eastern Pacific, followed by a suppression over South America that generates warm conditions in northern South America (Poveda et al., 1996, 2011; Waylen and Poveda, 2002). On the other hand,

during LN, normal conditions are reinforced, with sinking cold air in the tropical Pacific and deep convection over South America. This favors the occurrence of precipitation that can become extreme. However, during neutral years, omega anomalies are little, and positive values tend to dominate, showing a pattern similar to LN but with very low magnitudes.

The velocity potential at 200 hPa provides information about the divergence in the upper atmosphere, which is related to convective activity. Figure **4-3** shows the climatology of the velocity potential, and we can observe that initially, from August to December, there is convergence in the upper level due to divergence in the lower level, as expected in Walker's circulation. However, this divergence shifts from Central America in August to southern South America in the following months due to the movement of the ITCZ in response to the insolation cycle.

During the LN 2010 event, convergence is observed in the upper level from the Pacific Ocean into the continent in August, while divergence is kept in the Atlantic. In September 2010, positive convergence values were concentrated far from the coast in the Pacific Ocean, and divergence persists in the Atlantic. In October, the month selected with the highest extreme event activity, convergence is observed across the territory. This coincides with the results shown by Omega in Figure **4-2**, which indicates a weakening in the middle levels in the ascent of air masses toward low-pressure levels. In November and December, divergence is present over Colombia, showing strong convection and convergence values in the Pacific and eastern Atlantic.

When analyzing the LN composite, we can observe similarities in the spatial pattern of the velocity potential (Figure **4-3**). During August and September, the convergence covers both the Pacific Ocean and the continent. Then, the convergence shifts to the northern Pacific, and no clear divergence pattern can be identified in the north of South America. However, the October LN composite shows no consistency with the October 2010 event, indicating that a particular LN event may have unique characteristics that cannot be generalized to the composite. Moreover, other phenomena on different temporal and spatial scales may also affect atmospheric circulation conditions simultaneously with LN.

We can observe changes in the velocity potential variable (Figure **4-3**) when comparing EN and neutral years. During EN years, a pronounced divergence is noticeable in the Pacific Ocean commencing from August. However, this anomaly recedes towards the Pacific as the year ends, and convergence anomalies occur over the north of Brazil. Regarding neutral years, the changes in potential velocity hover near zero, indicating that the disparities between the neutral years' composite and the overall climatology are rather negligible. This suggests a relative stability of hydroclimatological conditions during neutral years compared to EN years.

The upper-level vertical motion is described in more detail in Figure **4-4**, which displays the divergent wind and is consistent with the horizontal field of divergence magnitude shown

in Figure **4-3**. While the spatial pattern of divergence magnitude exhibits considerable variability, certain notable aspects can be distinguished. The eastern Pacific Ocean displays convergence during the 2010 LN event, but regions of divergence are also found further north, such as in western South America and the Andes to the south of South America in August. Divergence is also observed in the Caribbean, as in the velocity potential. Convergence is found in the eastern Pacific near Colombia and northern South America in October. Finally, in November and December, the anomalies show divergence in the eastern tropical Pacific. Based on the velocity potential and divergence anomalies patterns, the convective upward motion in northern South America undergoes a sequence of weakening in August, strengthening in September, a subsequent weakening in October, and a further intensification during November and December.

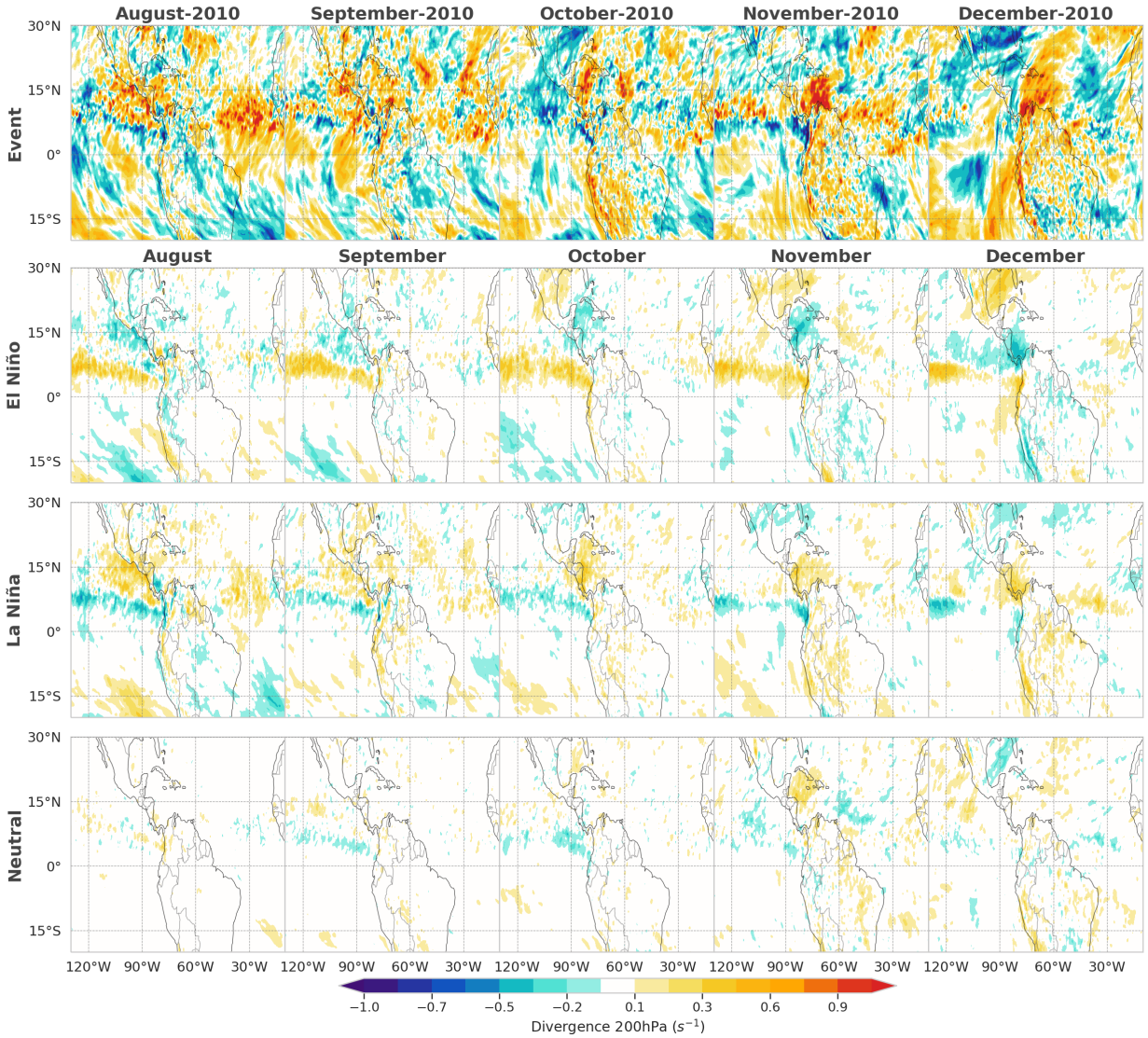

Figure **4-4**.: 200 hPa divergence magnitude anomalies from August to December, in the 2010 LN event (first row), EN composite (second row), LN composite (third row), and neutral years composite (fourth row).

In contrast, the composite of EN and LN reveals a distinct pattern (Figure **4-4**). EN is characterized by divergence in the tropical Pacific and convergence in northern South America, although the anomalies register relatively small magnitudes. Conversely, LN exhibits convergence in the tropical Pacific and divergence in Colombia. However, neutral years do not significantly differ from climatology, with some negative values indicating convergence in the eastern tropical Pacific and divergence in Colombia.

During the analysis of anomaly fields, it becomes feasible to identify unique characteristics

within the atmospheric circulation that may be instrumental in catalyzing extreme events. A particularly relevant variable in this context is specific humidity, a measure signifying moisture concentration in the atmosphere. Notably, regions with elevated specific humidity levels present a higher propensity for the occurrence of extreme precipitation events.

A distinctive pattern is observed when comparing the specific humidity at 850 hPa composite for LN, EN, neutral years, and the specific event. Higher moisture availability is found at the lower levels of the atmosphere, which is affected during ENSO. During October of LN 2010 (first row of Figure **4-5**), positive anomalies are prominently noticeable across regions of South America and parts of the northern Atlantic. The central cold tongue region of the tropical Pacific also features these positive anomalies, whereas negative anomalies are predominant over the remaining expanse of the ocean. In the preceding months, positive anomalies covered regions of the Atlantic and Central America, accompanied by pronounced positive values congregating around the Colombian Andes. Meanwhile, South America's Pacific coast and southern parts exhibited negative anomalies. Transitioning into November and December, noticeable increases in humidity are discernible in the Atlantic and eastern Pacific regions. Despite central Colombia registering relatively moderate values, negative anomalies continue to prevail along the coastline and within the Amazon region.

The LN composite anomalies (third row of Figure **4-5**) exhibit a less pronounced magnitude compared to the specific event under consideration. Concurrently, during EN (second row of Figure **4-5**), the anomaly patterns appear to be inverse in relation to those observed in LN events. Specifically, there is a notable augmentation in humidity in October across most of the studied territory, except the western Atlantic proximal to the continent. During the preceding months of August and September, an increase in humidity is evident across northern South America and the eastern Pacific, contrasted by a decrease in Central America, the Atlantic, and the southeastern Pacific. Moreover, September and October witness the manifestation of negative anomalies in the Atlantic and positive anomalies in the Pacific, with the magnitudes exhibiting more profound intensity along the coast of South America.

On the other hand, in the neutral years (fourth row of Figure **4-5**), no distinctive pattern is observed. However, in December, the anomalies were negative in the eastern Pacific, indicating a decrease in the humidity in that area. This is consistent since the waters east of the Pacific are usually colder, resulting in less evaporation and reduced moisture availability for December.

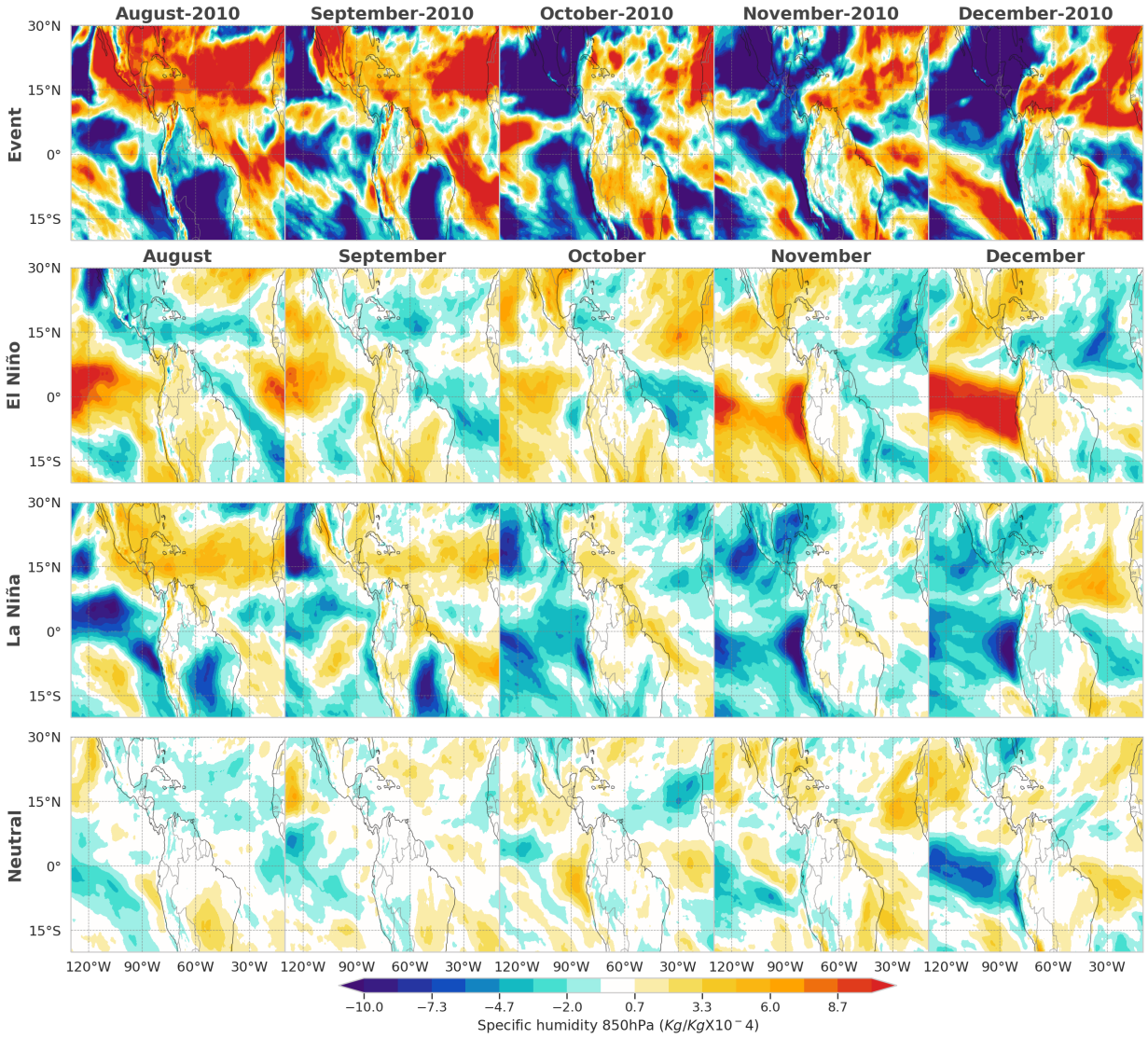

Figure **4-5**.: 850 hPa specific humidity anomalies from August to December, in the 2010 LN event (first row), EN composite (second row), LN composite (third row), and neutral years composite (fourth row).

The transportation of moisture from various sources to different regions plays a fundamental role in precipitation occurrence in the Colombian Andes. As depicted in second row of Figure **4-6**, during the LN composite, starting in August, there is an evident increase in moisture convergence from the Pacific Ocean towards the northern region of South America. Concurrently, in the eastern Pacific, between 13°N and 15°N, there is a noticeable reduction in moisture transport, accompanied by a robust eastward flow. Nevertheless, a decrease in moisture is also observed in Colombia and neighboring areas, with an outflow towards the

Atlantic Ocean occurring between August and September. In October, moisture convergence improves in the eastern Pacific, facilitating the ongoing transport towards the interior of northern South America, with fewer outflows from that particular region. November and December witness an improvement in humidity in north of South America, and in December, moisture inflow from the Caribbean Sea becomes prominent. Conversely, a decline in column moisture is observed towards the southern part of South America, which is being transported toward the South Atlantic.

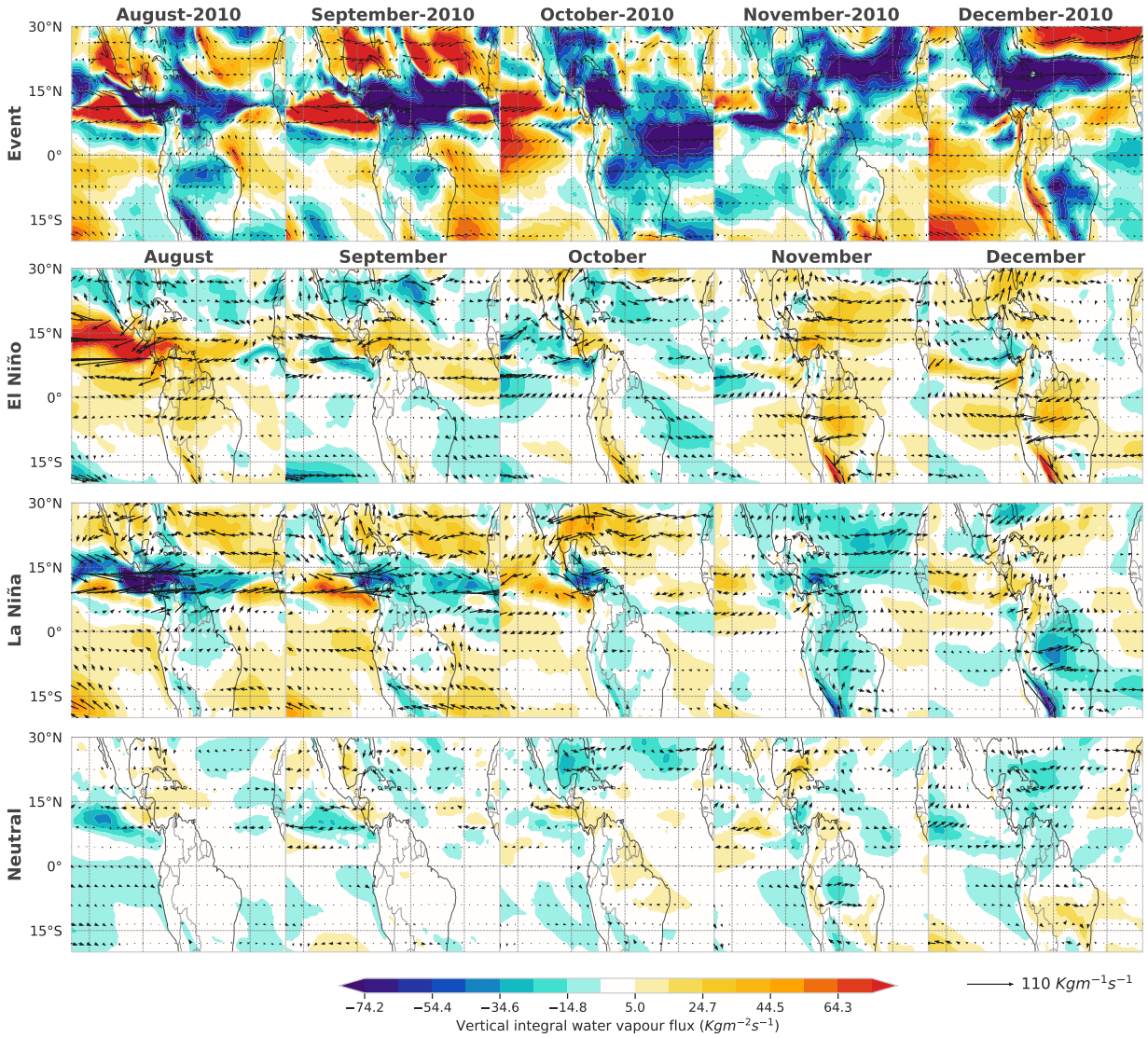

Figure **4-6**.: Vertically integrated moisture flux (vectors) and moisture convergence (shades) anomalies from August to December in the 2010 LN event (first row), EN composite (second row), LN composite (third row), and neutral years composite (fourth row). Vertically integrated moisture flux magnitude is indicated by the arrow at the right-bottom corner for the composite, but the event magnitude corresponds to 200 kgm-1s-1.

For the EN composite (second row Figure **4-6**), the atmospheric circulation during August demonstrates a notable convergence in the eastern Pacific and tropical Atlantic, as shown in the second row of Figure **4-6**. This convergence favors a westward transport of moisture originating from the Atlantic. During September, there is a discernible decline in the moisture flux over the eastern Pacific. By October, the moisture flow pivots from the Pacific

towards northern South America, culminating in an amplified convergence within this region. Conversely, there is a simultaneous decrease in moisture across the Pacific, as well as in the northern and southern sectors of the Atlantic. The subsequent months of November and December witness a shift in moisture transport towards the west across South America, which precipitates an enhancement in regional convergence, as clearly illustrated in Figure **4-6**.

Numerous studies have demonstrated that for northern South America, precipitation increases during LN but decreases during EN (Ávila et al., 2019; Cai et al., 2020; Espinoza et al., 2020; Poveda et al., 2011, 2020). However, a compelling question arises from these findings: Why, during EN events, is there an elevated level of specific humidity and enhanced convergence in northern South America during EN, despite the expected decrease in precipitation? Ruiz-vásquez et al. (2021) identified several mechanisms that may explain precipitation inhibition during EN. Firstly, they showed that precipitable water is higher in EN years than in LN from February to July due to increased moisture transport. Secondly, to understand what happens to the extra moisture that does not precipitate during EN, four indices were examined to explain the thermodynamic conditions of the atmosphere, leading to the conclusion that precipitation inhibition in EN is due to higher values of Lifting Condensation Level (LCL), high Convective Inhibition (CIN) and lower Relative Humidity (RH) in the lowest levels of the atmosphere. These combinations of factors make the condensation process more challenging during EN.

The 2010 LN event exhibited several similarities to the LN composite in various aspects. From August to October 2010 (first row Figure **4-6**), significant moisture convergence occurred in the northern tropical Pacific, accompanied by a slight moisture divergence to the south of that region. Both cases involved the transport of moisture toward Central America and Colombia. However, in October 2010, there was a shift in the direction of moisture transport, resulting in an outflow from northern South America towards the Pacific, alongside convergence over the region. November witnessed moisture divergence in the Pacific, Atlantic, Central America, and southern South America, with convergence observed in Colombia. By December 2010, moisture convergence prevailed over northern South America, the Pacific, and the tropical Atlantic, transporting moisture from the Caribbean Sea. The 2010 LN event exhibited more substantial and extended moisture divergence anomalies than the composite LN during October, November, and December.

During the 2010-2012 LN event, northern South America experienced above-average humidity levels. This phenomenon was linked to two LN events, one occurring from 2010 to 2011 and a less intense event in 2011 – 2012. Previous studies have demonstrated that the moisture flow from the eastern Pacific, Caribbean Sea, and tropical Atlantic resulted in a pronounced moisture convergence in the region (Arias et al., 2015). Moreover, there was an observed increase in moisture transport from the Caribbean Sea compared to other sources. These patterns were attributed to the strengthening of the Chocó low-level jet and the weakening of the Caribbean low-level jet (CLLJ). Arias et al. (2015) also highlighted that the

anomaly gradient between the northern and southern tropical Atlantic contributed to the weakening of the CLLJ, and they emphasized the existence of ENSO-independent variability in the tropical Atlantic. Specifically, the gradient in sea surface temperature anomalies was associated with a robust South Atlantic Mode with variability independent of ENSO. These findings suggest that, within each ENSO event, there can be distinct variations in moisture sources.

The purpose of studying horizontal fields and those variables that affect vertical motion is to explain why EPEs are more frequent during LN than in EN and neutral years. Since a high frequency of extreme events is expected during LN, it does not mean that the occurrence of events during EN and neutral years is negligible. In the first chapter, it was shown that the activity of extreme events is high throughout the year and that the intensities do not show differences between any of the ENSO phases with neutral years. This is due to the different sources of humidity that are transported into the Andes and can change during the year. In December - January - February, when the ITCZ is positioned southernmost, moisture sources come from the northern tropical Atlantic, the Caribbean, and even from the northern subtropical Atlantic, then when the ITCZ moves northward between 3°N and 6°N, local recycled moisture has a high percentage in March-April-May in the first rainy season, as well as moisture from the tropical Atlantic and the Orinoco. In June-July-August, when the ITCZ is further north, moisture is strongly contributed from the Amazon basin and the southern tropical Atlantic. Finally, in the second pass of the ITCZ, the second wet season occurs, with high local moisture recycling, important moisture transport from the Orinoco, and essential contributions from the northern and southern tropical Pacific due to the intensification of the low-level Chocó jet (Arias et al., 2015; Builes-Jaramillo et al., 2022; Hoyos et al., 2018). This pattern of moisture transport shows that there are inflows throughout the year in all directions into the Andes, allowing precipitation throughout the year and the development of EPE—taking into account the two well-marked dry and wet seasons.

To gain a deeper understanding of atmospheric dynamics, we computed the cross-sectional representations for specific humidity, omega, and geopotential anomalies for the region encompassing all of the Colombian Andes (-80°W, -60°W, 10°N, 15°S), over the same five-month period. Analyzing the cross-section of these variables is pivotal as it allows us to visualize their vertical distribution, thereby aiding in the detection of any altitude-dependent patterns or anomalies that may be crucial for comprehending the initiation and propagation of extreme events.

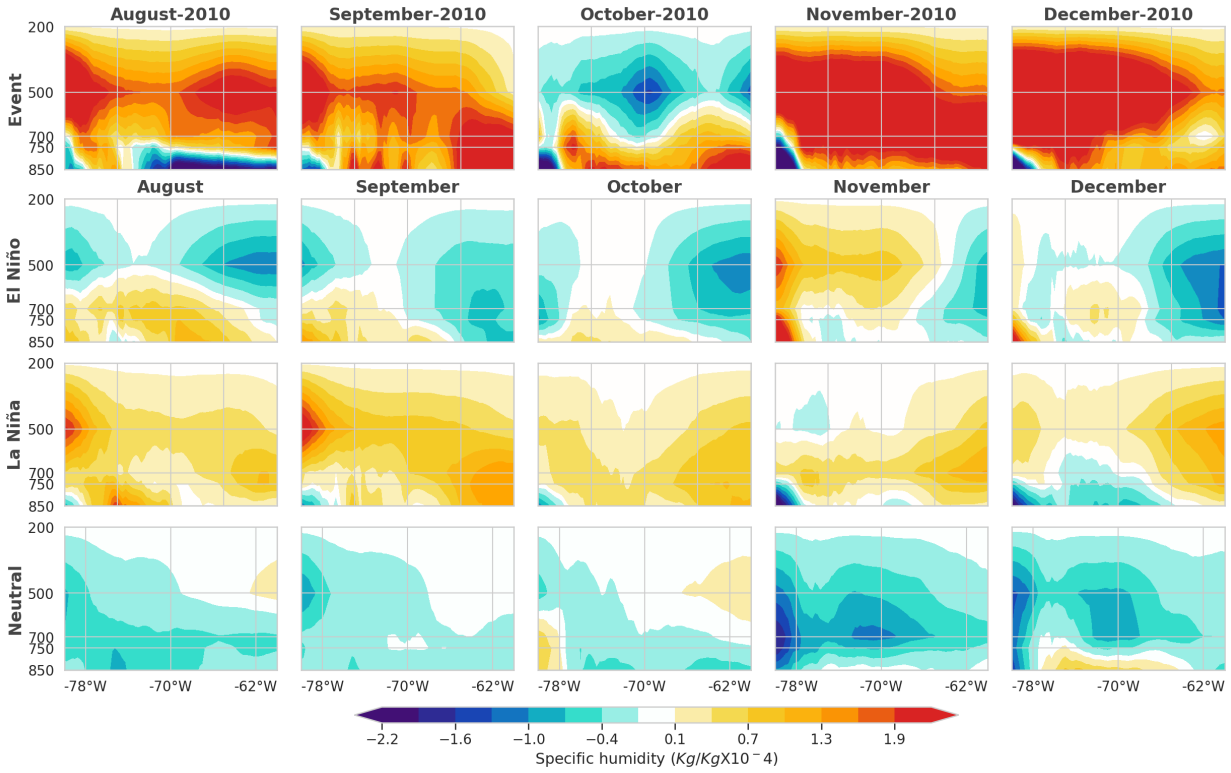

Figure **4-7**.: Meridional specific humidity anomalies cross-section from August to December in the 2010 LN event (first row), EN composite (second row), LN composite (third row), and neutral years composite (fourth row).

Figure **4-7** shows the specific humidity anomalies for the 2010 event, EN, LN, and neutral years composite. The vertical profile during the 2010 LN event had higher than average humidity values up to 200hPa for August and September, while in October, high humidity values only reached up to 700hPa, and negative anomalies in the following pressure levels. However, at all altitudes, these humidity anomalies are again high for November and December. LN composite shows some similarities in August and September. In October, low specific humidity is found at low-pressure levels, which is not observed in the preceding and following months, additional external factors may have contributed to lower-than-average.

For November 2010 and December 2010, there are notable differences in composite humidity anomalies at lower altitudes in LN, EN, and neutral years. It is worth noting that in neutral years, specific humidity is lower than normal across all months, with November and December experiencing the most significant decreases. However, during EN years, the trend shifts - positive anomalies are observed at low to medium levels of the atmosphere in August, followed by negative anomalies from 500 to 200 hPa in August and September. Only positive anomalies are found in October at 850 hPa in the Andes, while negative values are

observed along the easternmost Andes. In November, positive anomalies are present at all pressure levels, while in December, they are only found at low levels. These results align with those presented in Figure **4-5** at 850 hPa and other pressure levels (500, 700, 750, and 200 hPa; not shown), where LN results in negative anomalies in the eastern Pacific and positive anomalies over northern South America. Moisture analysis shows that during LN, there is moisture for convective systems to develop, while in EN, moisture levels are generally below average, resulting in drier conditions. In Chapter 2, we found that during neutral years there is a high activity of EPEs, so we would expect higher humidity values, especially in SON, where the rainy season occurs in the Andes. This suggests that other factors influence the occurrence of rain in the region during this season.

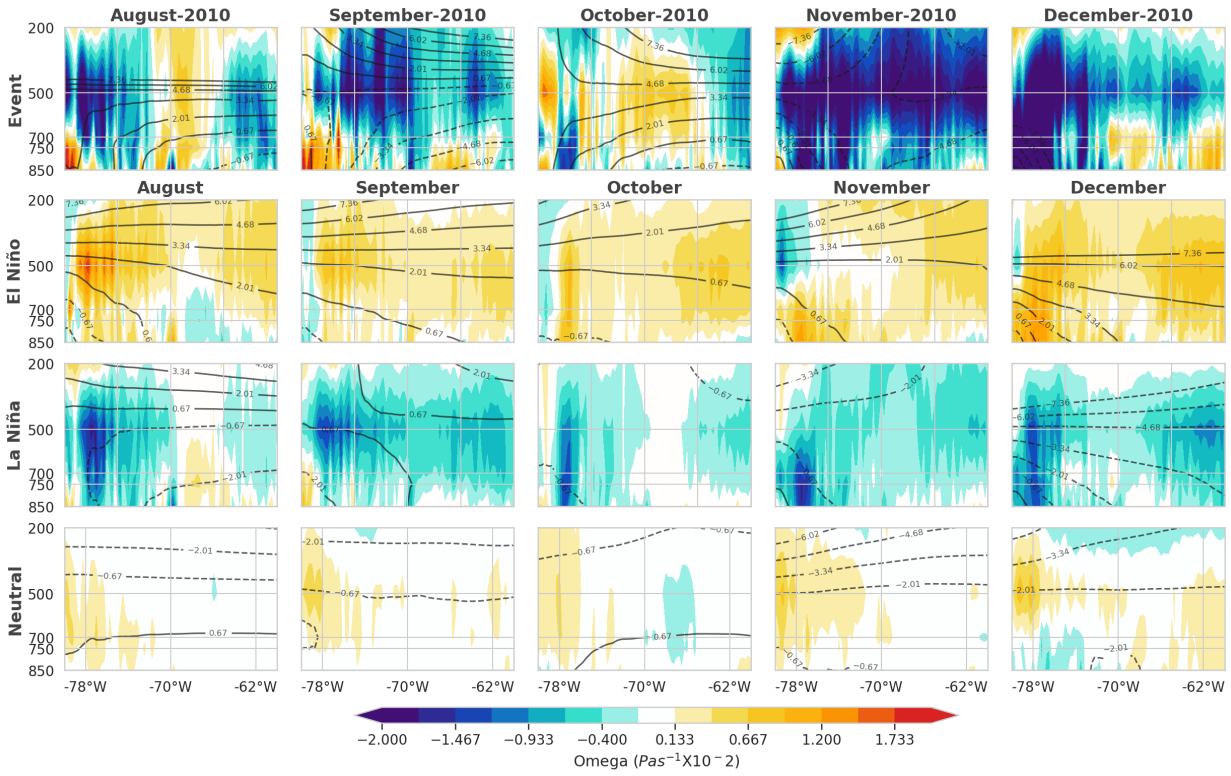

Figure **4-8**.: Meridional omega (shades) and geopotential height (contours) anomalies cross-section from August to December in the 2010 LN event (first row), EN composite (second row), LN composite (third row), and neutral years composite (fourth row). Solid (dotted) contours indicate positive (negative) geopotential height anomalies.

The omega (vertical velocity) anomalies (Figure **4-8**) differ between the specific event and the LN composite for the Colombian Andes. Between August and October, negative anomalies are shown mainly in the composite LN, indicating strengthening in the vertical ascent and negative geopotential anomalies at low levels, and positive anomalies at high

levels. Positive omega values are observed east of the Andes in August and in all the Andes in October in LN 2010 event, i.e., a weakening of the uplift, accompanied by positive geopotential anomalies. Both in the event and in the composite, there is an improvement in the vertical ascent in November and December, in addition to negative geopotential anomalies.

On the other hand, during EN, the ascent is generally weakened in the Andes (positive anomalies), with higher-than-average geopotential height in the five months of analysis. Neutral years show slightly weakened vertical ascent, which varies in each month and pressure level; even during December, some negative anomalies are shown in the lower atmosphere over the Andes; negative anomalies are found throughout the profile (Figure **4-8**).

A distinctive atmospheric circulation in the Colombian Andes region is observed regarding the LN and EN phenomena. During LN, the vertical ascent strengthens, while during EN, this process weakens (Cai et al., 2015; Chen et al., 2019; Trenberth, 2019). This phenomenon is relevant since vertical motion plays a crucial role in atmospheric convection and is explained by y Ruiz-vásquez et al. (2021). They found anomalies exist in the tropical Pacific's Walker and Hadley circulation. These findings indicate that during LN, favorable conditions for cloud development and subsequent precipitation at higher altitudes are created. However, in October 2010, specific characteristics were observed in this movement, such as reduced humidity in the upper levels due to the weakening of rising air, which hinders moisture transport to the top atmosphere. This, in turn, inhibits convection, likely precipitation, and favors low occurrences of EPE during this month.

Choosing October as the month with the highest extreme event activity does not indicate that the previous or following months did not have extreme events. The purpose was to determine how much the atmospheric conditions weakened or strengthened by having a reference month for EPE activity. Chapter 2 shows that the intensity and frequency of extreme events are high during the year, with September-October-November being the season with the most increased occurrence of events in the Colombian Andes; however, it should be noted that the activity of extreme events varies spatially, and dependins on the source of moisture transport.

4.3. Conclusions

Extreme weather events are an everyday feature in the Colombian Andes and can be influenced by anomalies in the atmospheric circulation pattern during ENSO phases. We analyzed several variables, including geopotential height anomalies, specific humidity, velocity potential, omega, divergence, vertically integrated moisture flux, and moisture convergence to better understand the mechanisms and patterns associated with these events. By examining how horizontal and vertical movement affects convective development, we aimed to identify factors that promote or inhibit precipitation. Our analysis revealed that EPEs occur more

frequently during LN than EN or neutral years. We also examined the characteristics of a strong event in 2010-2011, focusing on October when precipitation was highest, and extreme events were more frequent. This involved studying the atmospheric circulation pattern two months before and after October.

We discovered some similarities between the 2010 LN event and the LN composite in the anomaly fields. However, there were also some notable differences in the velocity potential. Specifically, we observed divergence in the Atlantic and South America during the 2010 event, which was not present in the composite (Figure **4-3**). Furthermore, as depicted in(Figure **4-4**, the divergence anomalies during the months of the LN event exhibited a heterogeneous pattern, contrasting with the more uniform profile observed in the LN composite.

Comparing LN and EN composites, we found an opposite pattern in all the analyzed variables. In general, during EN, the high sea surface temperatures in the eastern Pacific generate positive geopotential height anomalies at 200 hPa (Figure **4-1**), in addition to positive omega anomalies at 500 hPa (Figure **4-2**), indicating strengthening in the ascent of air masses, high specific humidity at 850 hPa (Figure **4-5**) and divergence at high levels at 200 hPa (Figure **4-4**). These results imply that during EN, it is possible to obtain convective systems in the Pacific Ocean, although these conditions change over land. In northern South America, due to Walker's circulation anomalies, air suppression is generated in the region, generating drier and warmer conditions. This pattern can be slightly appreciated in the variables. As mentioned in several studies, LN mirrors the changes in hydroclimatological variables in EN, so during LN, normal conditions strengthen, and convective processes will intensify over the Colombian Andes, increasing precipitation.

In contrast, the cross-section for omega, specific humidity, and geopotential height shows marked differences between the 2010 LN event and the composite. In the composite, all months from 850 hPa to 200 hPa show positive anomalies of specific humidity (Figure **4-7**) in the Colombian Andes, i.e., there is more humidity during LN than in the average. Although this humidity pattern is very similar in the event, October shows an exception with lower values from the middle to high levels. Although omega and geopotential height anomalies are different in all months, in the LN composite, a pattern is observed throughout the vertical of negative anomalies of vertical motion (Figure **4-8**), indicating strengthening in the ascent of air and favoring conditions for convection. In contrast, the 2010 event exhibited positive omega values in August, October, and December, with October notably displaying a pervasive weakening of the upward air motion across nearly the entire region. Regarding geopotential height, negative anomalies predominantly characterize the LN composite. However, this pattern displays noticeable variations in terms of both altitude and temporal progression during the event.

EN and neutral years also had an interesting pattern in the cross-section of omega and humidity. In the analysis of the horizontal circulation, LN exhibited a similar pattern to

the neutral years in some variables; however, this changes entirely in the vertical motion. Regarding anomalies in the neutral years, it shows lower than average humidity values in almost the entire vertical. In omega, the values are positive, suggesting weakening in the ascent (Figure **4-7** and **4-8**). In the context of neutral years, the observed anomalies resemble those seen during EN, with specific humidity predominantly evident at lower atmospheric levels between August and October. There is a corresponding decrease in humidity from the mid-to-upper atmosphere. During the months of November and December, these anomalies generally exhibit positive values across the entire vertical atmospheric column. Further, patterns akin to those found during EN conditions can be discerned in the omega (vertical motion) and geopotential height parameters. Namely, positive anomalies are exhibited in vertical motion and geopotential height, a correlation which is further clarified in Figure **4-7** and **4-8**.

Figure **4-6** shows that During EN, moisture convergence prevails, leading to increased sources of moisture for precipitation. In contrast, LN exhibits moisture divergence in northern South America, resulting in limited sources of moisture for precipitation. Studies have demonstrated that during EN phases, northern South America exhibits a greater quantity of precipitable water compared to LN phases. This can be attributed to convergence dynamics, indicative of a moist air flow accumulation in this region. However, available high humidity does not guarantee precipitation development due to other thermodynamic factors that prevent it, such as high values of CIN, LCL, and low RH values characteristic in EN (Ruiz-vásquez et al., 2021). This combination of factors suggests that even though the moisture sources may be limited in LN, the vertical movement is stronger than in EN (Figure **4-8**), as has been shown by several authors due to the strengthening of the ascending branch of Walker's circulation in South America (Cai et al., 2020; Chen et al., 2019; Trenberth, 2019).

By comparing the 2010 LN event with the composite, it is possible to gain insight into the behavior of certain variables contributing to increased precipitation in northern South America during any LN event. However, it is important to note that moisture sources may vary between different events, and the interaction of other phenomena, besides ENSO, at different scales should also be considered, as indicated by Arias et al. (2015). This research reveals that atmospheric conditions favorable for precipitation occur during LN in northern South America. It is worth mentioning that the effects of EN and LN are not linear: while a decrease in rainfall is observed in the Colombian Andes during EN, extreme precipitation events can still occur. In fact, as mentioned in the first chapter, precipitation extremes occur during LN, EN, and neutral years, and their intensities can be similar. However, the frequency of extreme precipitation events varies, with a higher frequency during LN.

5. General conclusions

The aim of this study was to characterize EPEs and ETEs in the Colombian Andes during ENSO phases and neutral years. We utilized three precipitation databases (TRMM, CHIRPS, and IDEAM stations) and reanalysis data from the ERA5 product for temperature. Our findings differ from previous research in the region, as our methodology and objective were focused on characterizing these events rather than identifying trends (Cerón et al., 2022; Pabón-Caicedo et al., 2020; Rodríguez et al., 2019).

The characterization of extreme events in our study was based on a defined threshold derived from the 95th and 99th percentile for precipitation. This percentile was individually calculated for each pixel in the satellite observations and at each station. At the same time, the 90th and 10th percentile was selected to characterize the ETEs, considering the maximum and minimum temperature, daytime and nighttime (Barlow et al., 2019; Grotjahn et al., 2016).

The characterization of the intensity of EPEs showed no differences between ENSO phases and neutral years. However, a distinct contrast was observed in the frequency of EPEs, which demonstrated seasonal variations between LN, EN, and neutral years. For the Colombian Andes, the events at the 95th percentile in DJF across all three databases revealed that the occurrence of events is higher in the western region. This trend then shifts during MAM, with the frequency increasing to the north and east of the Andes. In the JJA season, events become prevalent across the entire Andes range, while during SON, they converge predominantly in the north.

The pattern presented in the 95th percentile is also observed in the 99th percentile, with the difference that the occurrence of events decreases, due to the higher threshold required for classification. The seasonal fluctuations of the EPEs appear to be associated with the biannual movement of the ITCZ, underscoring the relevance of this climatic modulator in the region's precipitation regime and its interplay with ENSO. When comparing ENSO and neutral years, our results suggest that during LN, EPEs occur more frequently than during EN and neutral years. However, at certain stations, events during EN may indeed surpass the frequency observed in neutral years.

Additionally, we performed a cluster analysis using the k-means method (Jia et al., 2019; Steinley, 2006) to identify regions with similar daily EPEs characteristics at both percentiles. This analysis was applied to the TRMM and CHIRPS databases. Our analysis classified five

distinct regions in both databases, where the spatial distribution of the clusters demonstrated similar patterns at the 95th percentile. However, notable differences emerged at the 99th percentile, particularly in the central Andes. In particular, the cluster analysis was similar to the spatial distribution of the EPEs when comparing the threshold of both percentiles (Figures **2-22** and **2-23**). This pattern was mirrored in both the TRMM and CHIRPS databases and followed the spatial distribution of the stations. The behavior remained consistent across ENSO events and neutral years.

On the other hand, before performing the characterization of ETEs, we first evaluated the data trends and subsequently removed these trends to discount the effects of climate change (Foster and Rahmstorf, 2011, Figure **3-1**). Comparison between ENSO and neutral years in the TXx and TNn indices were only performed for the DJF and JJA seasons. The results showed that difference between ENSO and neutral years in ETEs are significant and intense during EN and neutral years compared to LN. However, the difference between EN and neutral years in terms of daytime and nighttime temperatures revealed less significance within the Andean region, but it was evident that TXx and TNn were more pronounced during EN, specifically during the day (Figures **3-9**, **3-10**, **3-11**, **3-12**). The frequency analysis of ETEs indicated that extreme TXx occur more frequently during EN, while extreme TNn are more common during LN. In addition, TXx ETEs during EN are more intense and frequent during the daytime, while TNn are less intense yet more frequent at nighttime during LN.

We were also interested in investigating the atmospheric circulation patterns that could be associated with the EPEs. Specifically, our focus was on the intense La LN event from 2010-2012. Our aim was to determine whether the horizontal fields of certain hydroclimatic variables during this LN event mirrored those found in a composite LN event. The objective was to discern if there's a general pattern to LN events or if each one is unique, as well as how these patterns differ from EN composite and neutral years. Interestingly, we found that the horizontal fields of variables such as geopotential height, omega (vertical velocity), velocity potential, specific humidity, vertical integrated moisture flux, and divergence wind showed patterns that were similar between the 2010-2012 LN event and the composite LN. These patterns exhibited a contrast with those of EN events.

However, during certain months, cross-sectional analysis of variables like omega (vertical velocity), specific humidity, and geopotential height revealed discrepancies between the specific LN event and the composite. This suggests that the primary distinctions may be predominantly associated with vertical movements. The combined results of the horizontal fields and the cross section of the variables show us in an exploratory way the behavior of convection in northern South America during ENSO.

During LN, dry conditions are favored in the tropical Pacific due to suppression, cooler than average SST temperature anomalies, causing the evaporation rate to be low, as well as the humidity; and therefore the vertical movement is weakened (Figures **4-1**, **4-2**, **4-3**,

4-5,**4-7**,**4-8**). The moisture transport in the air column, inhibiting deep convection, and together affecting the transport of humidity in the horizontal (Figure **4-6**). While in the north of South America the ascending branch of Walker's circulation and the change in pressure favors evaporation in the region and therefore the triggering of precipitation. These patterns are observed in the opposite way in EN.

Our research raises important questions regarding the prevalence and intensity of EPEs during LN years, and why these characteristics do not significantly differ between ENSO and neutral years. We conducted an exploratory analysis of circulation patterns to shed light on these inquiries and drew insights from Ruiz-vásquez et al. (2021) findings. The authors investigated thermodynamic indices to elucidate why convection is not favored during EN in the northern region of South America. Additionally, Arias et al. (2015) identified changes in moisture sources that influenced precipitation anomalies during the 2010-2012 LN event.

As underscored in previous studies, we observed that the Andes are influenced by different sources of moisture that can affect the EPEs (Hoyos et al., 2018). For instance, north of the Andes, moisture recycling from the Magdalena basin is prominent, coupled with moisture inflow from the Atlantic via the Caribbean low-level jet. The west features moisture inflow from the Chocó jet stream, while the east and south are influenced by the Orinoco jet stream and moisture sources from the Amazon (Builes-Jaramillo et al., 2022; Jiménez-Sánchez et al., 2019; Bedoya-Soto et al., 2019; Poveda and Mesa, 2000). This may also explain the regions categorized by the cluster analysis, in addition to other atmospheric circulation patterns.

We conducted an exploratory analysis of horizontal fields and cross-sections to gain insights into the atmospheric conditions during El Niño-Southern Oscillation (ENSO) and neutral years in the months preceding and following October. This analysis was conducted for the LN 2010-12 event, as well as for the EN, LN, and neutral year composites. As the modulation of the ENSO phenomenon over South America could promote convective activity in the region, it is necessary to analyze moisture sources to study the evolution of the EPEs.

To study the EPEs, we utilized three databases, enabling us to compare satellite observations with station measurements. The analysis of the CHIRPS database's heatmaps (see Figure) revealed inconsistencies in the months of June, July, and August. Specifically, we observed more intense values of EPEs in the 95th percentile that were not evident in the station measurements and TRMM data. Hence, it is crucial for future investigations to assess extreme values using different sources of information specific to our region.

Finally, there are several remaining questions and future work regarding extreme precipitation and temperature events. For example, the characterization of extreme precipitation and temperature events on an hourly scale. In addition, is it important to explore if there are available registers in situ data to characterize extreme temperature events. Also, it would be valuable to explore if the implementation of other indices would lead to different conclusion and to define methodologies to analyze the mechanism behind extreme precipitation and

temperature evento during ENSO.

A. Appendix: Complementary Figures

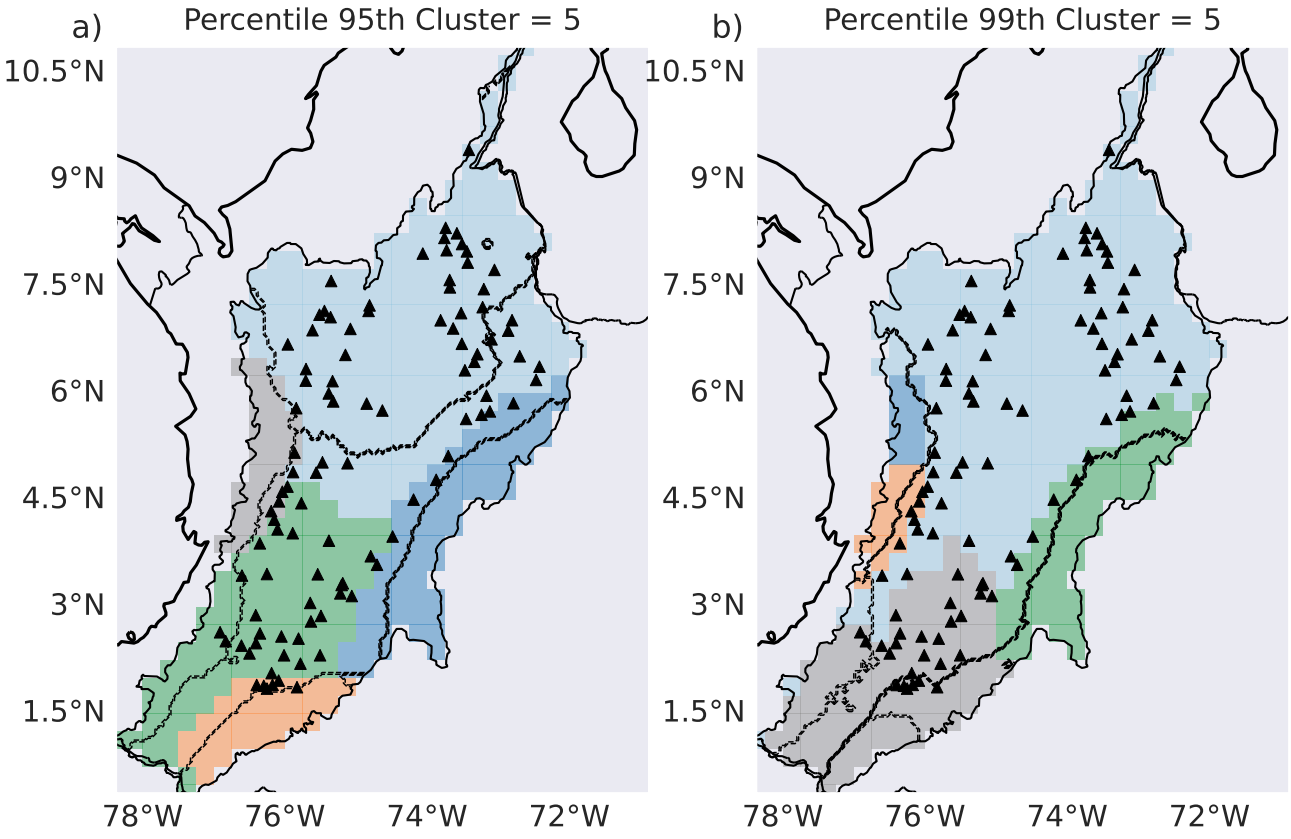

Figure **A-1**.: Regional cluster classification in the Colombian Andes. The shading is the TRMM classification, the overlay (black) contour is the CHIRPS classification and the triangle symbol corresponds to the IDEAM stations. For a) 95th percentile and b) 99th percentile.

B. Appendix: Complementary Tables

Station code	Latitude (°)	Longitude (°)	Elevation (m.a.m.s.l)
27011100	7.15880556	-74.8218333	600
24035430	5.74591667	-73.1163611	2470
24030160	5.86035722	-72.7847914	2486
23190140	7.46472222	-73.2013889	500
24035260	6.52072222	-72.6966111	1160
23210010	8.185	-73.7552778	90
24050070	7.12716667	-73.5205556	150
26140180	4.8925	-75.8827778	922
27020200	7.07072222	-75.3555833	2400
23210160	8.32666667	-73.7377778	150
23190110	7.83805556	-73.4280556	164
21110330	3.18738889	-75.2184167	429
21110070	3.15033333	-75.0573333	615
24010830	5.64	-73.4504444	2985
26080290	3.89088889	-76.3508333	962
21010040	1.96147222	-76.0856944	1334
26230160	7.10527778	-75.5116667	1440
26125061	4.45472222	-75.7663889	1229
21050160	2.31705556	-76.0101389	1745

Station code	Latitude (°)	Longitude (°)	Elevation (m.a.m.s.l)
24030750	6.88111111	-72.8583333	2400
24011070	6.32361111	-73.4672222	1800
21205740	5.11772222	-73.7014167	2709
26180170	5.99833333	-75.3813889	2530
23145020	6.69638889	-73.51	805
26070170	3.45972222	-76.2502778	155
24050110	6.91194444	-73.6322222	216
24010660	6.44361111	-73.3338889	150
26010020	2.34336111	-76.4955	2419
26255020	7.15727778	-75.4422222	1132
21255120	5.01685278	-75.1176111	269
21115060	3.32922222	-75.1840556	400
26115080	4.48091667	-76.0798889	945
21010160	1.89944444	-76.3941667	1724
26185020	5.88636111	-75.3186389	2408
26020460	2.48758333	-76.4046667	2507
21010170	1.90138889	-76.1725	1700
25020690	9.42327778	-73.4109444	500
26230130	6.88719444	-75.6096111	2830
26020020	2.62466667	-76.3491389	2446
23080640	6.17108333	-75.328	2150
23180080	7.48944444	-73.6783333	90
24055040	6.54972222	-73.292	940
22020060	3.05333333	-75.6419167	2326
21190090	3.98697222	-74.4835556	1900
37010060	7.02777778	-72.8044444	3824
22055020	3.45577778	-75.5363611	699
21050090	2.55144444	-75.8065	1545
26105140	4.03305556	-75.8880278	332

Station code	Latitude (°)	Longitude (°)	Elevation (m.a.m.s.l)
26105140	4.03305556	-75.8880278	332
23070020	5.85552778	-74.8483611	449
26250030	7.57905556	-75.3478333	95
27010850	6.90555556	-75.0772222	1530
24025030	5.96638889	-73.1638914	2700
21205720	4.50575	-74.1892778	2900
27030140	7.23611111	-74.8079444	100
21120090	2.87033333	-75.4909722	700
21110120	3.30533333	-75.2007778	400
26030030	2.64066667	-76.9090278	2658
23060150	5.75827778	-74.6273333	1836
26110040	4.34294444	-76.1904444	972
26100830	4.68841667	-75.9616667	940
26110300	4.61638889	-76.0344444	940
26130170	4.88555556	-75.5580556	2134
21050230	2.58180556	-76.0468056	1595
27010770	6.17833333	-75.7050833	255
26080280	3.43819444	-76.6015556	1637
21010190	1.84894444	-76.2497222	1700
22050040	3.92805556	-75.3791667	468
21015030	1.88847222	-76.2949722	1800
21080080	2.79305556	-75.632	1800
23190210	7.59333333	-73.6813889	89
23190520	7.99555556	-73.4397222	271
26035030	2.45288889	-76.60875	1752
26170150	5.79105556	-75.8388056	2100
21160170	3.70933333	-74.7908333	140
23195180	7.73527778	-73.0516667	1882
26100070	4.22380556	-76.1473056	964

Station code	Latitude (°)	Longitude (°)	Elevation (m.a.m.s.l)
23210130	8.24944444	-73.58	250
26155110	5.02977778	-75.4699167	2104
26040290	2.88052778	-76.4075	293
23155030	7.02638889	-73.8086111	126
27015190	6.54038889	-75.14675	1440
26100700	4.08725	-76.1008056	1314
26140090	5.16705556	-75.8627778	1609
21206980	4.78427778	-73.8708056	3100
24030530	5.69872222	-73.2342222	2580
23190380	7.21108333	-73.2178889	855
21145080	3.58977778	-74.7029444	1410
24060050	6.75916667	-73.0927778	1460
21010220	2.06588889	-76.185	1625
26030090	2.515	-76.8297222	1628
24030660	6.37511111	-72.419	3409
21035040	1.86838889	-75.8277778	145
26220090	6.68805556	-75.9572222	10
21060100	2.31716667	-75.5035833	1460
23190480	8.09888889	-73.5075	228
23205030	7.96527778	-74.0591667	650
21040060	2.19936111	-75.7793611	805
23190710	8.01183333	-73.7244444	50
24035250	6.18833333	-72.4663333	2888
26205080	6.34105556	-75.7009444	1737

Table **B-1**.: Information from IDEAM stations located in the Andes region.

Bibliography

Aceituno, P. (1989). On the functioning of the Southern Oscillation in the South American sector. Part II. Upper-air circulation. *Journal of Climate*, 2(4):341–355.

Aceituno, P., Prieto, M. D. R., Solari, M. E., Martínez, A., Poveda, G., and Falvey, M. (2009). The 1877-1878 El Niño episode: Associated impacts in South America. *Climatic Change*, 92(3-4):389–416.

Aguilar, E., Peterson, T. C., Obando, P. R., Frutos, R., Retana, J. A., Solera, M., Soley, J., García, I. G., Araujo, R. M., Santos, A. R., Valle, V. E., Brunet, M., Aguilar, L., Álvarez, L., Bautista, M., Castañón, C., Herrera, L., Ruano, E., Sinay, J. J., Sánchez, E., Oviedo, G. I., Obed, F., Salgado, J. E., Vázquez, J. L., Baca, M., Gutiérrez, M., Centella, C., Espinosa, J., Martínez, D., Olmedo, B., Espinoza, C. E., Núñez, R., Haylock, M., Benavides, H., and Mayorga, R. (2005). Changes in precipitation and temperature extremes in Central America and northern South America, 1961-2003. *Journal of Geophysical Research Atmospheres*, 110(23):1–15.

Alexander, L. V. (2016). Global observed long-term changes in temperature and precipitation extremes: A review of progress and limitations in IPCC assessments and beyond. *Weather and Climate Extremes*, 11:4–16.

Almazroui, M., Ashfaq, M., Islam, M. N., Rashid, I. U., Kamil, S., Abid, M. A., O'Brien, E., Ismail, M., Reboita, M. S., Sörensson, A. A., Arias, P. A., Alves, L. M., Tippett, M. K., Saeed, S., Haarsma, R., Doblas-Reyes, F. J., Saeed, F., Kucharski, F., Nadeem, I., Silva-Vidal, Y., Rivera, J. A., Ehsan, M. A., Martínez-Castro, D., Muñoz, Á. G., Ali, M. A., Coppola, E., and Sylla, M. B. (2021). Assessment of CMIP6 Performance and Projected Temperature and Precipitation Changes Over South America. *Earth Systems and Environment*, 5(2):155–183.

Araujo, R. S. P., Vila, D. A., Rodrigues, D. T., Pareja, D. Q., Cassineli, R. P., Almeida, R. d. S., and de Sousa Afonso, J. M. (2020). Assessment of the Extreme Precipitation by Satellite Estimates over South America. *Remote Sensing*, 12(13):2085.

Arblaster, J. M. and Alexander, L. V. (2012). The impact of the El Nio-Southern Oscillation on maximum temperature extremes. *Geophysical Research Letters*, 39(20):2–6.

Arias, P. A., Martínez, J. A., and Vieira, S. C. (2015). Moisture sources to the 2010–2012 anomalous wet season in northern South America. *Climate Dynamics*, 45(9-10):2861–2884.

Ávila, Á., Guerrero, F. C., Escobar, Y. C., and Justino, F. (2019). Recent precipitation trends and floods in the Colombian Andes. *Water (Switzerland)*, 11(2):1–22.

Banauthor, N., Fischerauthor, E. M., Rajczakauthor, J., Schmidliauthor, J., Freiauthor, C., Giorgiauthor, F., Karlauthor, T. R., Kendonauthor, E. J., Tankauthor, A. M. K., Gormanauthor, P. A. O., et al. (2015). Percentile indices for assessing changes in heavy precipitation events.

Barkhordarian, A., von Storch, H., Zorita, E., Loikith, P. C., and Mechoso, C. R. (2018). Observed warming over northern South America has an anthropogenic origin. *Climate Dynamics*, 51(5-6):1901–1914.

Barlow, M., Gutowski, W. J., Gyakum, J. R., Katz, R. W., Lim, Y. K., Schumacher, R. S., Wehner, M. F., Agel, L., Bosilovich, M., Collow, A., Gershunov, A., Grotjahn, R., Leung, R., Milrad, S., and Min, S. K. (2019). North American extreme precipitation events and related large-scale meteorological patterns: a review of statistical methods, dynamics, modeling, and trends. *Climate Dynamics*, 53(11):6835–6875.

Bastianin, A., Lanza, A., and Manera, M. (2018). Economic impacts of El Niño southern oscillation: evidence from the Colombian coffee market. *Agricultural Economics (United Kingdom)*, 49(5):623–633.

Beck, F., Bárdossy, A., Seidel, J., Müller, T., Fernandez Sanchis, E., and Hauser, A. (2015). Statistical analysis of sub-daily precipitation extremes in Singapore. *Journal of Hydrology: Regional Studies*, 3:337–358.

Bedoya-Soto, J. M., Poveda, G., Trenberth, K. E., and Vélez-Upegui, J. J. (2019). Interannual hydroclimatic variability and the 2009–2011 extreme ENSO phases in Colombia: from Andean glaciers to Caribbean lowlands. *Theoretical and Applied Climatology*, 135(3-4):1531–1544.

Borges, P. d. A., Bernhofer, C., and Rodrigues, R. (2018). Extreme rainfall indices in Distrito Federal, Brazil: Trends and links with El Niño southern oscillation and Madden–Julian oscillation. *International Journal of Climatology*, 38(12):4550–4567.

Builes-Jaramillo, A., Valencia, J., and Salas, H. D. (2023). The influence of the El Niño-Southern Oscillation phase transitions over the northern South America hydroclimate. *Atmospheric Research*, 290(May).

Builes-Jaramillo, A., Yepes, J., and Salas, H. D. (2022). The Orinoco Low-Level Jet and Its Association with the Hydroclimatology of Northern South America. *Journal of Hydrometeorology*, 23(2):209–223.

Cai, W., McPhaden, M. J., Grimm, A. M., Rodrigues, R. R., Taschetto, A. S., Garreaud, R. D., Dewitte, B., Poveda, G., Ham, Y.-G., Santoso, A., Ng, B., Anderson, W., Wang, G., Geng, T., Jo, H.-S., Marengo, J. A., Alves, L. M., Osman, M., Li, S., Wu, L., Karam-

peridou, C., Takahashi, K., and Vera, C. (2020). Climate impacts of the El Niño–Southern Oscillation on South America. *Nature Reviews Earth Environment*, 1(4):215–231.

Cai, W., Santoso, A., Wang, G., Yeh, S. W., An, S. I., Cobb, K. M., Collins, M., Guilyardi, E., Jin, F. F., Kug, J. S., Lengaigne, M., Mcphaden, M. J., Takahashi, K., Timmermann, A., Vecchi, G., Watanabe, M., and Wu, L. (2015). ENSO and greenhouse warming. *Nature Climate Change*, 5(9):849–859.

Carvalho, M., Melo-Gonçalves, P., Teixeira, J., and Rocha, A. (2016). Regionalization of europe based on a k-means cluster analysis of the climate change of temperatures and precipitation. *Physics and Chemistry of the Earth, Parts A/B/C*, 94:22–28.

Cerón, W. L., Andreoli, R. V., Kayano, M. T., Canchala, T., Ocampo-Marulanda, C., Avila-Diaz, A., and Antunes, J. (2022). Trend Pattern of Heavy and Intense Rainfall Events in Colombia from 1981-2018: A Trend-EOF Approach. *Atmosphere*, 13(2).

Chen, N., Thual, S., and Stuecker, M. F. (2019). *El Niño and the Southern Oscillation: Theory*. Elsevier Inc.

Condom, T., Martínez, R., Pabón, J. D., Costa, F., Pineda, L., Nieto, J. J., López, F., and Villacis, M. (2020). Climatological and Hydrological Observations for the South American Andes: In situ Stations, Satellite, and Reanalysis Data Sets. *Frontiers in Earth Science*, 8(April).

de Barros Soares, D., Lee, H., Loikith, P. C., Barkhordarian, A., and Mechoso, C. R. (2017). Can significant trends be detected in surface air temperature and precipitation over South America in recent decades? *International Journal of Climatology*, 37(3):1483–1493.

Dracup, J. A. and Gutie, F. (2001). An analysis of the feasibility of long-range streamflow forecasting for Colombia using El Niño–Southern Oscillation indicators. *Journal of Hydrology*, 246:181–196.

Dunn, R. J., Alexander, L. V., Donat, M. G., Zhang, X., Bador, M., Herold, N., Lippmann, T., Allan, R., Aguilar, E., Barry, A. A., Brunet, M., Caesar, J., Chagnaud, G., Cheng, V., Cinco, T., Durre, I., de Guzman, R., Htay, T. M., Wan Ibadullah, W. M., Bin Ibrahim, M. K. I., Khoshkam, M., Kruger, A., Kubota, H., Leng, T. W., Lim, G., Li-Sha, L., Marengo, J., Mbatha, S., McGree, S., Menne, M., de los Milagros Skansi, M., Ngwenya, S., Nkrumah, F., Oonariya, C., Pabon-Caicedo, J. D., Panthou, G., Pham, C., Rahimzadeh, F., Ramos, A., Salgado, E., Salinger, J., Sané, Y., Sopaheluwakan, A., Srivastava, A., Sun, Y., Timbal, B., Trachow, N., Trewin, B., van der Schrier, G., Vazquez-Aguirre, J., Vasquez, R., Villarroel, C., Vincent, L., Vischel, T., Vose, R., and Bin Hj Yussof, M. N. A. (2020). Development of an Updated Global Land In Situ-Based Data Set of Temperature and Precipitation Extremes: HadEX3. *Journal of Geophysical Research: Atmospheres*, 125(16):1–28.

Erfanian, A., Wang, G., and Fomenko, L. (2017). Unprecedented drought over tropical

South America in 2016: Significantly under-predicted by tropical SST. *Scientific Reports*, 7(1):22–24.

Espinoza, J. C., Garreaud, R., Poveda, G., Arias, P. A., Molina-Carpio, J., Masiokas, M., Viale, M., and Scaff, L. (2020). Hydroclimate of the Andes Part I: Main Climatic Features. *Frontiers in Earth Science*, 8(March).

Firat, M., Dikbaş, F., Koc, A. C., and Güngör, M. (2012). Classification of annual precipitations and identification of homogeneous regions using k-means method. *Teknik Dergi*, 23(115):1609–1622.

Foster, G. and Rahmstorf, S. (2011). Global temperature evolution 1979–2010. *Environmental Research Letters*, 6(4):044022.

Funk, C., Peterson, P., Landsfeld, M., Pedreros, D., Verdin, J., Shukla, S., Husak, G., Rowland, J., Harrison, L., Hoell, A., and Michaelsen, J. (2015). The climate hazards infrared precipitation with stations - A new environmental record for monitoring extremes. *Scientific Data*, 2:1–21.

Gershunov, A. (1998). ENSO influence on intraseasonal extreme rainfall and temperature frequencies in the contiguous United States: Implications for long-range predictability. *Journal of Climate*, 11(12):3192–3203.

Ghasemi, A. R. (2015). Changes and trends in maximum, minimum and mean temperature series in Iran. *Atmospheric Science Letters*, 16(3):366–372.

Giraldo-Osorio, J. D., Trujillo-Osorio, D. E., and Baez-Villanueva, O. M. (2022). Analysis of ENSO-Driven Variability, and Long-Term Changes, of Extreme Precipitation Indices in Colombia, Using the Satellite Rainfall Estimates CHIRPS. *Water (Switzerland)*, 14(11):1–33.

Grimm, A. M. (2011). Interannual climate variability in South America: Impacts on seasonal precipitation, extreme events, and possible effects of climate change. *Stochastic Environmental Research and Risk Assessment*, 25(4):537–554.

Grimm, A. M. and Natori, A. A. (2006). Climate change and interannual variability of precipitation in South America. *Geophysical Research Letters*, 33(19):1–5.

Grimm, A. M. and Tedeschi, R. G. (2009). ENSO and extreme rainfall events in South America. *Journal of Climate*, 22(7):1589–1609.

Grotjahn, R., Black, R., Leung, R., Wehner, M. F., Barlow, M., Bosilovich, M., Gershunov, A., Gutowski, W. J., Gyakum, J. R., Katz, R. W., Lee, Y. Y., Lim, Y. K., and Prabhat (2016). *North American extreme temperature events and related large scale meteorological patterns: a review of statistical methods, dynamics, modeling, and trends*, volume 46. Springer Berlin Heidelberg.

Hellström, C. (2005). Atmospheric conditions during extreme and non-extreme precipitation events in Sweden. *International Journal of Climatology*, 25(5):631–648.

Hersbach, H., Bell, B., Berrisford, P., Hirahara, S., Horányi, A., Muñoz-Sabater, J., Nicolas, J., Peubey, C., Radu, R., Schepers, D., Simmons, A., Soci, C., Abdalla, S., Abellan, X., Balsamo, G., Bechtold, P., Biavati, G., Bidlot, J., Bonavita, M., De Chiara, G., Dahlgren, P., Dee, D., Diamantakis, M., Dragani, R., Flemming, J., Forbes, R., Fuentes, M., Geer, A., Haimberger, L., Healy, S., Hogan, R. J., Hólm, E., Janisková, M., Keeley, S., Laloyaux, P., Lopez, P., Lupu, C., Radnoti, G., de Rosnay, P., Rozum, I., Vamborg, F., Villaume, S., and Thépaut, J. N. (2020). The ERA5 global reanalysis. *Quarterly Journal of the Royal Meteorological Society*, 146(730):1999–2049.

Hirata, F. E. and Grimm, A. M. (2016). The role of synoptic and intraseasonal anomalies in the life cycle of summer rainfall extremes over South America. *Climate Dynamics*, 46(9-10):3041–3055.

Hoyos, I., Baquero-Bernal, A., Jacob, D., and Rodríguez, B. A. (2013a). Variability of extreme events in the Colombian Pacific and Caribbean catchment basins. *Climate Dynamics*, 40(7-8):1985–2003.

Hoyos, I., Dominguez, F., Cañón-Barriga, J., Martínez, J. A., Nieto, R., Gimeno, L., and Dirmeyer, P. A. (2018). Moisture origin and transport processes in Colombia, northern South America. *Climate Dynamics*, 50(3-4):971–990.

Hoyos, N., Escobar, J., Restrepo, J. C., Arango, A. M., and Ortiz, J. C. (2013b). Impact of the 2010-2011 La Niña phenomenon in Colombia, South America: The human toll of an extreme weather event. *Applied Geography*, 39(September 2011):16–25.

Hu, S., Zhou, B., Gao, C., Xu, Z., Wang, Q., and Chou, J. (2020). Theory of three-pattern decomposition of global atmospheric circulation. *Science China Earth Sciences*, 63(9):1248–1267.

Huang, W., Yang, Z., He, X., Lin, D., Wang, B., Wright, J. S., Chen, R., Ma, W., and Li, F. (2019). A possible mechanism for the occurrence of wintertime extreme precipitation events over South China. *Climate Dynamics*, 52(3-4):2367–2384.

Huffman, G. J., Adler, R. F., Bolvin, D. T., and Nelkin, E. J. (2010). The TRMM Multi-Satellite Precipitation Analysis (TMPA). In Gebremichael, M. and Hossain, F., editors, *Satellite Rainfall Applications for Surface Hydrology*, pages 3–22. Springer Netherlands, Dordrecht.

IPCC (2021). Weather and climate extreme events in a changing climate. *Cambridge University Press, Cambridge*.

Jennrich, G. C., Furtado, J. C., Basara, J. B., and Martin, E. R. (2020). Synoptic Characteristics of 14-Day Extreme Precipitation Events across the United States. *Journal of*

Climate, 33(15):6423–6440.

Jia, K., Ruan, Y., Yang, Y., and Zhang, C. (2019). Assessing the performance of CMIP5 global climate models for simulating future precipitation change in the Tibetan Plateau. *Water (Switzerland)*, 11(9).

Jiménez-Sánchez, G., Markowski, P. M., Jewtoukoff, V., Young, G. S., and Stensrud, D. J. (2019). The Orinoco Low-Level Jet: An Investigation of Its Characteristics and Evolution Using the WRF Model. *Journal of Geophysical Research: Atmospheres*, 124(20):10696–10711.

Jones, C. and Carvalho, L. M. (2018). The influence of the Atlantic multidecadal oscillation on the eastern Andes low-level jet and precipitation in South America. *npj Climate and Atmospheric Science*, 1(1):1–7.

Julian, P. R. and Chervin, R. M. (1978). A study of the Southern Oscillation and Walker Circulation phenomenon. *Monthly Weather Review*, 106(10):1433–1451.

Kayano, M. T. and Capistrano, V. B. (2014). How the Atlantic multidecadal oscillation (AMO) modifies the ENSO influence on the South American rainfall. *International Journal of Climatology*, 34(1):162–178.

Kim, Y. H., Min, S. K., Zhang, X., Sillmann, J., and Sandstad, M. (2020). Evaluation of the CMIP6 multi-model ensemble for climate extreme indices. *Weather and Climate Extremes*, 29:100269.

Krishnamurthy, V. and Misra, V. (2010). Observed ENSO teleconnections with the South American monsoon system. *Atmospheric Science Letters*, 11(1):7–12.

Leon, G. E., Zea, J. A., and Eslava, J. A. (2000). Circulación general del tropico y la zona de confluencia intertropical en Colombia. *Meteorología Colombiana*, 1:31–38.

Li, Z., Chao, Y., and McWilliams, J. C. (2006). Computation of the streamfunction and velocity potential for limited and irregular domains. *Monthly Weather Review*, 134(11):3384–3394.

Marengo, J. A., Jones, R., Alves, L. M., and Valverde, M. C. (2009). Future change of temperature and precipitation extremes in South America as derived from the PRECIS regional climate modeling system. *International Journal of Climatology*, 29(15):2241–2255.

Martínez, R., Zambrano, E., Nieto López, J. J., Hernández, J., and Costa, F. (2017). Evolución, vulnerabilidad e impactos económicos y sociales de El Niño 2015-2016 en América Latina. *Investigaciones Geográficas*, (68):65.

Meseguer-Ruiz, O., Ponce-Philimon, P. I., Quispe-Jofré, A. S., Guijarro, J. A., and Sarricolea, P. (2018). Spatial behaviour of daily observed extreme temperatures in Northern Chile (1966–2015): data quality, warming trends, and its orographic and latitudinal effects.

Stochastic Environmental Research and Risk Assessment, 32(12):3503–3523.

Pabón-Caicedo, J. D. (2012). Cambio climático en Colombia: tendencias en la segunda mitad del Siglo XX y escenarios posibles para el siglo XXI. *Revista de la Academia Colombiana de Ciencias Exactas, Físicas y Naturales*, 36(139):261–278.

Pabón-Caicedo, J. D., Arias, P. A., Carril, A. F., Espinoza, J. C., Borrel, L. F., Goubanova, K., Lavado-Casimiro, W., Masiokas, M., Solman, S., and Villalba, R. (2020). Observed and Projected Hydroclimate Changes in the Andes. *Frontiers in Earth Science*, 8(March).

Palomino-Ángel, S., Anaya-Acevedo, J. A., and Botero, B. A. (2018). Evaluation of 3B42V7 and IMERG daily-precipitation products for a very high-precipitation region in northwestern South America. *Atmospheric Research*, 217(July 2018):37–48.

Peng, Y., Zhao, X., Wu, D., Tang, B., Xu, P., Du, X., and Wang, H. (2018). Spatiotemporal variability in extreme precipitation in China from observations and projections. *Water (Switzerland)*, 10(8):1–17.

Posada-Marín, J. A., Rendón, A. M., Salazar, J. F., Mejía, J. F., and Villegas, J. C. (2019). WRF downscaling improves ERA-Interim representation of precipitation around a tropical Andean valley during El Niño: implications for GCM-scale simulation of precipitation over complex terrain. *Climate Dynamics*, 52(5-6):3609–3629.

Poveda, G. (2004). La hidroclimatología de Colombia: Una síntesis desde la escala interdecadal hasta la escala diurna. *Revista de la Academia Colombiana de Ciencias Exactas, Fisicas y Naturales*, (January 2004).

Poveda, G., Álvarez, D. M., and Mesa, O. J. (1996). Las fases extremas del fenomeno ENSO (El Nino y La Nina) y su influencia sobre la hidrologia de Colombia. *Ingenieria Hidraulica en Mexico*, 11(1):21–37.

Poveda, G., Álvarez, D. M., and Rueda, Ó. A. (2011). Hydro-climatic variability over the Andes of Colombia associated with ENSO: a review of climatic processes and their impact on one of the Earth's most important biodiversity hotspots. *Climate Dynamics*, 36(11-12):2233–2249.

Poveda, G., Espinoza, J. C., Zuluaga, M. D., Solman, S. A., Garreaud, R., and van Oevelen, P. J. (2020). High Impact Weather Events in the Andes. *Frontiers in Earth Science*, 8(May):1–32.

Poveda, G., Jaramillo, A., Gil, M. M., Quiceno, N., and Mantilla, R. I. (2001). Seasonality in ENSO-related precipitation, river discharges, soil moisture, and vegetation index in Colombia. *Water Resources Research*, 37(8):2169–2178.

Poveda, G. and Mesa, O. (2000). On the existence of Lloró (the rainiest locality on Earth): enhanced ocean–atmosphere–land interaction by a low level jet. 27(11):1675–1678.

Poveda, G., Mesa, O., Agudelo, P., Álvarez, J., Arias, P., Moreno, H., Salazar, L., Toro, V., Vieira, S., Jaramillo, A., and Guzman, O. (2002). Diagnóstico del ciclo diurno de la precipitación en los Andes tropicales de Colombia. *Meteorología Colombiana*, (5):23–30.

Poveda, G. and Mesa, O. J. (1997). Feedbacks between hydrological processes in tropical South America and large-scale ocean-atmospheric phenomena. *Journal of Climate*, 10(10):2690–2702.

Poveda, G., Mesa, O. J., Salazar, L. F., Arias, P. A., Moreno, H. A., Vieira, S. C., Agudelo, P. A., Toro, V. G., and Alvarez, J. F. (2005). The Diurnal Cycle of Precipitation in the Tropical Andes of Colombia. *Monthly Weather Review*, 133(1):228–240.

Reboita, M. S., Ambrizzi, T., Crespo, N. M., Dutra, L. M. M., Ferreira, G. W. d. S., Rehbein, A., Drumond, A., da Rocha, R. P., and de Souza, C. A. (2021). Impacts of teleconnection patterns on South America climate. *Annals of the New York Academy of Sciences*, 1504(1):116–153.

Renom, M., Rusticucci, M., and Barreiro, M. (2011). Multidecadal changes in the relationship between extreme temperature events in Uruguay and the general atmospheric circulation. *Climate Dynamics*, 37(11-12):2471–2480.

Ridder, N., De Vries, H., and Drijfhout, S. (2018). The role of atmospheric rivers in compound events consisting of heavy precipitation and high storm surges along the Dutch coast. *Natural Hazards and Earth System Sciences*, 18(12):3311–3326.

Rivera, J. A., Marianetti, G., and Hinrichs, S. (2018). Validation of CHIRPS precipitation dataset along the Central Andes of Argentina. *Atmospheric Research*, 213:437–449.

Rodríguez, M., Arias, P., and Ochoa, A. (2019). precipitación diaria en Colombia : observaciones , simulaciones y proyecciones. *M.S. thesis, Geoscience and Environment Department, National University of Colombia*.

Ruiz-vásquez, M., Arias, P. A., Martínez, J. A., Arias, P. A., and Alejandro, J. (2021). ENSO Influence on Regional Atmospheric Circulation and Thermodynamics Over Northern South America circulation and thermodynamics over. *Research Square*.

Rusticucci, M. (2012). Observed and simulated variability of extreme temperature events over South America. *Atmospheric Research*, 106:1–17.

Rusticucci, M., Barrucand, M., and Collazo, S. (2017). Temperature extremes in the Argentina central region and their monthly relationship with the mean circulation and ENSO phases. *International Journal of Climatology*, 37(6):3003–3017.

Salas, H. D., Poveda, G., Mesa, Ó. J., and Marwan, N. (2020). Generalized Synchronization Between ENSO and Hydrological Variables in Colombia: A Recurrence Quantification Approach. *Frontiers in Applied Mathematics and Statistics*, 6(March):1–20.

Salio, P., Hobouchian, M. P., García Skabar, Y., and Vila, D. (2015). Evaluation of high-resolution satellite precipitation estimates over southern South America using a dense rain gauge network. *Atmospheric Research*, 163:146–161.

Salvador, M. A. and de Brito, J. I. (2018). Trend of annual temperature and frequency of extreme events in the MATOPIBA region of Brazil. *Theoretical and Applied Climatology*, 133(1-2):253–261.

Santoso, A., Mcphaden, M. J., and Cai, W. (2017). The Defining Characteristics of ENSO Extremes and the Strong 2015/2016 El Niño. *Reviews of Geophysics*, 55(4):1079–1129.

Schumacher, V., Justino, F., Fernández, A., Meseguer-Ruiz, O., Sarricolea, P., Comin, A., Peroni Venancio, L., and Althoff, D. (2020). Comparison between observations and gridded data sets over complex terrain in the Chilean Andes: Precipitation and temperature. *International Journal of Climatology*, 40(12):5266–5288.

Shinker, J. J. and Bartlein, P. J. (2009). Visualizing the large-scale patterns of ENSO-related climate anomalies in North America. *Earth Interactions*, 13(3):1–50.

Skansi, M. d. l. M., Brunet, M., Sigró, J., Aguilar, E., Arevalo Groening, J. A., Bentancur, O. J., Castellón Geier, Y. R., Correa Amaya, R. L., Jácome, H., Malheiros Ramos, A., Oria Rojas, C., Pasten, A. M., Sallons Mitro, S., Villaroel Jiménez, C., Martínez, R., Alexander, L. V., and Jones, P. D. (2013). Warming and wetting signals emerging from analysis of changes in climate extreme indices over South America. *Global and Planetary Change*, 100:295–307.

Steinley, D. (2006). K-means clustering: A half-century synthesis. *British Journal of Mathematical and Statistical Psychology*, 59(1):1–34.

Sun, Q., Miao, C., Qiao, Y., and Duan, Q. (2017). The nonstationary impact of local temperature changes and ENSO on extreme precipitation at the global scale. *Climate Dynamics*, 49(11-12):4281–4292.

Tan, M. L., Juneng, L., Tangang, F. T., Chung, J. X., and Radin Firdaus, R. B. (2021). Changes in temperature extremes and their relationship with ENSO in Malaysia from 1985 to 2018. *International Journal of Climatology*, 41(S1):E2564–E2580.

Tan, Y., Yang, S., Zwiers, F., Wang, Z., and Sun, Q. (2022). Moisture budget analysis of extreme precipitation associated with different types of atmospheric rivers over western North America. *Climate Dynamics*, 58(3-4):793–809.

Tedeschi, R. G., Grimm, A. M., and Cavalcanti, I. F. (2015). Influence of Central and East ENSO on extreme events of precipitation in South America during austral spring and summer. *International Journal of Climatology*, 35(8):2045–2064.

Tedeschi, R. G., Grimm, A. M., and Cavalcanti, I. F. (2016). Influence of Central and East ENSO on precipitation and its extreme events in South America during austral autumn

and winter. *International Journal of Climatology*, 36(15):4797–4814.

Tencer, B., Bettolli, M. L., and Rusticucci, M. (2016). Compound temperature and precipitation extreme events in southern South America: Associated atmospheric circulation, and simulations by a multi-RCM ensemble. *Climate Research*, 68(2-3):183–199.

Tootle, G. A., Piechota, T. C., and Gutiérrez, F. (2008). The relationships between Pacific and Atlantic Ocean sea surface temperatures and Colombian streamflow variability. *Journal of Hydrology*, 349(3-4):268–276.

Trenberth, K. E. (2019). *El Niño southern oscillation (ENSO)*. Number September. Elsevier Inc.

Urrea, V., Ochoa, A., and Mesa, O. (2019). Seasonality of Rainfall in Colombia. *Water Resources Research*, 55(5):4149–4162.

Valencia, S., Marín, D. E., Gómez, D., Hoyos, N., Salazar, J. F., and Villegas, J. C. (2023). Spatio-temporal assessment of Gridded precipitation products across topographic and climatic gradients in Colombia. *Atmospheric Research*, 285(October 2022).

Vallejo-Bernal, S. M., Urrea, V., Bedoya-Soto, J. M., Posada, D., Olarte, A., Cárdenas-Posso, Y., Ruiz-Murcia, F., Martínez, M. T., Petersen, W. A., Huffman, G. J., and Poveda, G. (2021). Ground validation of TRMM 3B43 V7 precipitation estimates over Colombia. Part I: Monthly and seasonal timescales. *International Journal of Climatology*, 41(1):601–624.

Vincent, L. A., Peterson, T. C., Barros, V. R., Marino, M. B., Rusticucci, M., Carrasco, G., Ramirez, E., Alves, L. M., Ambrizzi, T., Berlato, M. A., Grimm, A. M., Marengo, J. A., Molion, L., Moncunill, D. F., Rebello, E., Anunciação, Y. M., Quintana, J., Santos, J. L., Baez, J., Coronel, G., Garcia, J., Trebejo, I., Bidegain, M., Haylock, M. R., and Karoly, D. (2005). Observed trends in indices of daily temperature extremes in South America 1960-2000. *Journal of Climate*, 18(23):5011–5023.

Wang, X., Luo, M., Wu, S., Ning, G., Liu, Z., Wang, S., Wang, P., Zhang, H., and Li, X. (2022a). Spatiotemporal Evolution Patterns of Contiguous Extreme Precipitation Events Across China From a 3D Perspective. *Geophysical Research Letters*, 49(16).

Wang, X., Luo, M., Wu, S., Ning, G., Liu, Z., Wang, S., Wang, P., Zhang, H., and Li, X. (2022b). Spatiotemporal evolution patterns of contiguous extreme precipitation events across china from a 3d perspective. *Geophysical Research Letters*, 49(16):e2022GL098840.

Ward, J. H. (1963). Hierarchical Grouping to Optimize an Objective Function. *Journal of the American Statistical Association*, 58(301):236–244.

Warner, M. D., Mass, C. F., and Salatheé, E. P. (2012). Wintertime extreme precipitation events along the Pacific Northwest Coast: Climatology and synoptic evolution. *Monthly Weather Review*, 140(7):2021–2043.

Waylen, P. and Poveda, G. (2002). El Nino-Southern Oscillation and aspects of western South American hydro-climatology. *Hydrological Processes*, 16(6):1247–1260.